Spatial and temporal variability of soil CO_2 efflux in a spruce-dominated forest in the Eifel National Park, Germany

Dissertation

zur

Erlangung des Doktorgrades (Dr. rer. nat.)

der Mathematisch-Naturwissenschaftlichen Fakultät

der

Rheinischen Friedrich-Wilhelms-Universität Bonn

vorgelegt von

Daniela Dwersteg

aus Steinfurt

Bonn, August 2011

Angefertigt mit Genehmigung der Mathematisch-Naturwissenschaftlichen Fakultät der Rheinischen Friedrich-Wilhelms-Universität Bonn.

1. Referent: Prof. B. Diekkrüger

2. Referent: Prof. J. Löffler

Tag der Promotion: 28.02.2012

Erscheinungsjahr: 2012

ACKNOWLEDGEMENTS

This work is supported by the German Research Foundation (Deutsche Forschungsgemeinschaft – DFG) in the frame of the special collaboration program Transregio 32 ‘Patterns in Soil-Vegetation-Atmosphere systems: Monitoring, Modelling and Data assimilation‘ of the University of Bonn, the University of Cologne, the University of Aachen and the Research Centre Jülich.

I would like to thank Professor B. Diekkrüger for his scientific support and his helpful advice, guiding me through this research.

Dr. Alexander Graf from the Research Centre Jülich is gratefully acknowledged for providing me with invaluable information and assistance whenever a problem came along.

Thanks to Hanna Post, Mareike Hees and Caroline Homm for an outstanding assistance in field work, labour work and computer work.

Guido Sciuto is acknowledged for a delightful teamwork and great support.

Table of Contents

List of Tables

List of abbreviations

B	Cambisol
BD	Bulk Density
B-S	Cambisol-Planosol
COSMO-CLM	model system for numerical weather prediction and regional climate modelling
CV	coefficient of variation
dbh	diameter at breast height
DWD	Deutscher Wetterdienst (German Weather Service)
E_{pot}	potential evaporation
ET_{act} or ETR	actual evapotranspiration
ET_{pot} or ETP	potential evapotranspiration
G	Gleysol
G-Q	Gleysol-Regosol
G-S	Gleysol-Planosol
GHn	Histosol-Gleysol (Niedermoorgley)
GM	Histosol-Gleysol (Anmoorgley)
HN	Histosol (Niedermoor)
LAI	leaf area index
LH	Latin Hypercube
MRD	mean relative difference
PATCIS	**P**roduction **A**nd **T**ransport of **C**O_2 **I**n the **S**oil (soil respiration model)
Q	Regosol
Q_{10}	temperature coefficient (rate of change of a system by a temperature increase of 10°C)
Q-G	Regosol-Gleysol
rFRB	relative fine root biomass
R^2	coefficient of determination
S-B	Planosol-Cambisol
SD	Standard deviation
S-G	Plansosol-Gleysol
SIMLAB	tool for sensitivity and uncertainty analysis
SIMULAT	physically-based 1-dimensional model to simulate water fluxes in soil
T_{pot}	potential transpiration
VESPER	**V**ariogram **E**stimation and **S**patial **P**rediction plus **ER**ror (tool for spatial prediction)
θ	relative soil water content
ψ	matric potential

1 Introduction

In view of the increased concern about an upcoming global change, the understanding of soil processes and soil-atmosphere exchange processes gains in importance. The major greenhouse gas CO_2 with its spatial and temporal variability in the different compartments is in the focus of several research projects.

1.1 Statement of problem

In the context of an upcoming global change the relevance of soil CO_2 emissions has increased drastically, as pointed out in numerous studies (IPCC 2007, Schlesinger & Andrews 2000). With regard to soil respiration, knowledge of processes is still poor and experimental data remains insufficient in combination with a weak geographical representation (Yuste et al. 2007, Saiz et al. 2007).

In general three main components contribute to total soil respiration. Those components are the respiration from live roots, the respiration of root-derived carbon (root exudates) by mycorrizhae or other microfauna in the rhizosphere and the respiration of soil carbon by soil fauna. It is a common approach to combine root and root-associated respiration into one component called rhizosphere or autotrophic respiration due to the difficulty of separating both components from each other (Hanson et al. 2000, Meharg 1994). Respiration of soil carbon by soil fauna is often referred to as microbial or heterotrophic respiration. Microorganisms decompose litter, while consuming oxygen and producing carbon dioxide. Soil CO_2 efflux is the combined result of production and gas transport (Suarez & Šimunek 1993, Fang & Moncrieff 1999). The main environmental factors controlling soil CO_2 efflux are temperature and soil water content (Davidson et al. 1998, Janssens et al. 2001). Among other influencing factors are the amount and quality of carbon stored in the soil and the litter layer and mineral soil and plant root activities (Nadelhoffer & Raich 1992, Bowden et al. 1993). There is still insufficient information on the extent to which environmental parameters such as temperature, soil moisture or litter availability control rhizosphere or microbial respiration.

Nevertheless research has been carried out to study the factors controlling soil CO_2 efflux. The most common approach to quantify soil CO_2 efflux has been the development of empirical models based on relationships between soil CO_2 efflux, soil temperature and soil water content (Davidson et al. 1998, Buchmann 2000).

There is an increasing interest in using process-based models, which take into account physiological properties and environmental regulations affecting soil respiratory processes. Each developed process-based model focuses on different aspects, serving the particular situation it was set up for.

1.2 The aim of this study

The project presented here is part of the Transregio Collaborative Research Centre 32 „Patterns in Soil-Vegetation-Atmosphere Systems: monitoring, modelling and data assimilation“, funded by the German Research Foundation DFG. The aim is to achieve a better understanding of complex spatial and temporal patterns in heat, water and matter fluxes on a catchment scale.

We conducted a study on a 60-year-old spruce stand (*Picea abies*) located in Western Germany from April 2008 to December 2010 with weekly measurements for 89 measurement points arranged in two setups. Our objectives were to reveal reasons for spatial and temporal patterns of soil CO_2 efflux in a spruce forest of temperate climate through field measurements and the application of a process-based model for soil CO_2 efflux to back up field data and improve the understanding of temporal patterns as a prerequisite for understanding spatial patterns. One central research question aims at the importance of the factor temperature. Is temperature the main factor controlling soil CO_2 efflux? Does it play a major role in the spatial patterns of soil CO_2 efflux? Which other factors determine spatial and temporal patterns of soil respiration? Another important goal is to study the feasibility of upscaling from the existent monitoring network to catchment scale. Further research questions concerned the applicability of the soil respiration model PATCIS (Fang & Moncrieff 1999). Does the model PATCIS help to answer the stated research questions?

1.3 The practical approach

1.3.1 Research area

The study area is located in the northern part of the Eifel National Park, which is part of the so-called Rureifel, in the catchment area of the Wüstebach stream (Figure 1). Measurements were concentrated in the upper part of the Wüstebach catchment area, including the headwaters. The area has a size of approximately 27 ha and shows a distance in altitude of up to 34 m (ranging from 595 m a.s.l. to 629 m a.s.l.). The borders of the considered catchment area are partly of natural and partly of anthropogenic origin. The motorway 258 defines the southern border of the catchment, while a small rural road in the western part of the catchment displays a water divide.

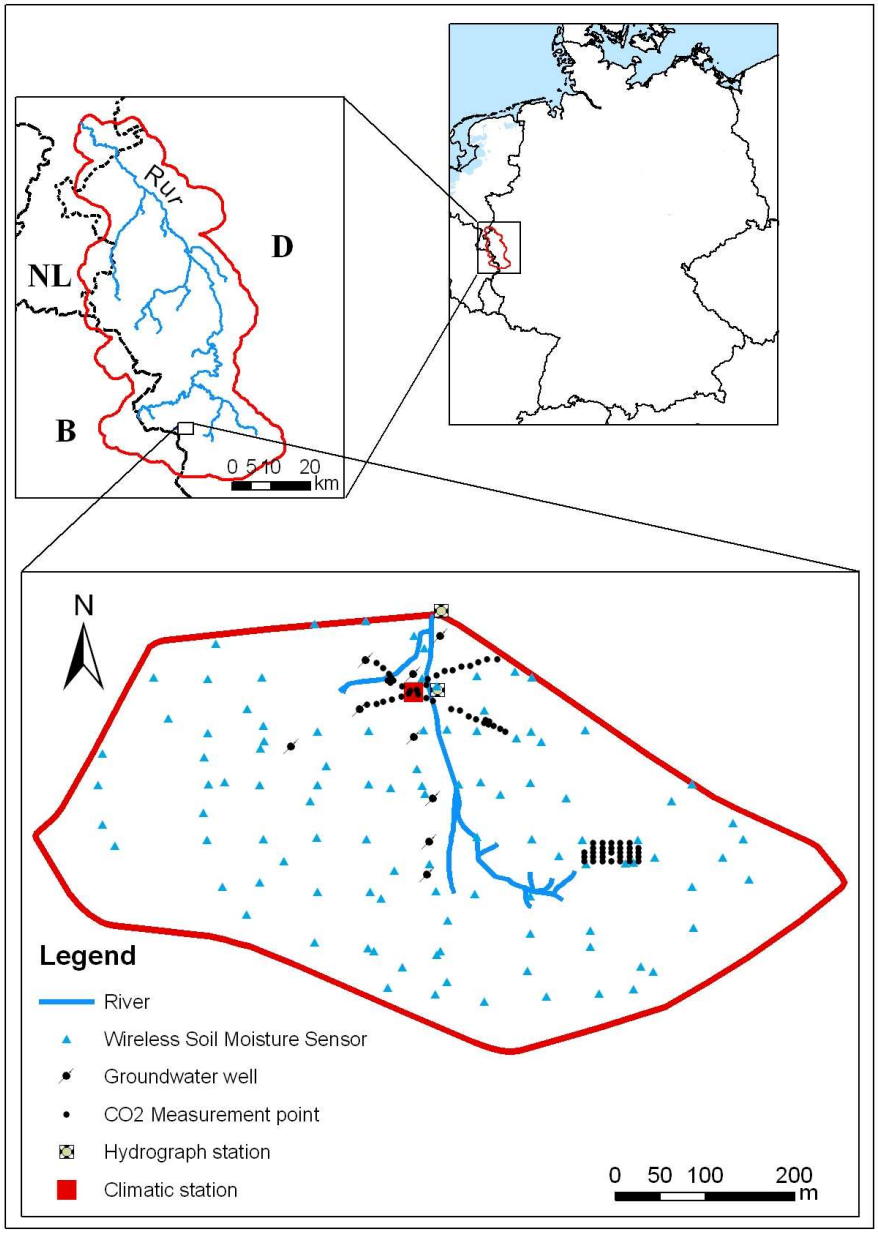

Figure 1 Location of the Wüstebach research area (modified after Sciuto & Diekkrüger, 2010)

1.3.2 Soil characterization

Underlying bedrock consists of a stratigraphic sequence of clay shales, the so called "Wüstebach-Schiefer", which is dark blue-grey to black-grey in colour and can be weathered from light grey to white. Sporadically sandstone banks with a fine grained or medium grained structure can occur. During the Pleistocene talus material built up due to solifluction and cryofracturing. (Meyer 1994)

Soils are alkali-poor and nutrient poor and are dominated by cambisols, which are normally well aerated, but are partly affected by tail water. In the groundwater influenced floodplains alongside the Wüstebach stream Gleysols, Stagnosols or Histosols are present. The Geological Survey North Rhine-Westphalia (Geologischer Dienst Nordrhein-Westfalen) developed a soil map at a scale of 1:5,000 m, (figure 2) which was used in this study.

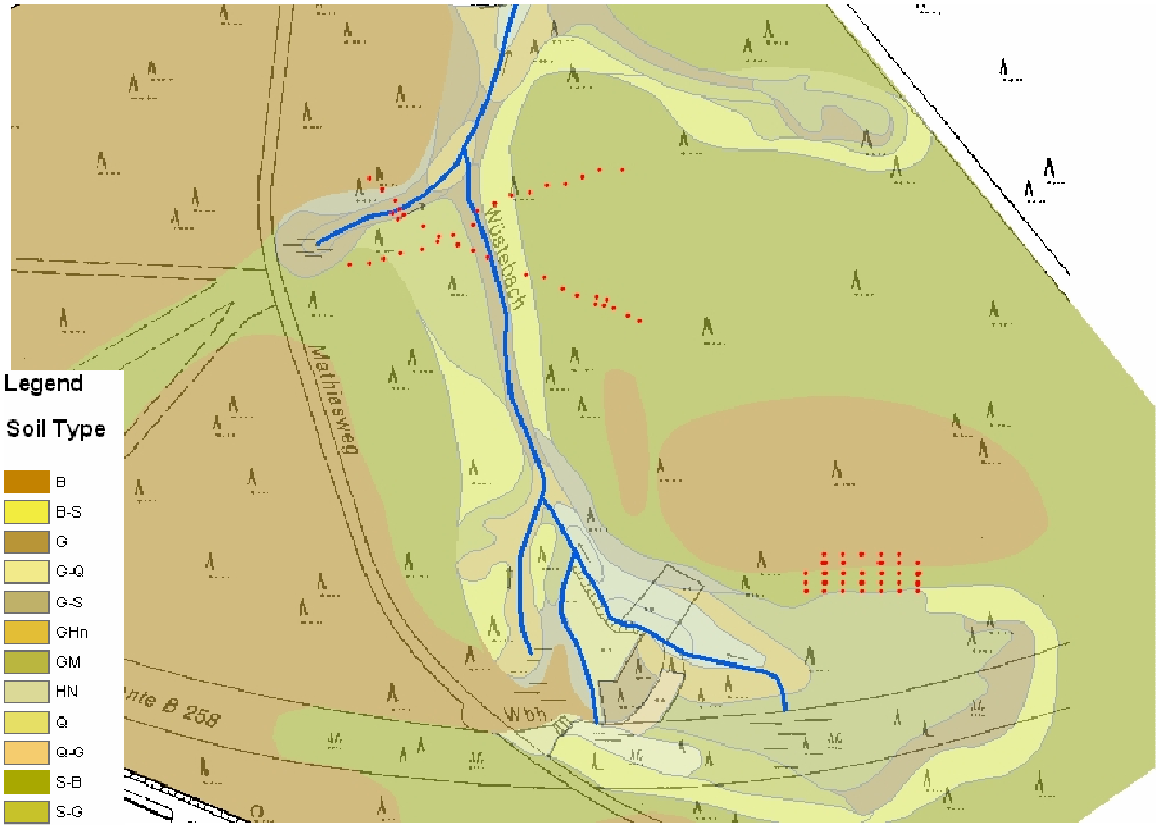

Figure 2: Soil map of the Wüstebach catchment area. *Soil types*: B – Cambisol; B-S – Cambisol-Planosol; G – Gleysol; G-Q – Gleysol-Regosol; G-S – Gleysol-Planosol; GHn – Histosol-Gleysol, GM – Histosol-Gleysol; HN – Histosol (Niedermoor); Q – Regosol; Q-G – Regosol-Gleysol; S-B – Planosol-Cambisol; S-G – Planosol-Gleysol. The red dots display the measurement points of the soil CO_2 efflux measurement setup. (own illustration based on data from the Geological Survey North Rhine Westphalia)

Typical soil profiles of a Cambisol (a), Gleysol (b) and Histosol (c) are illustrated in figure 3.

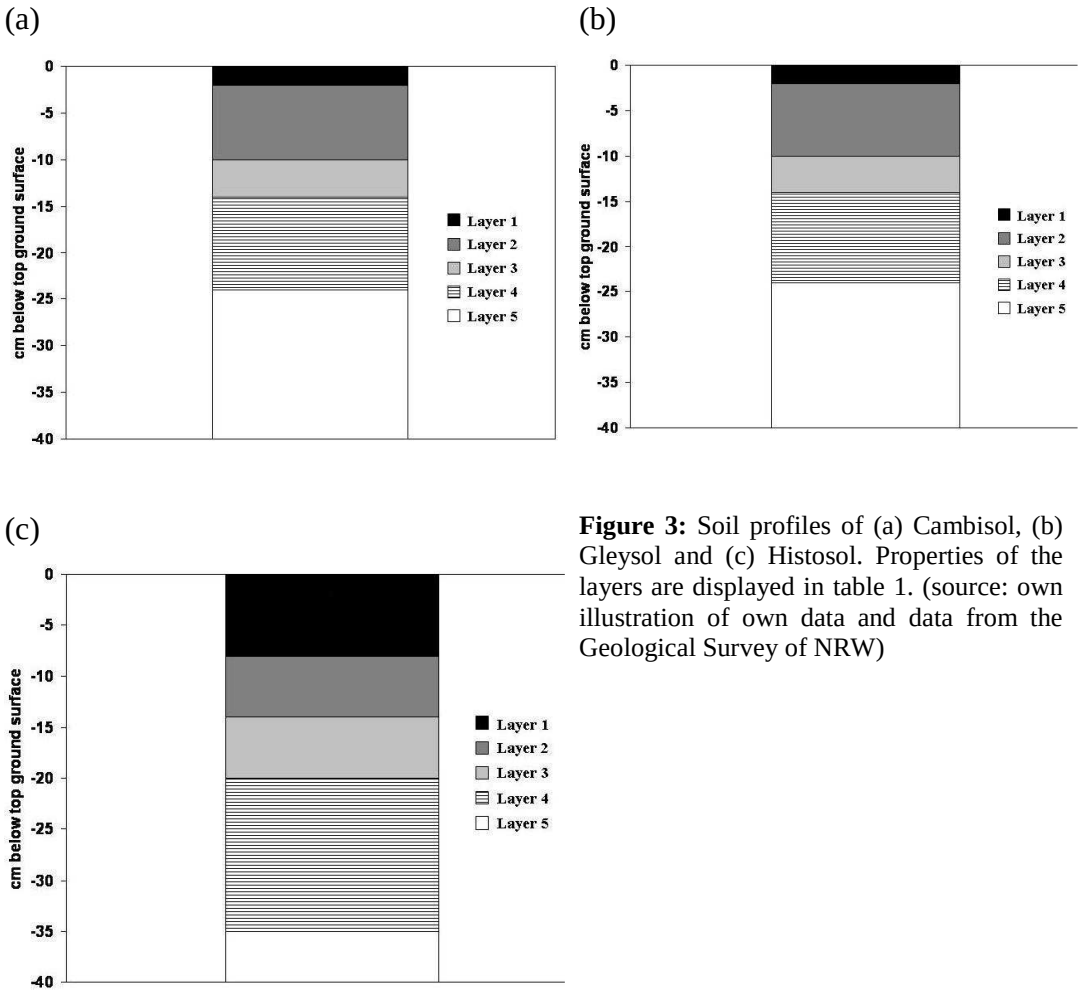

Figure 3: Soil profiles of (a) Cambisol, (b) Gleysol and (c) Histosol. Properties of the layers are displayed in table 1. (source: own illustration of own data and data from the Geological Survey of NRW)

Table 1: Layer properties of different soil types at the research site (BD = Bulk Density)

	Cambisol	**Gleysol**	**Histosol**
Layer 1	BD=0.11, needle litter	BD=0.11, needle litter	BD=0.26, silt loam, clay loam
Layer 2	BD=0.61, medium clay loam	BD=0.53, medium clay loam	BD=0.23, silt loam, clay loam
Layer 3	BD=0.69, medium clay loam	BD=0.60, strong clay loam	BD=0.36, silt loam, clay loam
Layer 4	BD=0.85, strong clay loam	BD=0.99, strong clay loam	BD=0.67, clay loam, silt loam
Layer 5	BD=1.15, strong clay loam	BD=1.53, silt loam	BD=0.90, clay loam, silt loam

1.3.3 Vegetation

Spruce (*Picea abies*) stands are dominating the vegetation in the catchment area, with an average age of 60 years, partly juvenescence occurs (age 10-20 years). The mature *Picea abies* shows a sinker root system consisting of horizontally spreading roots from which vertical or sinker roots develop (Gruber 1994). The root system can be modified, depending on soil conditions, to plate-root systems (without any vertical roots). Spruce roots are very sensitive to waterlogging and anoxia. Therefore the development of vertical roots is encouraged by nutrient-rich soils with high base saturation under well-aerated conditions. (Puhe 1994). Due to the unfavourable soil conditions with high acid saturation present in the Wüstebach catchment, the spruce stands here have developed a plate-root system. On poor soil conditions the trees can not linger and are prone to windfall (figure 4)

Figure 4: Spruce tree affected by windfall (photo by Guido Sciuto)

Common alder (*Alnus glutinosa*) appears alongside the stream, while scattered European beeches (*Fagus sylvatica*) can be found throughout the area. The density of the tree vegetation and the unfavourable soil conditions with a low nutrient content and a thick litter layer result in a low diversity of species in the understorey with ferns, herbage, mosses, few shrubs and phanerogams. The potential native vegetation of the upper Wüstebach valley is the *Luzula-Fagetum typicum* forest with *Fagus sylvatica* as a keystone species. Current vegetation originated from an extensive anthropogenic impact

on the area. Native wood was clear-cut for utilization in the context of wood charcoal production. Written records reveal that most parts of the Eifel region were deforested during mediaeval times (Schwind 1984). Only towards the beginning of the 19th century the state of the forest gained an increasing interest. *Picea abies* was preferred for afforestation due to its fast growth. Both world wars involved repeated forest clearance, soon after which *Picea abies* was again used for further afforestation.

The vegetation period (= period of days with an average temperature above 10°C) in the Wüstebach forest lies between 127 days (2008) and 138 days (2007) during the considered period of analysis. In comparison to this, the vegetation period in the northern region of the Eifel National Park (around Nideggen, see figure A8) lasts 160 days. Unfavourable conditions for the vegetation are late frost and cold air, which accumulates on the plateaus of the Rureifel and can not run off immediately due to low slope.

1.3.4 Climate

The climate in the catchment area is oceanic with a mean annual temperature of 6.5°C to 7.5°C and a mean annual precipitation of 1100 to 1200 mm (see table 2 and figures 5 & 6). A snow cover is present on 20-30 days per year. The wind predominantly originates from a western direction. Precipitation data was available from two meteorological stations, with numerous data gaps. For 2007 complete data was also available through a simulation with the model COSMO, developed by the German Weather Service (DWD) for numerical weather forecasts, and called "reanalysis". Air temperature was measured directly in the Wüstebach catchment.

Table 2: Nearby climate stations with precipitation data (source: DWD; *from COSMO model)

Name	**Coordinates**		**Height**	**Resolution**	**Mean annual rainfall [mm]**		
	Easting	*Northing*	*[m]*		*2007*	*2008*	*2009*
Schleiden-Schöneseiffen	2528366	5597820	572	Daily	1391	935	1082
Monschau - Kalterherberg	2515365	5597766	535	daily, 6 hours	1455	1318	1224
Reanalysis*	2523669	5596549	598	hourly	1603	-	-

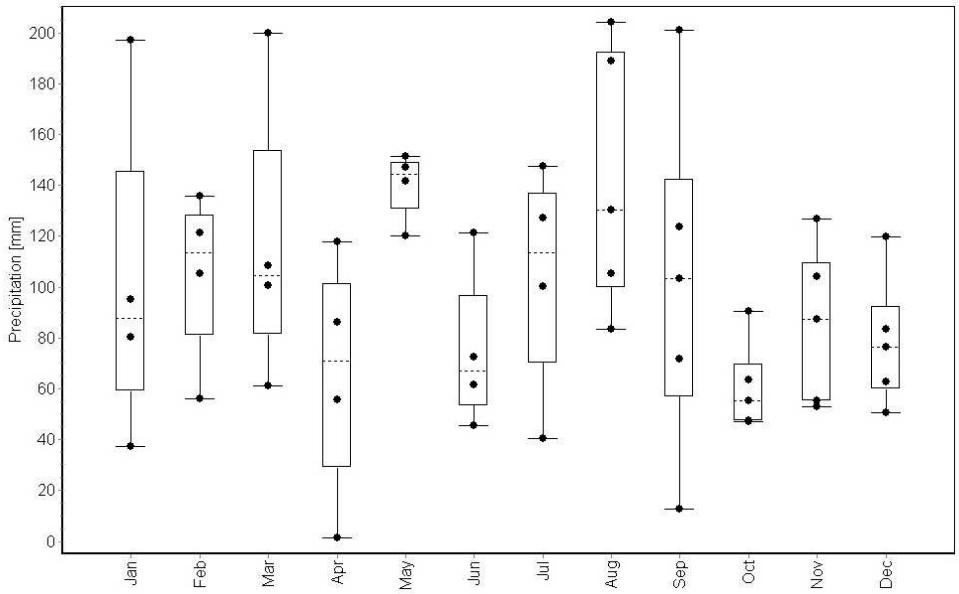

Figure 5: Boxplots of mean monthly precipitations for the station Kall-Sistig for the years 2004 (from August 04) – 2008. (source: own illustration with data from the DWD)

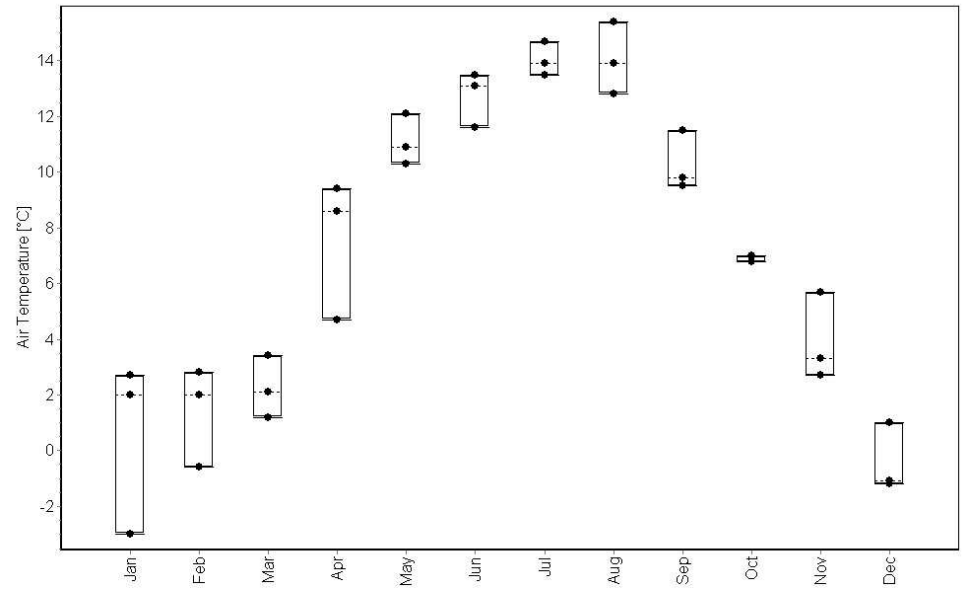

Figure 6: Boxplots of mean monthly temperatures for the Wüstebach station for the years 2007-2009. (source: own illustration of data collected in the frame of the Transregio 32)

1.3.5 Historical land use

The contemporary vegetation structure of the Eifel National Park originated from profound anthropogenic influences of the last centuries. Due to climatic conditions and the presence of nutrient-poor soils, the region was primarily affected by forest management since the start of settlement in the 13th century and to a lesser extent by agriculture. Natural forest was cut down and the wood was used for wood charcoal production to satisfy a growing energy demand of the iron industry during the 18th century (Schwind 1984).

Most woodland areas of the Eifel region are so called age-group forests (Schöller 2002), which characterizes coeval and comparably unstructured tree stands. In economically used forests, trees are taken out in their vital phase and are replaced by young growth. Therefore the decay and alteration phase with the formation of deadwood stands, which is relevant for a natural forest, is nonexistent. Through forest tending strategies such as pruning or selective cutting, coniferous trees are stimulated to a straight and fast growth and therefore build uniform and dense stands (Schöller 2002).

Towards the end of the 19th century most parts of the Eifel region were passed on to state-run forestry. Along with natural beech trees, coniferous wood such as spruce was introduced and used for afforestation. Further deforestation occurred during the two world wars, accompanied by visible signs in the soil structure of the forest (i.e. bomb craters, trenches). Afforestation after the Second World War lead to a further large-scale distribution of spruce trees (*Picea abies*).

In 2004 110 km² of the Eifel region were declared as Eifel National Park in order to protect people and landscape and to abandon wood harvest.

1.4 Analysis and modelling concept

To achieve a comprehensive data set of soil temperature and soil moisture for several soil layers and time periods, a model had to be chosen, which is able to simulate water as well as heat fluxes. The model SIMULAT (Diekkrüger 1996) was chosen because it provides a substantial output by requiring moderate input parameters, which could sufficiently be provided with a relatively low uncertainty.

For transport of CO_2 in soil ordinary gaseous diffusion and convective flow are considered to be the most important mechanisms (Freijer & Leffelaar 1996). A mass balance model for the soil is commonly used to quantify CO_2-efflux and the spatial distribution of CO_2 within the soil (Suarez & Šimunek 1993, Wood et al. 1993). Describing CO_2 production and its dependence on soil conditions is linked to uncertainty, no existing model is wholly appropriate. The number of published soil CO_2 efflux models, which are based on CO_2 release in decomposition in soil and on molecular diffusion of CO_2 into the atmosphere, is rather small.

The model PATCIS after Fang & Moncrieff (1999) was chosen because it shows a more complex model structure, with separate determination of microbial and root respiration, which is especially important for forest ecosystem. Soil moisture, temperature and even O_2-influence are sufficiently taken into account. The only drawback is the need of numerous parameters, which require extensive field and laboratory studies and lead to an increase of model uncertainty. A scheme of the modelling approach can be found in figure 7.

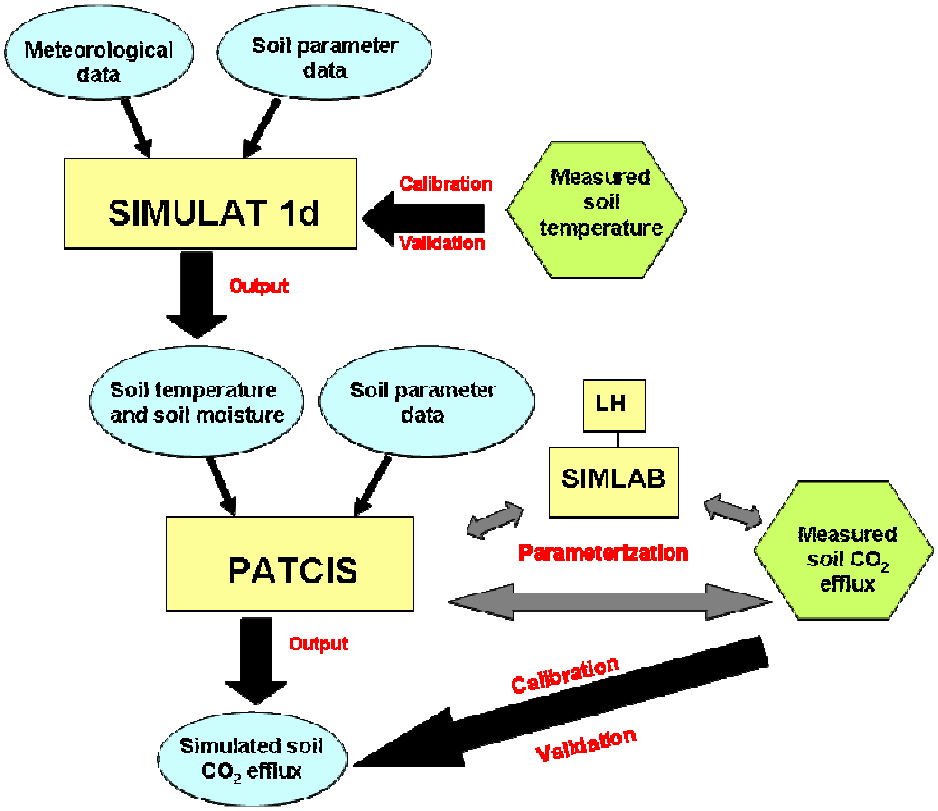

Figure 7: Scheme of the modelling approach. Meteorological and soil parameter data are used as input for the soil water budget model SIMULAT 1d, the model is calibrated and validated with measured soil temperature data. Simulated soil temperature and soil moisture along with measured soil parameter data is then used as input for the soil respiration model PATCIS. PATCIS is parameterized with the model SIMLAB and the Latin Hypercube analysis. Measured soil CO_2 efflux is used for calibration and validation of the model, as well as for parameterization. (source: own illustration)

1.5 Structural Overview

After introducing aims and objectives of this study and the research area, chapter 2 will provide the present status of knowledge concerning carbon soil fluxes and aspects of measuring and modelling them. Chapter 3 describes the methodological approach concerning measurements and the simulation of soil CO_2 efflux and several environmental parameters. The results of several methods of analysis are discussed in chapter 4, while model application, including model parameterization and modification, are illustrated in chapter 5. Results are summarized in chapter 6 and general conclusions are presented in chapter 7.

2 Research context

It is apparent that no lifetime is long enough in which to explore
the resources of a few square yards of ground.
(Alice M. Coats)

In recent years research on soil respiration has gained in importance due to the importance of CO_2 as one of the driving forces of climate change. As early as 1932, an analysis of total humus content in the upper layers of several soil profiles was conducted by Romell (1932). At the beginning of the 20th century Lundegardh (1927) noted that soil respiration was correlated with various factors, such as temperature, soil moisture and the nutrient content of the soil.

Schlesinger (1977), who published a comparative study of early soil respiration research, characterized soil respiration as a major CO_2 flux within terrestrial ecosystems as well as between biosphere and atmosphere. It is widely acknowledged that temperature exerts a dominating influence on soil respiration (Buchmann 2000, Davidson et al. 1998, Subke et al. 2006). The relationship between soil temperature and soil respiration is typically described by an empirical Q_{10} function (Davidson et al. 1998, Graf et al. 2008). The Q_{10} factor describes the increase in soil respiration with an increase in temperature by 10 Kelvin. Lloyd and Taylor (1994) emphasize the temperature dependency of Q_{10} itself, leading to higher values of Q_{10} in colder climates. Furthermore Q_{10} is affected by soil moisture (Kirschbaum et al. 1995). Davidson et al. (1998) point out that Q_{10} increases with depth, which complicates comparisons among different studies. In most studies soil temperature is measured in one depth only, while the measured value of soil respiration includes the CO_2 production from several depth with various temperature regimes (Graf et al. 2008). Some researchers have analysed which temperature depth yields the highest coefficient of determination (R^2) (Tang et al. 2003, Shi et al. 2006). Q_{10} is not constant throughout the year; it changes seasonally (Janssens & Pilegaard 2003). An increase in temperature and a decrease in soil moisture lead to a decrease in soil respiration (Kirschbaum 1995, Rayment & Jarvis 2000, Xu & Qi 2001). There are major restrictions on the Q_{10} function (Davidson et al. 2006). Enzyme activity, diffusion of oxygen and soluble carbon substrates through soil air and water, the growth of microbial populations and root tissues can have multiplicative effects on soil respiration (Davidson et al. 2006). Although empirical relationships between soil respiration, soil temperature and soil moisture are not sufficient and site specific (Bunnell et al. 1977, Hanson et al. 1993), they

are commonly applied due to the lack of a full mechanistic understanding of all processes involved.

While an increase in temperature generally leads to an increase in decomposition of organic material (Buchmann 2000, Subke et al. 2006, Fang & Moncrieff 1999, Pumpanen et al. 2003), it can also lead to dehydration of soils and therefore limited water content. A low soil water content leads to a limitation of substrate diffusion in water films and therefore to desiccation stress (Orchard & Cook 1983, Skopp et al. 1990), while a high soil water content results in a limitation of oxygen diffusion in pore spaces (Linn & Doran 1984, Skopp et al. 1990).

Hanson et al. (2003) pointed out the effects of drought periods on microbial respiration. While dry periods cause cumulative death of microbial cells and therefore a decrease in microbial soil respiration, even a small precipitation event shortly after this period leads to a significant increase in soil respiration due to the sudden substrate availability. CO_2 flux from the soil is commonly modelled as a function of soil temperature and soil moisture (Qi & Xu 2001). While scientists agree upon the effect of soil temperature on soil respiration (Lloyd & Taylor 1994), the function form of the moisture effect remains controversial. Different functions to combine the effects of soil temperature and soil moisture on soil respiration exist in literature. In several studies the effects of soil moisture and soil temperature are assumed to be multiplicative (Parton et al. 1993, Potter et al. 1993, Raich et al. 1991). With the availability of large data sets the effect of soil temperature and soil moisture in combination is often fitted using multiple linear equations (Leiros et al. 1999, Rout & Gupta 1989).Various function forms can be found in different studies (Davidson et al. 1998, Epron et al. 1999, Orchard & Cook 1983).Qi & Xu (2001) separated the effects of soil moisture and soil temperature using a two-step procedure and applied a partial correlation analysis afterwards to detect these effects. The combined effect of soil temperature and soil moisture is modelled using two power functions.

Other factors such as soil texture, substrate quality and quantity can also exert influence on soil respiration (Randerson et al. 1996, Boone et al. 1998). Soil components like clay minerals have the ability to adsorb organic compounds which could result in a decrease of heterotrophic respiration. Soils with a higher content of aggregates might also show a lower heterotrophic respiration due to C-compounds being embedded in between aggregates (Scheffer & Schachtschabel 2002).

Heterotrophic and autotrophic respiration react differently to changes in environmental conditions (Kirschbaum 1995, Boone et al. 1998). Autotrophic respiration is characterized more sensitive to temperature than heterotrophic respiration, displaying different Q_{10} values (Boone et al. 1998). A general opinion is that soil warming will lead

to an increase of microbial decomposition and with it an increase of heterotrophic and autotrophic respiration, due to the plant nutrient release and the overall plant productivity increase (Van Cleve et al. 1983). This would indicate an increase in total soil respiration with a soil temperature increase. However, studies have shown that the soil respiration enhancement is not sustained at high levels in response to warming (Jarvis & Linder 2000, Rustad et al. 2001). Instead root respiration may decrease or remain constant with warming because of temperature adaptation. Roots adapt to warmer average temperatures by respiring less at a given temperature (Sowell & Spomer 1986, Luo et al. 2001).

High soil water content can impede root respiration in mineral soil. Moncrieff and Fang (1999) show that microbial respiration in the upper soil is left unhindered, from which the conclusion is drawn that soil moisture is no influencing factor in the litter layer. With low soil moisture conditions, dissolved carbon, which is seen as the most important substrate for heterotrophic respiration, is limited. The diffusion of enzymes needed for decomposition of organic material can only take place in liquid phase. Moncrieff and Fang (1999) defined the maximum of soil CO_2 efflux at a volumetric soil water content of 20-35%. Less than 15% would lead to a decrease of respiration due to the limitation on substrate availability, while more than 35% would lead to a decrease in oxygen and therefore likewise limit soil respiration. Low soil water content leads to desiccation stress which results in closure of stomata, exfoliation etc. (Borken et al. 2005). It remains unclear to which extent root respiration is battered from desiccation stress of the plant. Recent radiocarbon data suggest that respiration of young carbon substrates, such as those respired by live roots, is less affected by drought in forest ecosystems than is microbial decomposition of older substrates in the litter layer (Borken et al. 2005). If this is true, then variation of soil water content within an intermediate range may affect soil respiration primarily through its effect on diffusion of solutes to soil microorganisms. (Davidson et al. 1998)

Soil texture plays an important role with regard to soil moisture and oxygen availability. The high-level groundwater in bogs and half-bogs leads to oxygen deficiency which inhibits organic matter decomposition. (Scheffer & Schachtschabel 2002).

Several methods to achieve the separation of heterotrophic and autotrophic respiration are discussed in literature (Subke et al. 2006, Hanson et al. 2000). While the use of isotopes seems to be a reliable way to distinguish between microbial and root respiration, so-called root exclusion methods, including root trenching, root removal and gap analysis, often provide an easier and more cost-efficient way (Hanson et al. 2000).

The contribution of root respiration to total soil respiration can be anything from 10…95% (Hanson et al. 2000). Buchmann (2000) discovered a percentage of less than 30% of autotrophic respiration to total soil respiration in her study on a *Picea abies* forest

stand in Northeast Germany using the method of trenching. Saiz et al. (2007) identified autotrophic respiration as the dominant soil respiration component with 54.7% for their Sitka spruce stand using the process-based model PATCIS, which differentiates between heterotrophic and autotrophic respiration. Díaz-Pinés et al. (2008) gained 25% autotrophic respiration of total soil respiration from their study in a spruce-dominated Austrian mountain forest, which is supported by studies from Epron et al. (1999) and Lee et al. (2003). Brumme (1995) applied the method of gap analysis for a 146 year old beech stand. Two years after clear-cutting the contribution of root respiration to total soil respiration was identified as 40%. The use of ^{14}C pulse labelling on hybrid poplar trees by Horwarth et al. (1994) resulted in a contribution of 20% for root respiration to total soil respiration. Subke et al. (2006) point out that spatial variability of total soil respiration can be attributed to root respiration and therefore the spatial distribution of roots. Extensive research has been carried out to study the factors controlling soil CO_2 efflux. The most common approach to quantify soil CO_2 efflux has been the development of empirical models based on relationships between soil CO_2 efflux, soil temperature and soil water content (Davidson et al. 1998, Buchmann 2000). These models lack a biological framework, which makes it difficult to account for the role of the environment on soil respiration (Fang & Moncrieff 1999, Pumpanen et al. 2003). Therefore process-based models are more commonly applied, which take into account physiological properties and environmental regulations affecting soil respiratory processes.

For transport of CO_2 in soil ordinary gaseous diffusion and advective flow are considered to be the most important mechanisms (Freijer & Leffelaar 1996). A mass balance model for the soil is commonly used to quantify CO_2-efflux and the spatial distribution of CO_2 within the soil (Šimunek & Suarez 1993, Wood et al. 1993). Describing CO_2 production and its dependence on soil conditions is linked to uncertainty, no existing model is wholly appropriate. The number of published soil CO_2 efflux models, which are based on CO_2 release in decomposition in soil and on molecular diffusion of CO_2 into the atmosphere is rather small. Billings et al. (1998) calculated soil-surface CO_2-efflux for boreal forests based on soil-profile CO_2 concentration and the diffusion of gas through the soil profile. Cook et al. (1998) developed a one-dimensional steady-state model for CO_2 diffusion from soil for a stand of *Pinus radiata*. The model is based on vertical decrease of the source term described by a power function and a constant diffusion coefficient. The surface-flux density of CO_2 from the soil is derived from integration of the source term with depth. Suarez and Šimunek (1993) developed a complex simulation model SOILCO2, which includes one-dimensional water flow and multiphase transport of CO_2 utilizing the Richards' and the convection-dispersion equations as well as heat flow and a CO_2-production model. The model was set up for agricultural areas. Fang and Moncrieff

(1999) developed a process-based model (PATCIS) which simulates the production and transport of CO_2 in soil. CO_2 produced by respiration is transported in the soil by gaseous diffusion and liquid-based dispersion as well as gas convection and vertical water movement. Microbial respiration is related to the amount and quality of organic matter and root respiration to the distribution of roots in the soil. Temperature and moisture responses of soil respiration are included in the model. Reichstein et al. (2003) take into account the influence of substrate availability on soil respiration. As an indicator for substrate availability the leaf area index (LAI) is used. This was achieved by applying a general regression model and adding an empirical explicit dependency of soil respiration on maximum site leaf area index. The model was validated for several European forests. Pumpanen et al. (2003) partition the soil in several layers and the processes and soil properties are described separately for each layer. The CO_2 flux between the layers is driven by diffusion, depending on CO_2 concentration, porosity and temperature of the layers. The model was developed for a Scots Pine forest stand.

3 Measurement and simulation of soil CO_2 efflux and its environmental parameters

The spatial and temporal variability of soil CO_2 efflux is highly complex. This chapter will illustrate the experimental setup, the measurements of soil CO_2 efflux and its environmental parameters and the methods involved to characterize the soil CO_2 efflux in this particular area of the Eifel National Park. Subsequent to this, the analysis and the different approaches to analyse spatial and temporal variability of soil CO_2 efflux will be discussed.

3.1 Measurement setup

The installation of 35 measurement points, arranged in two crossing transects, was conducted before the start of this study in 2006. The crossing point of the transects WA and WB was located close to the Wüstebach stream and the idea was to capture a possible CO_2 gradient from the stream uphill. In 2008 the two transects were modified (one point was taken out, 6 new measurement points were added; figure 8) and a new measurement grid (M) was established.

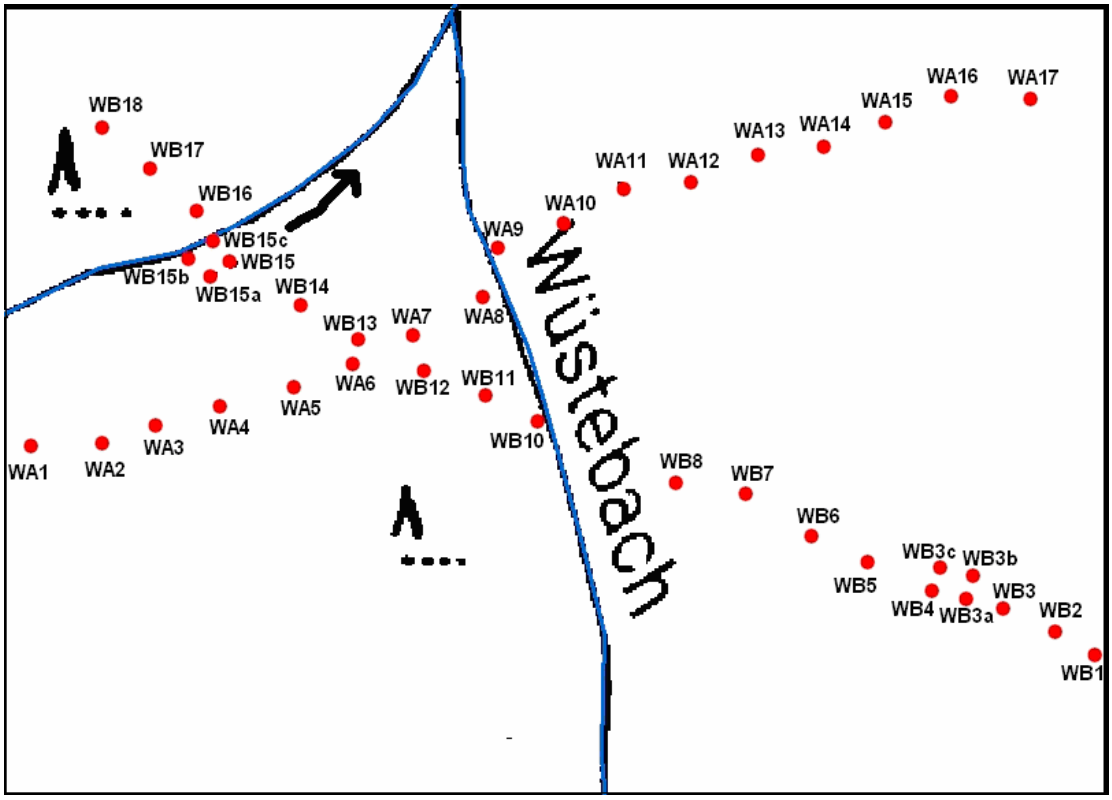

Figure 8: Position of soil CO_2 measurement transects WA and WB. For exact position see figure 1. (source: own illustration)

The new grid M contained 35 points, which were modified by and by to a current measurement grid of 49 measurement points (figure 9). For two of those 49 measurement points the litter layer (2-4 cm) was removed, while litter layer and organic layers (up to ~ 12 cm) were removed for two further points.

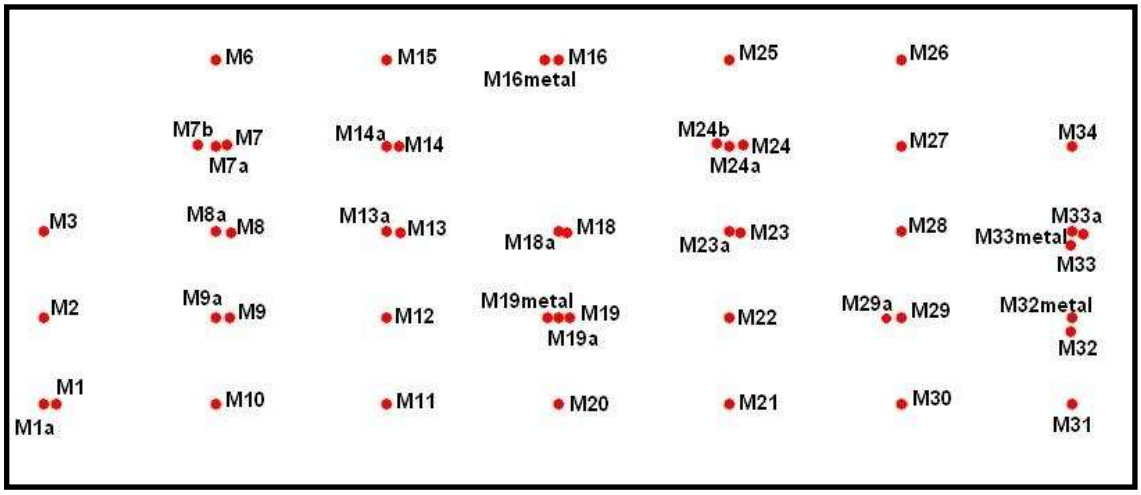

Figure 9: Position of soil CO_2 measurement grid M. For exact position see figure 1. M1a, M7a/b, M16metal, M18a, M19metal/a, M23a, M24a/b, M29a, M32metal, M33a/metal are points affected by root separation techniques. M8a, M9a, M13a, M14a are control points for adjacent layer removal points. (source: own illustration)

In order to explain possible different reactions of heterotrophic and autotrophic respiration to changes in temperature, soil moisture, organic matter content etc. the two components of soil respiration were separated (figure 10).

Figure 10: Installation of collars used for root exclusion (photo by Guido Sciuto)

Several methods to achieve this separation are discussed in literature (Subke et al. 2006, Hanson et al. 2000). While the use of isotopes seems to be a reliable way to distinguish

between microbial and root respiration, so-called root exclusion methods often provide an easier and more cost-efficient way. Root exclusion methods (Hanson et al. 2000) can be divided into three groups:

1. Root elimination

The soil is excavated and all roots are removed. Afterwards the soil is replaced in reverse order. Barriers are constructed to avoid reintroduction of roots into the measured spot. One advantage of this method is the immediate removal of all roots; no root litter is left for degradation by microbes. The low costs involved display another advantage. Major drawbacks of this method are the heavy disturbance of the soil structure and possible compression of soil due to the soil replacement. The separation of roots and soil is time-consuming. In case larger roots are present, the application of this method might be difficult or even impossible.

2. Root trenching

The roots are cut with the collar used for the soil CO_2-chamber. A rest period of several months is needed to allow for the roots to be totally degraded. Fine roots need to be monitored carefully. Measurement spots should be in adequate distance from trees to avoid large roots. The advantages of this method are the easy handling and the low costs and efforts involved. The soil structure is not disturbed. The major drawback is the root litter left for microbial degradation. This method is not advisable for plants with deep roots, root ingrowth from below might be a major problem there.

3. Gap analysis

Elimination of complete vegetation, e.g. clear cut of forests. The advantage is the immediate elimination of live roots and therefore the autotrophic respiration. There are several large drawbacks however. A large amount of root litter is left for heterotrophic respiration on the one hand; on the other hand litter input from aboveground litter fall is not available for heterotrophic respiration anymore. The lack of vegetation results in a change of radiation and water budget, leading to changes in soil temperature and soil water content. The extreme alteration of the ecosystem makes it difficult to compare the former ecosystem before the gap analysis and the new ecosystem with regard to autotrophic and heterotrophic respiration. Parts of the Wüstebach catchment will be clear cut in the near future enabling us to test the method of gap analysis for measurement grid M.

For two of the 49 measurement points of grid M the method of root elimination was used. Due to the fact that steel collars with a length of 40 cm and a diameter of 20 cm were installed, we resigned from the construction of barriers. For nine further measurement points the method of root trenching was applied. In this case the steel (or plastic) collars, as described above, were used to cut the roots.

All measurement collars were installed at least 4-6 weeks prior measurements to reduce soil disturbance. A long term measurement chamber (LI-8100-101; Licor Biosciences Ltd) was installed outside the catchment area, close to the Feuerwachturm (figure 11) and diurnal soil CO_2 efflux was measured for individual days in September and October 2009. A detailed description of individual measurement points can be found on the CD (file "point characteristics").

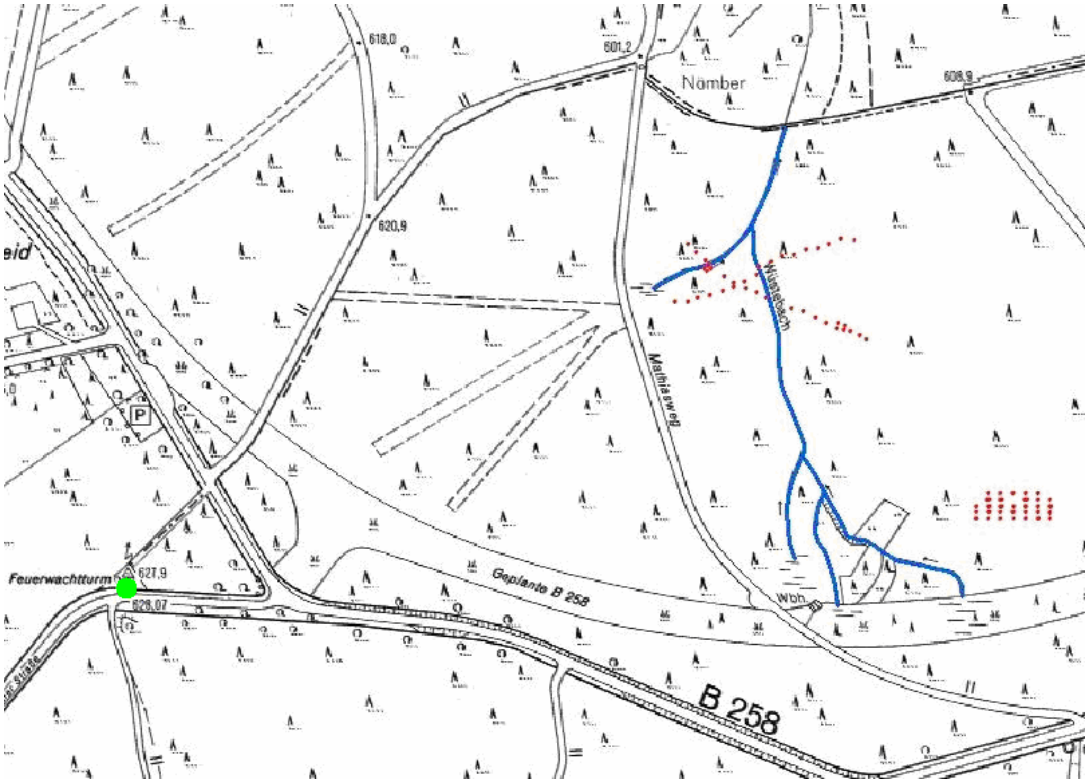

Figure 11: Position of the soil CO_2 measurement points; green dot: long term measurement chamber (Feuerwachturm) (source: map changed after data from Geological Survey of North Rhine-Westphalia)

3.2 Measurement of soil CO_2 efflux

Soil CO_2 efflux was measured on a weekly basis using a closed dynamic chamber system (LI 8100, Licor Biosciences Ltd). The chamber (figure 12) is placed on PVC collars (Ø 20 cm) to use the increase of CO_2 within the chamber for estimation of CO_2 diffusion from the soil. Insertion depth of collars was 5-8 cm into the forest floor.

Figure 12: LICOR-8100 measurement chamber (left) and plastic collar for soil respiration (right) (own photo material)

The LI-8100 uses the rate of increase of CO_2 in the measurement chamber to estimate the rate at which CO_2 diffuses into free air outside the chamber (measurement accuracy: 1.5% of reading). For such an estimate to be valid, conditions must be similar inside and outside the chamber; these conditions include the concentration gradients driving diffusion, barometric pressure, temperature and moisture of the soil. The CO_2 gradient between the soil surface layer and air are not exactly the same inside and outside the chamber, because there is an increase in CO_2 mole fraction inside the chamber. The diffusion rate is estimated and corrected by an analytical technique that takes into account the effects of increasing chamber CO_2 concentration on the diffusion gradient. This makes it possible to estimate the initial rate of CO_2 increase that occurred immediately after the chamber closed (manual LI-8100, Licor Biosciences Ltd). We used a 3 minute-measurement interval, recommended by the manufacturer.

The resulting regression line (figure 13) can be fitted in two ways: the traditional linear fit, and the theoretically more correct exponential fit. The LI-8100 uses all raw records after the start time (= deadband; the time until steady chamber mixing is established), but allows the user to shorten this by specifying a stop time. If the regression takes the maximum number of iterations and still hasn't converged, then the normalized sums of the squares of the residuals are compared to see which gave the better fit – linear or exponential. Strict guidelines concerning the choice of exponential and linear fit do not exist among scientists. The choice of a suitable fit remains subjective and the question whether it is advisable to mix linear and exponential values with regard to their comparability stays unresolved. With regard to the manufacturer linear fits are more robust than exponential fits, but tend to underestimate the soil CO_2 efflux. The exponential regression on the other hand is said to reproduce the data more precisely but is prone to "bumps" (up and down of values) in the measurement data (figure 13). Bumps could occur due to chamber restrictions or measurement errors. Measurement errors could

develop through disturbance of the measurement by moving the chamber (air inflow) or through loose tube fittings (figure 13d).

There is no unique recipe for dealing with raw data. Some examples may help to explain basic decisions on “irregular” data.

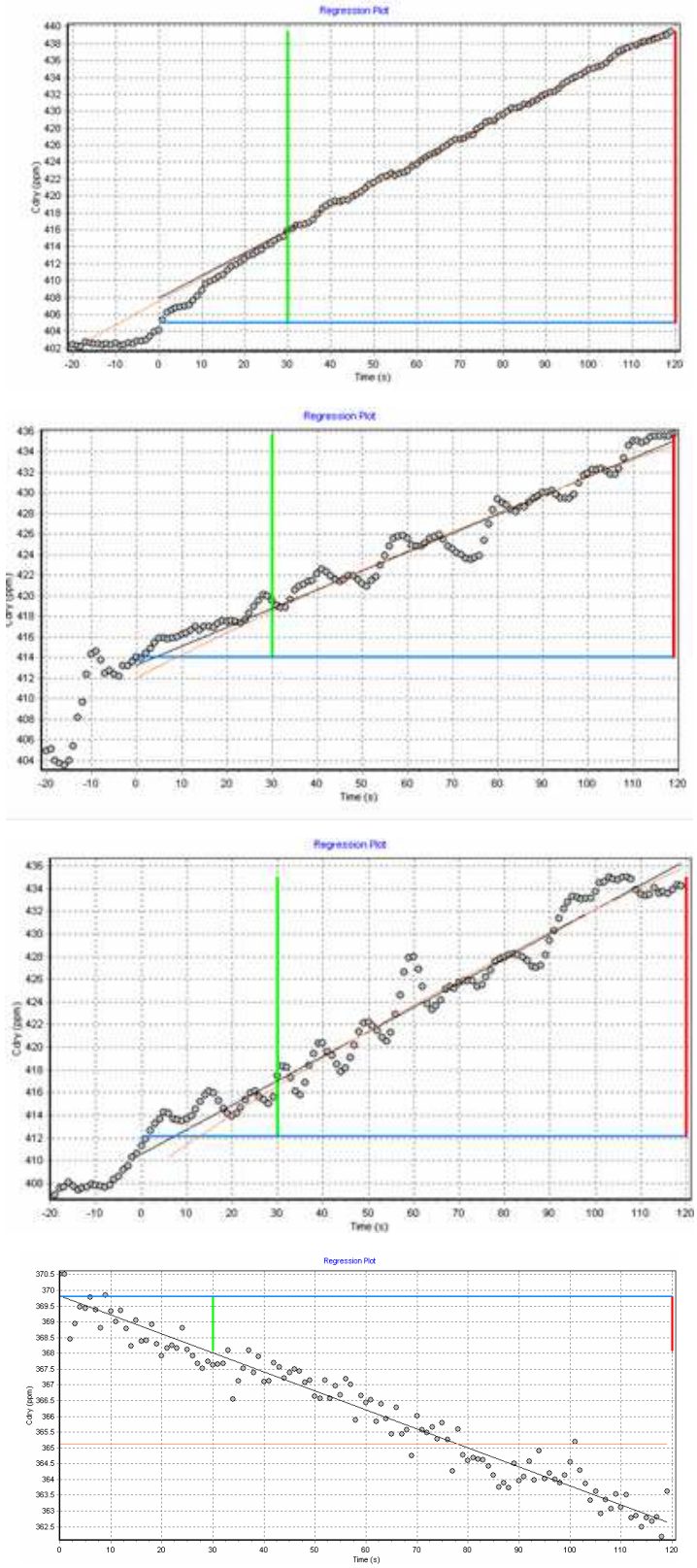

Figure 13: Examples for soil CO_2 measurement plots provided by LI-8100 viewer software. Figure 13 a shows a perfect measurement while 13 b & c show problems in the measurements but may still be interpretable. Figure 13 d shows a measurement which is not interpretable. More details are given in the text.

Figure 13b shows an irregular picture differing significantly from the ideal case (figure 13a), with several bumps. These bumps can be a “normal” phenomenon due to a not always consistently working chamber which does not necessarily have to refer to a measurement error. Nevertheless there could be a problem using the exponential fit, since data jumps up and down making it difficult to place an exponential curve. In this case a linear fit could be more appropriate. Figure 13c shows a different picture. The graph seems to consist solely of bumps – nevertheless an exponential fit is proposed, which turns out to be inappropriate. The unusual behaviour of the data with larger bumps and irregular features could hint at a measurement error. Anything looking like what can be seen in figures 13d should be discarded, since the totally erratic course points at a measurement error.

The measurement values used in this thesis were individually checked and, if applicable, corrected by one person only to minimize the error. An overview of data availability and missing data can be found in appendix (CD) and in appendix (figures A1-A2).

3.3 Measurement of environmental factors

Along with soil CO_2 efflux the parameters temperature and soil moisture were measured weekly and a soil survey analysis was conducted in 2009, including soil bulk density, root biomass, organic matter content and grain size distribution.

3.3.1 Soil temperature and soil moisture

Soil temperature was measured parallel to measurements at measurement depths of 35 cm (2006 and 2007), 11 cm (2008-2010) and 5 cm (May 2008-2010) with the LI-8100 temperature device (35 cm) and with a Testo 100 (Testo AG, Germany) temperature device (5 and 11 cm).

Soil moisture was measured with a TDR soil moisture probe (Trime-FM soil moisture probe, IMKO, Germany) over an interval of 15 cm (including soil litter). Continuous information on soil temperature and soil moisture were derived from the application of the soil water budget model SIMULAT (Diekkrüger 1996), see chapter 3.4.

3.3.2 Soil parameters

In June 2009 each measurement point was sampled for bulk density in 10 cm depth and bulk density of the litter layer using metal cylinders (Ø 8 cm), while detailed soil profiles for bulk density were generated for each soil type (in total 8 profiles) using soil core sampling (figure 14). Six soil profiles, representing six different soil types, were taken for determination of organic matter content and root biomass. The organic matter content in the soil, respectively litter, was determined using a Carbon/Nitrogen analyzer (Leco CNS-

2000). Soil bulk density was determined by retrieving undisturbed cores of known volume to subsequently oven-dry the samples at 105°C until constant weight was reached. Samples for determination of root biomass were rinsed and sieved to detach roots from soil mineral particles. Washed roots were then classified by diameter class and weighted after being oven-dried at 70°C for 48 h to determine root biomass. The grain size distribution was analysed after Köhn (DIN ISO 11277) and by using a Particle Analyzer (Analysette 22, Fritsch, Germany).

Soil information for model application was taken from a soil map (1:5,000; figure 2, chapter 1.3.2), produced by the Geologischer Dienst NRW and from literature (AG Bodenkunde 2005).

Figure 14: Metal cylinder used for bulk density analysis (left) and soil core (right) (own photo material)

3.4 The model SIMULAT

The model SIMULAT (Diekkrüger 1996) is a physically-based, one-dimensional model, which simulates water fluxes in the soil. An additional module to calculate soil temperature is available. The considered soil column used for calculation of fluxes can be divided into horizons, which again can be divided into user-defined numerical layers (figure 15). The state variables will then be calculated for the numerical layers. Input and output parameters of the model can be found in table 3.

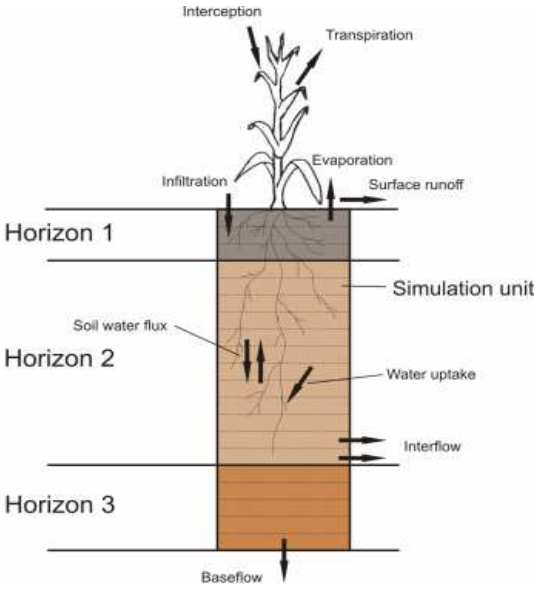

Figure 15: Illustration of hydrological processes and model components (Giertz et al. 2010)

Table 3: Input and output parameters of the soil water budget model SIMULAT (own illustration)

Input Parameters	**Output parameters**
Geographical latitude and longitude	Infiltration
Height of climate station	Transpiration
Mean soil temperature of lower boundary	Evaporation
Amplitude of soil temperature of lower boundary	Surface runoff
Day of year when temperature of lower boundary equals mean temperature	Interflow
Thickness of layers	Base flow
Parameters of the soil water retention curve: saturated water content, residual water content, parameters α and n (van Genuchten 1980)	Soil temperatures
Saturated soil hydraulic conductivity	Soil water content
Soil bulk density	
Clay content	
Heat capacity of the solid	
Quartz fraction of the solid	
Mineral fraction of the solid	
Minimum and maximum rooting depth	
Plant albedo	
Leaf area index	
Rainfall	
Relative humidity Wind velocity Air temperature Global radiation	**or** Potential evapotranspiration

3.4.1 Evapotranspiration

The potential evapotranspiration is calculated after Penman-Monteith (Monteith 1976):

$$\lambda \mathrm{ET}_{\mathrm{pot}} = \frac{\Delta(R_n - G) + c_\rho \frac{e_s - e_a}{r_a}}{\Delta + \gamma\left(1 + \frac{r_s}{r_a}\right)}$$

(1)

ET_{pot}	Potential evapotranspiration [kg m^{-2} s^{-1}]
Δ	Elevation of saturation vapour pressure curve [-]
λ	Latent enthalpy of vaporization [J kg^{-1}]
R_n	Radiation budget [W m^{-2}]
G	Soil heat flux [W m^{-2}]
c_p	Specific heat of air [1005 J $(kg\ K)^{-1}$]
e_s, e_a	Saturated vapour pressure or actual vapour pressure [hPa]
r_a	Aerodynamic resistance [s m^{-1}]
γ	Psychrometer constant [0.68 hPa K^{-1}]
r_s	Bulk-Stomata-Resistance [s m^{-1}]

For calculating the actual evapotranspiration the potential evapotranspiration is separated into potential evaporation and potential transpiration using the leaf area index (LAI). The actual evaporation (E_{pot}) is determined empirically after Ritchie (1972). For calculating the actual transpiration (T_{pot}) the approach by Feddes et al. (1978) is implemented in SIMULAT.

3.4.2 Interception

SIMULAT reduces the precipitation by the interception loss using an empirical approach. The maximum storage capacity of the plants is calculated empirically in relation to the leaf area index:

$$c_s = gLAI \qquad (2)$$

c_s	Maximum storage capacity of plants [mm]
g	Plant-dependent parameter [mm/LAI]

LAI Leaf area index [m²/m²]

The calculated intercepted amount of water evaporates with the potential evaporation rate.

3.4.3 Infiltration and Surface Runoff

Infiltration is calculated using the semi-analytical solution of the Richard's equation after Smith and Parlange (1978). For every precipitation event the Smith-Parlange-Infiltration equation is calculated. To consider spatial variability of the infiltration process a Latin Hypercube (LH) approach is implemented resulting in a number of infiltration simulations. The mean of executed simulations displays the net infiltration rate, transferred to the soil matrix.

The amount of water not infiltrating, is characterized as short-term surface storage, which infiltrates after the precipitation event. The resulting amount of water is defined as surface runoff.

3.4.4 Water transport into the soil matrix

The water flux in the soil matrix is calculated using the Richard's equation. Assuming vertical fluxes the Richard's equation reduces to:

$$C(\psi)\frac{\partial \psi}{\partial t} = \frac{\partial}{\partial z}(K(\theta)\frac{\partial}{\partial z}(\psi - z)) \pm Q \qquad (3)$$

$C(\psi)$	Specific water capacity [cm ^{3} cm^{-3} hPa^{-1}]
ψ	Matric potential [hPa]
Q	Sources and sinks [cm ^{3} cm^{-3} d^{-1}]
$K(\theta)$	Hydraulic water conductivity [cm d^{-1}]
z	Depth below ground level [cm]

This equation is solved iteratively and implicitly using a Quasi-Newton-method (Hornung & Messing 1984), which makes it possible to simulate both saturated and unsaturated conditions.

The water retention curve (relationship between θ and ψ) is described mathematically using either an approach by van Genuchten (1980) or a version of Brooks and Corey (1964) modified by Smith (1992):

$$\theta = \begin{cases} \dfrac{1}{\left(1+\left(\dfrac{\psi}{\psi_b}\right)^c\right)^{\frac{c}{\lambda}}} & for\,\psi \le 0 \\ 1 & for\,\psi > 0 \end{cases} \qquad (4)$$

θ	Relative saturation [-]
ψ_b	Point of air entry pressure [hPa]
c	Constant [-]
λ	Pore size index [-]

$$\theta = \frac{\theta_{vol} - \theta_{res}}{\theta_{sat} - \theta_{res}} \qquad (5)$$

θ	Relative saturation [-]
θ_{vol}	Volumetric water content [%]
θ_{res}	Residual water content [%]
θ_{sat}	Saturated water content [%]

The actual water conductivity in unsaturated soil is determined by "relative x saturated" water conductivity curves, calculated by Van Genuchten's approach (1980) or Brooks and Corey's (1964).

SIMULAT provides the following options for lower boundary conditions:

- Temporally variable water tension and respectively groundwater levels (Dirichlet boundary condition)
- Temporally variable water flux (Neumann boundary condition)
- Gradient of water tension is known (e.g. free drainage)
- Lysimeter boundary condition

3.4.5 Soil temperature

Parameters used in the following equations are:

q_h heat flux [W m^{-2}]
λ thermal conductivity [W m^{-1} K^{-1}]
T temperature [K]
z depth [m]
c_w specific heat capacity of water [J g^{-1} K^{-1}]
q_w water flux [m s^{-1}]
c_h volumetric heat capacity [J m^{-3} K^{-1}]

Soil heat flow driven by conduction and convection can be described by

$$q_h = -\lambda \frac{\partial T}{\partial z} - c_w T q_w \tag{6}$$

Combining conservation of heat with one-dimensional heat flow leads to

$$c_h \frac{\partial T}{\partial t} = \frac{\partial}{\partial z}\left(\lambda \frac{\partial T}{\partial z} \right) - c_w q_w T \tag{7}$$

This equation is valid if frost and thaw of ice is neglected.

Temperature boundary conditions

The soil surface temperature depends on the air temperature and the radiative and latent heat transfer. With regard to the upper boundary the surface temperature equals the air temperature when the radiative and latent heat transfer can be neglected, as given in forest ecosystems. In cases where the heat transfer can not be neglected, the radiative heat transfer can be calculated considering global radiation, long wave sky irradiance, surface albedo and air temperature. The latent heat flux can be computed by evaporation models like the Penman-Monteith equation (Monteith 1976).

At the lower boundary the annual fluctuation of temperature with time can be described by a sinusoidal cycle

$$T(t) = T_{mean} + T_{ampl} \sin\left(\frac{2\pi(t - t_0)}{365.25} \right) \tag{8}$$

T_{mean} mean annual temperature [°C]

T_{ampl} maximum amplitude at the lower boundary [°C]

t_0 time at which $T = T_{mean}$ [d]

3.4.6 Data input for SIMULAT

Precipitation data for 2007 was taken from reanalysis data (COSMO-CLM model, Rockel et al. 2008) provided by the Meteorological Institute, Bonn, Germany, because further data was not available at the time of model application. For 2008 and 2009 precipitation data from the DWD weather station Monschau-Kalterherberg was used, gaps were filled with interpolation methods. Air temperature data was used from the climate station located in the Wüstebach catchment. Soil profile information was taken from own soil surveys and from the soil map (1:5,000). The potential evapotranspiration was calculated after Penman-Monteith (Monteith 1965).

3.5 The model PATCIS

PATCIS (**P**roduction **A**nd **T**ransport of **C**O_2 **I**n the **S**oil) is a one-dimensional, process-based model developed by Fang and Moncrieff (1999) which simulates production and transport of CO_2 in soil. It can predict CO_2 efflux from the surface and respiration rates within the soil. CO_2 efflux from the soil is considered to be the result of two major processes: the production of CO_2 and gas transport through the soil which controls the movement of CO_2 from the soil to the atmosphere and of oxygen in the opposite direction. Gaseous diffusion (F_{dg}) and liquid phase dispersion (F_{ag}) are the major mechanisms governing the transport of CO_2 (figure 16).

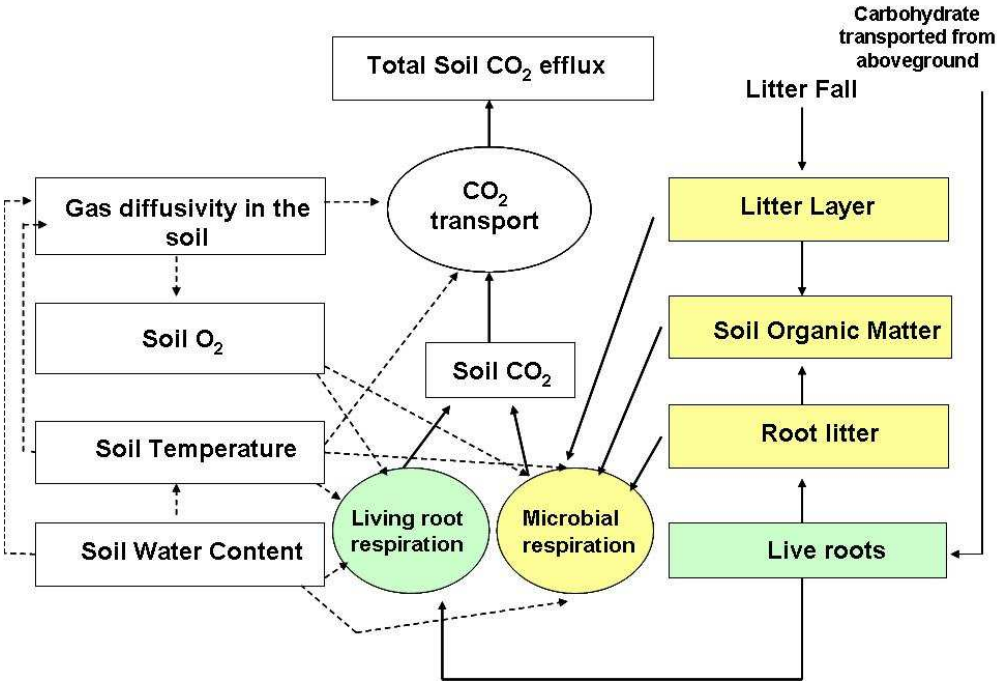

Figure 16: The concept of the soil respiration model PATCIS, changed after Fang & Moncrieff (1999)

Production of CO_2 in the soil is seen as the result of living root respiration and decomposition of soil organic matter by microbes. Live and dead biomass, soil temperature, moisture content and oxygen concentration in soil are considered as direct influencing factors on soil CO_2 production and transport. Different layers are defined which refer to given soil layers with individual soil characteristics (figure 17). A detailed description of model discretization for individual points can be found on the CD (file "point characteristics").

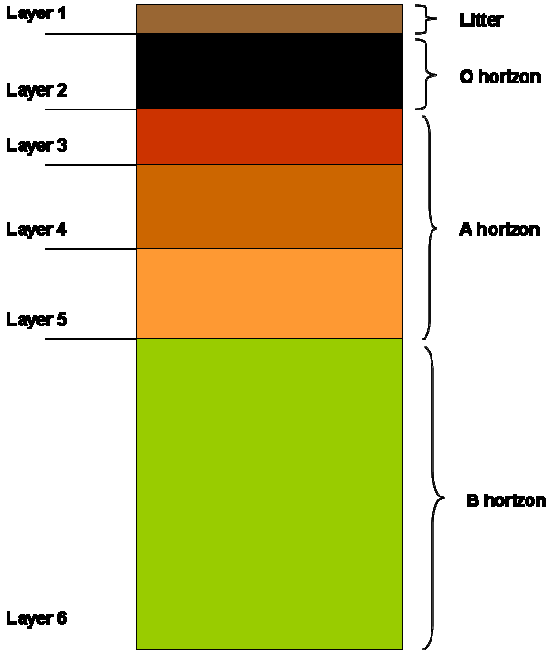

Figure 17: Layer structure for PATCIS (source: own illustration)

One-dimensional CO_2 transport in both the gas phase (g) and liquid (w) phase in the soil can be expressed using a mass balance equation (Suarez and Šimunek 1993), with the assumption of horizontal homogeneity:

$$\frac{\partial C_T}{\partial t} = -\frac{\partial}{\partial z}\left(F_{dg} + F_{ag} + F_{dw} + F_{aw}\right) \pm S \qquad (9)$$

F_{dg}	CO_2 flux caused by gas diffusion
F_{ag}	CO_2 flux resulting from gas convection
F_{dw}	Flux resulting from dispersion
F_{aw}	Flux resulting from vertical liquid transport
S	sources and sinks of CO_2

where C_T is the total concentration of CO_2 in both the gas and liquid phases, defined by eq.(10):

$$C_T = C_g V_g + C_w V_W \qquad (10)$$

C_g, C_w	CO_2 concentrations [mg CO_2 m^{-3}] in the gas and liquid phase
V_g, V_W	Volumetric fractions of air and water in the soil

Changes in soil water volume are always matched by changes in gas volume in the opposite direction:

$$V_g + V_W = \phi_T$$

(11)

Heterotrophic microbial respiration is a process of decomposition of soil organic matter by microbes. The decomposition rate for constant environmental conditions is

$$\frac{\partial M}{\partial t} = -kM \tag{12}$$

k	decomposition rate coefficient
M	amount of effective decomposing substance

However, soil organic matter is a mixture of different substances with different decomposition rates under the same environmental conditions. Hunt (1977) divides soil organic matter into labile and resistant fractions.

$$\frac{\partial M}{\partial t} = -k_{lab}\lambda M - k_{ris}(1-\lambda)M = -k_{lab}M' \tag{13}$$

λ	ratio of labile to total amount of organic matter
k_{lab} , k_{ris}	decomposition rates for labile and resistant organic matter

where $M' = \lambda M + k_{ris}(1-\lambda))M / k_{lab}$ can be considered as the equivalent amount of labile organic matter, to which microbial respiration is directly related.

Under the assumption that all carbon in decomposing soil organic matter is finally transformed into CO_2, the microbial respiration rate can be described as:

$$R_m = \alpha \frac{dM}{dt} = \gamma_m M' \tag{14}$$

α	coefficient representing the amount of CO_2 arising from the decomposition per unit of dry organic matter

The production of CO_2 from root respiration is related to the specific rate of root respiration and the root biomass. The total root respiration can be given as

$$R_r = \sum \gamma_{ri} B_i \tag{15}$$

γ_{ri} respiration rate parameter of root size class i

B_i root biomass of size class i

If the respiration rate of the finest root be γ_r, the equivalent root biomass B' is given by

$$B' = \sum \frac{\gamma_{ri}}{\gamma_r} B_i \tag{16}$$

and equation (15) becomes

$$R_r = \gamma_r B' \tag{17}$$

Under the assumption that the effects of environmental factors on soil respiration are multipliable, and that the influences of these factors are similar for both root and microbial respiration, we have

$$\gamma_r = \gamma_{r0} f(T) f(W) f(O_2) \tag{18}$$

$$\gamma_m = \gamma_{m0} f(T) f(W) f(O_2) \tag{19}$$

γ_{r0}, γ_{m0} maximum respiration rates of roots and microorganisms under optimal conditions at a given temperature T_0

$f(T), f(W), f(O_2)$ scaling factors for the dependence of soil respiration on temperature, water content and O_2 concentration

The response of soil respiration to soil temperature is described using an Arrhenius type equation:

$$f(T) = \exp\left(\frac{-E}{RT}\right)$$

(20)

E	activation energy for respiration [kJ mol^{-1}]
R	universal gas constant [J/(mol K)]
T	absolute temperature [K]

After Lloyd and Tayler (1994) E is assumed to be a variable parameter in PATCIS, having a larger value at low temperature than at high temperature. Assuming that f(T) = 1 at temperature T_{10} = 283.15 K, then the temperature dependence of soil respiration can be expressed as

$$f(T) = \exp\left(\frac{E}{RT}\frac{(T - T_{10})}{T_{10}}\right) \quad (21)$$

The dependence of soil respiration on soil moisture content is not yet clear. Different types of equations have been reported (Van Cleve & Sprague 1971, Orchard & Cook 1983, Oberbauer et al. 1992). Generally, low or high moisture contents impose a restriction on soil respiration. Under dry conditions the diffusion of liquid substances decreases due to the decline of soil water films. The diffusion of extra cellular enzymes which are produced by microbes for decomposition of organic matter and the diffusion of soluble C-substrates which can be bound by bacterial cells can only take place in liquid phase (Davidson et al. 2006). Higher soil moisture conditions on the other hand implicate a decrease in air-filled pores and therefore a decrease in oxygen which is required for microbial respiration (Fang & Moncrieff 1999). The respiratory potential of the soil cannot be fully realised when the soil is dry. An increase of water will lead to an increase of soil respiration, when other conditions are constant. The increasing rate of soil respiration will slow down with an ongoing increase in soil moisture. If the increase in soil respiration is linearly related to the unrealised respiratory potential, the direct effect of soil moisture content on soil respiration can be expressed as

$$\frac{\partial f(W)}{\partial W} = a\left[f(W)_{\max} - f(W)\right] \quad (22)$$

W	soil moisture content

a	parameter, defining the maximal increase in the rate of soil respiration with soil moisture
$f(W)_{max}$	maximum value of f(W) when soil moisture content does not limit respiration

Integrating equation (22) gives

$$f(W) = 1 - \exp(-aW + c) \tag{23}$$

where c is an integration constant.

Respiration rates of plant tissues have been observed to increase linearly with increasing ambient O_2 concentration when O_2 concentration is low. The increase in respiration rate will slow down, to a maximum, with further increase in O_2 concentration (Forward 1965). Applying this relationship to microbial respiration, the dependence of soil respiration rate on ambient oxygen concentration can be described by the Michaelis-Menten equation (Glinski & Stepniewski 1985):

$$V = \frac{V_{max}[O_2]}{[O_2] + K_M} \tag{24}$$

V	reaction rate
V_{max}	maximal reaction rate
K_M	Michaelis-Menten constant

O_2 uptake in the different layers is assumed to be responsible for the interaction of soil respiration between different soil layers. An increase in respiration in the upper layer goes along with less respiration in the lower layers due to the consumption of O_2. On the other hand, if soil respiration in a lower layer is accelerated, a steeper O_2 gradient through the soil profile will occur in order to supply sufficient O_2 to the soil layer. This leads to a lower O_2 concentration and therefore a decrease in soil respiration in the upper soil layers. Progressive iteration is used to simulate the interdependence of soil respiration rates between layers. The upper boundary condition is an initial oxygen concentration of 21% for the uppermost layer, while the lower boundary condition shows an initial oxygen concentration of 21%.

CO_2 profile in the soil and CO_2 efflux from the soil surface are simulated with respiration rates, soil diffusivity and the variations in soil CO_2 pool. Further details are given in Fang & Moncrieff (1999).

3.5.1 Data input for PATCIS

Climate data, soil temperature and soil moisture were used from the model SIMULAT (chapter 3.4). Soil profile information was taken from own soil surveys and from the soil map (1:5,000). Only few points were sampled for root biomass and soil organic matter content. Those values were extrapolated to other points, according to soil type and distance from trees.

3.5.2 Parameterization of the PATCIS model using SIMLAB 2.2

An automatic procedure for calibrating PATCIS is not available. To be able to perform automatic sensitivity analysis and to use the same methodology for determining optimal model parameters, PATCIS was linked to a procedure to automatically compute numerous data sets. SIMLAB 2.2 was applied to produce a specified number (here 150) of parameter combinations as model input for PATCIS using the Latin Hypercube method. These parameter combinations were used for the simulation of soil CO_2 efflux with PATCIS and the results compared with measured soil CO_2 efflux. The model output included the quality criterion of the simulations with the different parameter combinations, in particular the coefficient of determination of the regression (measured vs. simulated), the axis interception of the regression line and the slope of the regression line.

SIMLAB 2.2 (Simlab 2011) is a sensitivity analysis tool based on the Monte Carlo or Latin Hypercube method. Multiple model evaluations with probalistically selected model input can be performed. For that, range and distribution of each input variable are defined by the user and used to generate sets of parameters. The model is then fed with those parameter sets resulting in sets of model outputs which are used as the basis for model calibration and an uncertainty analysis. Statistical output, such as mean value, variance, coefficient of determination etc. is provided. These model evaluation results can be used as the basis for sensitivity analysis in a further step.

Latin Hypercube

The method of Latin Hypercube is a method of stratified sampling, which aims at achieving a better coverage of the sample space of input factors. Let the sample space S of the input vector X be partitioned into L disjoint strata $S_1 \ldots S_L$. Represent the size of

each S_i as $p_i = P(x \in S_i)$ and obtain a random sample x_h, $h = 1,...,n_i$ from S_i, where $\sum_{i=1}^{l} n_i = N$. In particular, when N = 1, the result is a random sample over the entire sample space. In the latin hypercube the range of each input factor, X_j, j = 1,2, …k, is divided into N intervals of equal marginal probability, 1/N, and one observation of each input factor is made in each interval using random sampling within that interval. Thus there are N non-overlapping realisations for each of the k input factors. One of the realisations on X_1 is randomly selected (each observation is equally likely to be selected) matched with a randomly selected realisation of X_2, and so on until X_k. These collectively constitute a first sample, x_1. One of the remaining realisations on X_1 is then matched at random with one of the remaining observations on X_2, and so on, to get x_2. A similar procedure is followed for x_3, …, x_N.

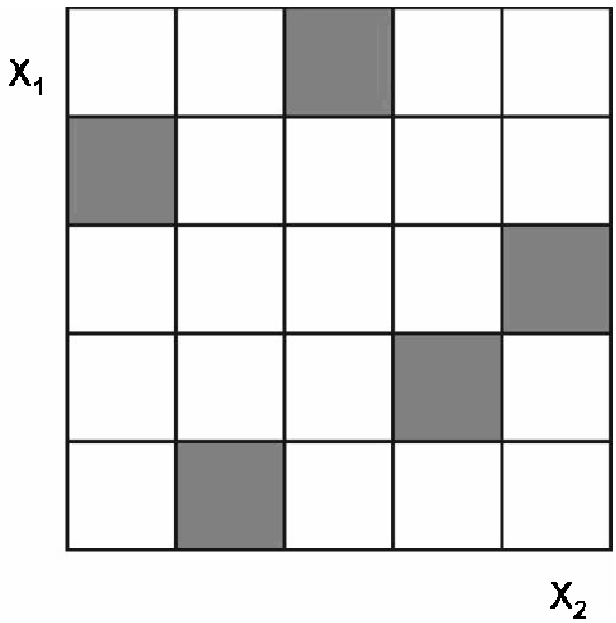

Figure 18: Latin square with parameters X_1 and X_2 and the resulting five samples in grey used for modelling (changed after Richter et al. (1996))

3.6 Fine root biomass

Ammer and Wagner (2005) developed a model to predict fine-root biomass distribution of Norway spruce trees. The model calculates the relative fine-root biomass for any point in a system of coordinates, taking into account the distance of single trees to that point and their dimensions. The model is based on the following assumptions:

- the maximum distance from the tree trunk, where roots can be found, depends on the dimension of the tree and exceeds the edges of the crown by a significant distance (Wiedemann 1927, Stone & Kalisz 1991, Parsons et al. 1994, Müller & Wagner 2003)

- fine-root biomass decreases with increasing distance from the tree trunk (Friedrich 2002, Drexhage 1994)
- fine-root biomass increases with diameter at breast height (dbh, 1.3 m) of the tree (Drexhage, 1994)
- the maximum fine-root biomass can be found at some distance from the stem (Hilf 1927, Taskinen et al. 2003)

These assumptions were transformed into two models. Model A defines a proportional decrease of fine-root with decreasing dbh, whereas model B assumes a stronger decrease.

1. Model A: $RD_3 = dbh/6$ assuming a maximum rootspread distance of 10 m for a tree of 60 cm in dbh (Ammer 2000)

   Model B: $RD_3 = dbh/6 + z$ with $z = -(dbh - 60)/10$ if dbh<60 (otherwise as in model A; applying the term z for thicker trees would lead to unreasonable distances of maximum root spread), where RD_3 is the maximum root spread distance in meters, and dbh is the diameter at breast height in centimetres.
2. Model A and B: $RD_2 = (2/3)RD_3$, $RD_1 = (1/3)RD_3$ and $RD_0 = 0$.
3. Model A: $rFRB_0 = dbh/100$

   Model B: $rFRB_0 = (dbh)/(100 + g)$ with g = -(dbh-60).
4. Model A and B: $rFRB_1 = (5/3)rFRB_0$, $rFRB_2 = (5/6)rFRB_0$ and $rFRB_3 = 0$, where

   $rFRB_1$, $rFRB_2$ and $rFRB_3$ are the relative fine-root biomasses at distance RD_1, RD_2 and RD_3, respectively.

Based on the distances RD_0 to RD_3 in both models a polynomial of third degree for the dbh of each tree is calculated using the Gregory-Newton procedures (Stöcker 1995). This allows the calculation of the rFRB of each tree of a stand at any point x,y.

1. If D ≥ RD3, then rFRB = 0, where D is the distance between the tree's trunk and x,y.
2. If D < RD3, then rFRB of a tree at point x,y is calculated as follows:

$$h = RD_2 - RD_1 \quad (25)$$

$$b_0 = rFRB_0 \quad (26)$$

$$b_1 = \frac{rFRB_1 - rFRB_0}{1!h}$$

(27)

$$b_2 = \frac{\left(\left(rFRB_2 - rFRB_1\right) - \left(rFRB_1 - rFRB_0\right)\right)}{2!h^2} \quad (28)$$

$$b_3 = \frac{\left(\frac{\left(\left(rFRB_3 - rFRB_2\right) - \left(rFRB_2 - rFRB_1\right)\right)}{-\left(\left(rFRB_2 - rFRB_1\right) - \left(rFRB_1 - rFRB_0\right)\right)}\right)}{3!h^3} \quad (29)$$

$$rFRB_{xy} = b_0 + b_1(D - RD_0) + b_2(D - RD_0)(D - RD_1) + b_3(D - RD_0)(D - RD_1)(D - RD_2) \quad (30)$$

An additive total rFRB (TrFRB) at point x,y was calculated as:

$$TrFRB = \sum_{i=1}^{n} rFRB_i \quad (31)$$

where i is the tree number of the stand. It is assumed that the total amount of fine roots at a given point results from additive contribution of the trees. Figure 19 illustrates the relative fine root biomass of a tree in relation to the distance from the stem trunk and the diameter at breast height (dbh).

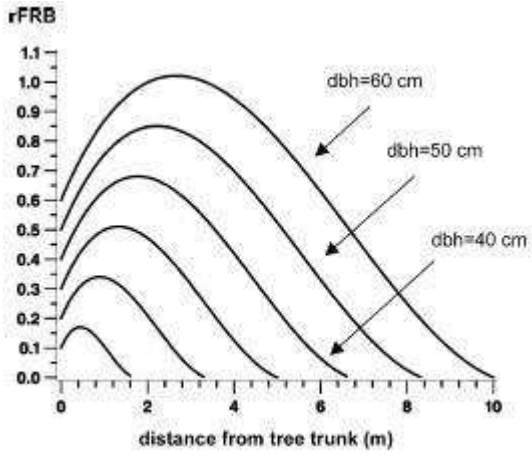

Figure 19: Relative fine root biomass of a tree in relation to the distance from the stem trunk and the diameter at breast height (dbh). (source: Ammer & Wagner 2005)

3.7 Geostatistical Analysis

Geostatistical methods are based on the theory of regionalized variables which consists of a structural and a random component and are used to characterize spatial or temporal autocorrelation.

Values of the observation variable for sampled locations $x_1,\ldots,x_n$ are defined as $z(x_1),\ldots,z(x_n)$. These are referred to as realisations of the random variables $Z(x_1),\ldots,Z(x_n)$. Unsampled locations are likewise related to random variables. To characterize spatial autocorrelation, the mean and the variance of the random variable are analysed. If weak stationarity can be assumed mean and variance of the increments Z(x+h)-Z(x) exists and are independent on x:

$$E[z(x+h)-Z(x)]=0$$

(32)

$$Var[Z(x+h)-z(x)]=2\gamma(h) \qquad (33)$$

in which h is the distance between measurements points. γ(h) is called semi-variogram and is computed as

$$\gamma(h)=\frac{1}{2n(h)}\sum_{i=1}^{n(h)}\left[Z(x_i)-Z(x_j)\right]^2 \qquad (34)$$

in which *n* is the number of measurements within a certain range of disctances like e.g. 50-100m. To be used for interpolation, this experimental variogram is fitted to a theoretical variogram. In this study the commonly used spherical model was chosen as a theoretical variogram. It has a simple polynomial expression and shows an almost linear growth up to a certain distance then stabilization (Armstrong 1998).

$$\gamma_s(h)=\begin{cases} c_0+c_1\left[1.5\frac{h}{a_1}-0.5\left(\frac{h}{a_1}\right)^3\right] & \text{for } h \le a_1 \\ c_0+c_1 & \text{for } h > a_1 \end{cases} \qquad (35)$$

To characterize the variogram three properties are required: The nugget variance **(c_0)** describes the small scale variability based on variability below the smallest measurement distance or errors in measurements. It is the intersection with the axis of the ordinate. As variance is limited in space, the sill **(c_1)** describes the largest variance which is reached at a certain distance. The total variance is the sum of c_0+c_1. The range *a* describes the maximum distance *h* in which the realisations Z(x) and Z(x+h) are not independent.

An example for a spherical model is shown in figure 20.

The program VESPER (Whelan et al. 2001) was used to create local variograms for soil CO_2 efflux, soil temperature and soil moisture.

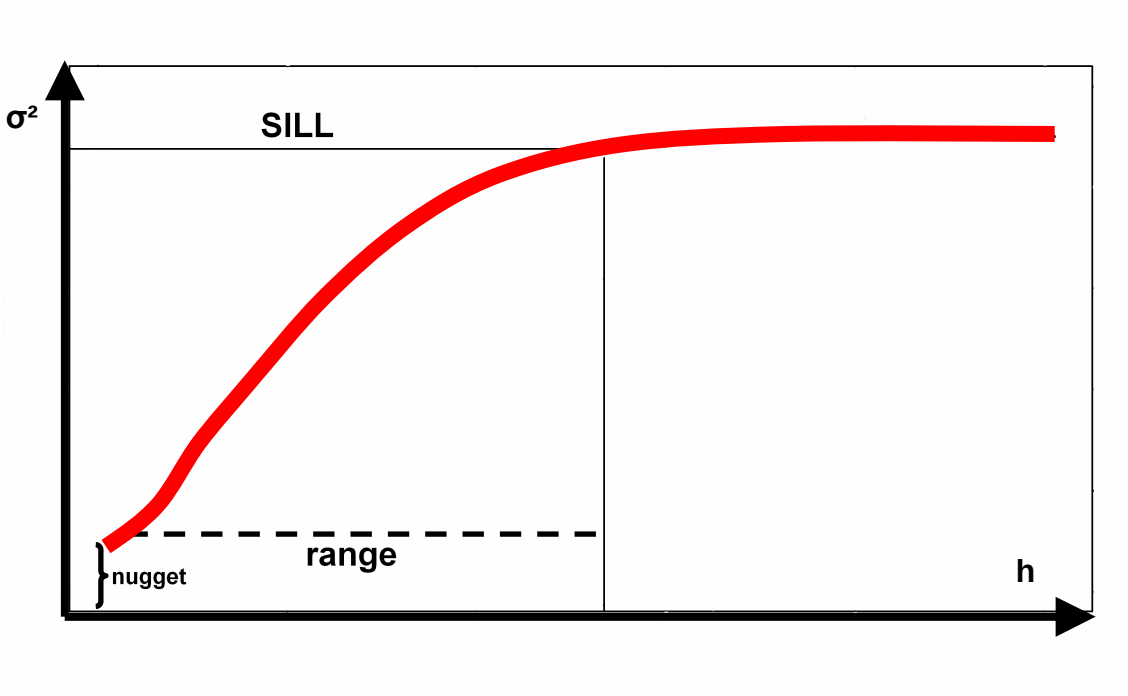

Figure 20: Typical variogram which reaches a sill at the range with a nugget effect. (source: own illustration)

3.8 Statistics of Temporal Persistence

When a location is repeatedly surveyed for an environmental parameter such as soil water content, sites often behave similar in time and show soil characteristics (such as wetness or drought) constantly higher or lower compared to the field average. Vachaud et al. (1985) characterized this phenomenon as temporal persistence or temporal stability.

Two methods, first suggested by Vachaud et al. (1985), were used to analyze temporal stability of the data. The first method includes the two-dimensional, linear Pearson coefficient of correlation, which is calculated by:

$$r = \frac{\sum_{i=1}^{n}(x_i - \bar{x})(y_i - \bar{y})}{\sqrt{\sum_{i=1}^{n}(x_i - \bar{x})^2 \sum_{i=1}^{n}(y_i - \bar{y})^2}} \qquad (36)$$

where $x_i - \bar{x}$ is the covariance of the measurement date and $y_i - \bar{y}$ is the covariance of the consecutive measurement dates. The index *i* represents the measurement points. We

used the Pearson correlation coefficient between two consecutive measurement dates to quantify temporal stability. The closer *r* is to 1, the more stable the process will be.

To characterize soil CO_2 efflux on a larger scale, it is useful either to calculate field averages or to use representative test sites. A representative test site can be defined as that site which always shows a mean behaviour at each measurement date. This can be determined using the mean relative differences method (MRD), first applied by Vachaud et al. (1985) for soil water content and by Herbst et al. (2009) for CO_2-efflux. For that, the ranked mean relative difference is computed which calculates the mean of the relative difference of the parameter at the n locations and each time of measurement. The relative difference for each measurement date *j* is calculated according as:

$$\xi_{i,j} = \frac{x_{i,j} - \bar{x}_j}{\bar{x}_j} \tag{37}$$

where *i* is the sampling point and *j* is the date. Next the mean relative difference for each sampling point *i* is calculated:

$$MRD_i = \frac{1}{m}\sum_{j=1}^{m} \xi_{i,j} \tag{38}$$

where *m* is the number of measurement dates. That site with a MRD close to zero shows a mean behaviour over time. To characterize variability, the standard deviation of the relative differences at each sampling point is also calculated. Because a large part of the data did not show a log normal distribution; therefore the data was logarithmically transformed prior to statistical analysis.

3.9 Relationship of soil CO_2 efflux and soil parameters

Nonlinear regression was used to test the relationship between soil CO_2 efflux, soil moisture and soil temperature (eq. 39). The Q_{10} value, which characterizes the increase of soil CO_2 efflux with an increase of 10°C in temperature, is described by eq. 40 after van't Hoff (Buchmann 2000, Davidson et al. 2006).

$$y = \beta_0 * e^{(\beta_1 * T)} \quad \text{or} \quad y = \beta_0 * e^{(\beta_1 * W)} \tag{39}$$

$$Q_{10} = e^{10*\beta_1} \tag{40}$$

where

T soil temperature (°C)

W	soil moisture [Vol%].
β_0, β_1	fitted parameters

The Q_{10} value can alternatively be calculated using a modified van't Hoff approach (Davidson et al. 2006, Fang & Moncrieff 2001):

$$Q_{10} = \frac{resp_{T2}}{resp_{T1}}^{\frac{10}{(T2-T1)}} \quad (41)$$

where

$resp_{T1}$	Respiration rate observed at temperature T1
$resp_{T2}$	Respiration rate observed at temperature T2
T1	Temperature T1
T2	Temperature T2

A bimodal or polynomial regression was proposed by Xu and Qi (2001) to describe the relationship between soil respiration and soil moisture:

$$y = \beta_0 W^2 + \beta_1 W + \beta_2 \quad (42)$$

where

W	soil moisture [Vol%]
β_0, β_1, β_2	fitted parameters

4 Analyzing soil CO_2 efflux and other environmental parameters

4.1 Temporal variability in soil CO_2 efflux measurements

Soil CO_2 efflux ranged from 0.13 g/m²/d to 58.8 g/m²/d during all measurement years, 2006-2010. Mc Dowell et al. (2000) investigated soil CO_2 efflux over snow and reported soil CO_2 efflux values as low as 0.42 g/m²/d. In most publications maximum soil CO_2 efflux did not exceed 35 g/m²/d (Hanson et al. 1993, Crill 1991, Certini et al. 2003). An overview of measured soil CO_2 efflux rates can be found in table 4.

Table 4: Minimum and maximum measured soil CO_2 efflux for all measurement points for the years 2006-2010 in g/m²d (own data)

Year	Transects WA and WB		Grid M	
	CO_2 efflux (min)	CO_2 efflux (max)	CO_2 efflux (min)	CO_2 efflux (max)
2006	2.1	32.9	--	--
2007	1.9	35.7	--	--
2008	1.3	41.2	0.1	27.9
2009	1.1	42.2	0.3	58.8
2010	0.5	38.6	0.3	54.7

A higher range of values is noticeable for the measurement grid M compared to the transects WA and WB. The year 2008 features rather low maximum values of soil CO_2 efflux for grid M compared to the transects WA and WB. This can be attributed to the fact that measurements for grid M started in August, while transects WA and WB were sampled from April on. The highest values for WA and WB in 2008 were detected for the month June.

4.1.1 Seasonal patterns of soil CO_2 efflux

The seasonal trend of soil CO_2 efflux in transects WA and WB was similar for all measurement years (figure 21). Soil CO_2 efflux increased during spring and summer, and reached mean maximum values of 22.3 g CO_2 m^{-2} d^{-1} in July 2008. During fall (October), soil CO_2 efflux rates declined again, reaching values close to those in spring (April).

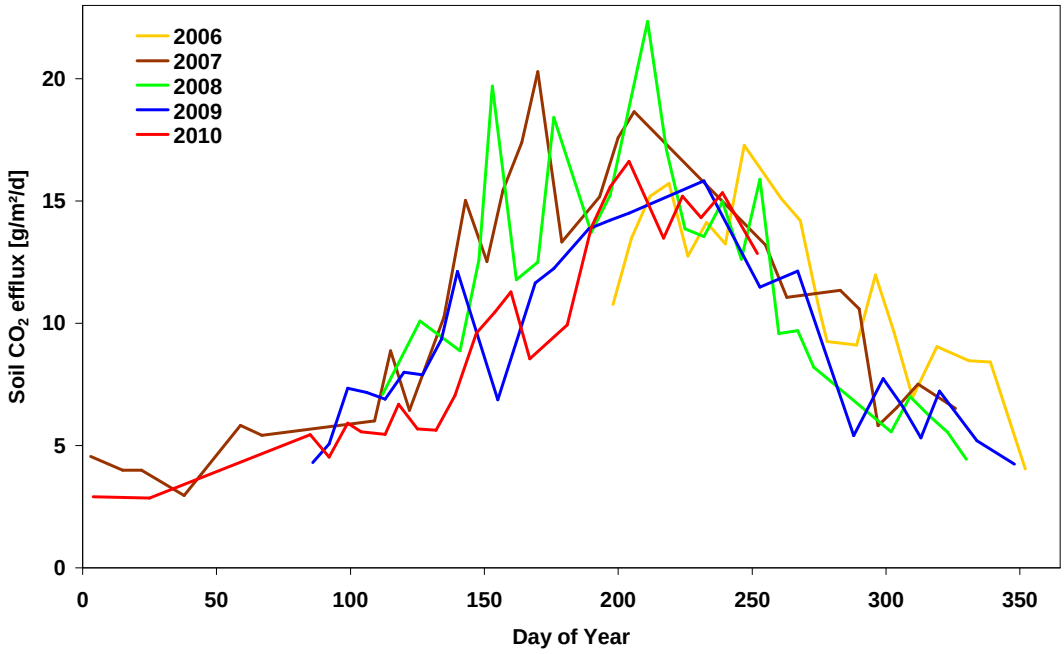

Figure 21: Seasonal trend of soil CO_2 efflux measurements for transects WA and WB for the years 2006 – 2010 (source: illustration of own data)

The seasonal trend of soil CO_2 efflux for the measurement grid M was comparable to transects WA and WB (figure 22). Soil CO_2 efflux increased during spring and summer, and reached mean maximum values of 15.8 g m^{-2} d^{-1} in July 2009. During fall (October), soil CO_2 efflux rates declined again, reaching values close to those in spring (April).

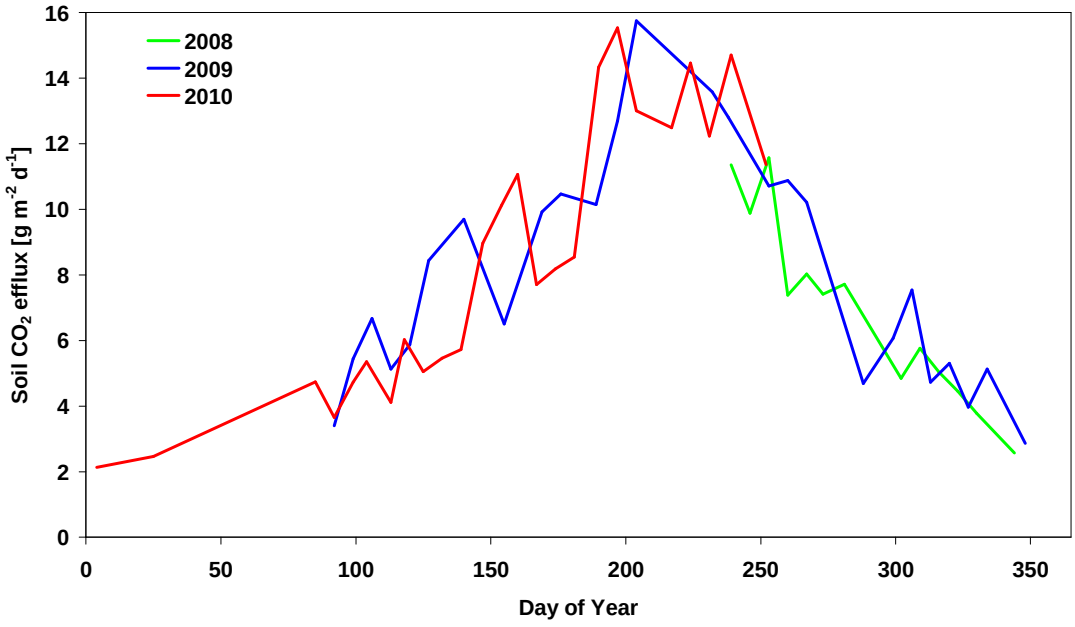

Figure 22: Seasonal trend of soil CO_2 efflux measurements for grid M for the years 2008 – 2010 (source: illustration of own data)

For a better overview figures 23a-c illustrate mean soil CO_2 efflux rates for all measurement grids for 2008-2010. It is clearly visible, that mean values for all measurement grids were similar for the considered years.

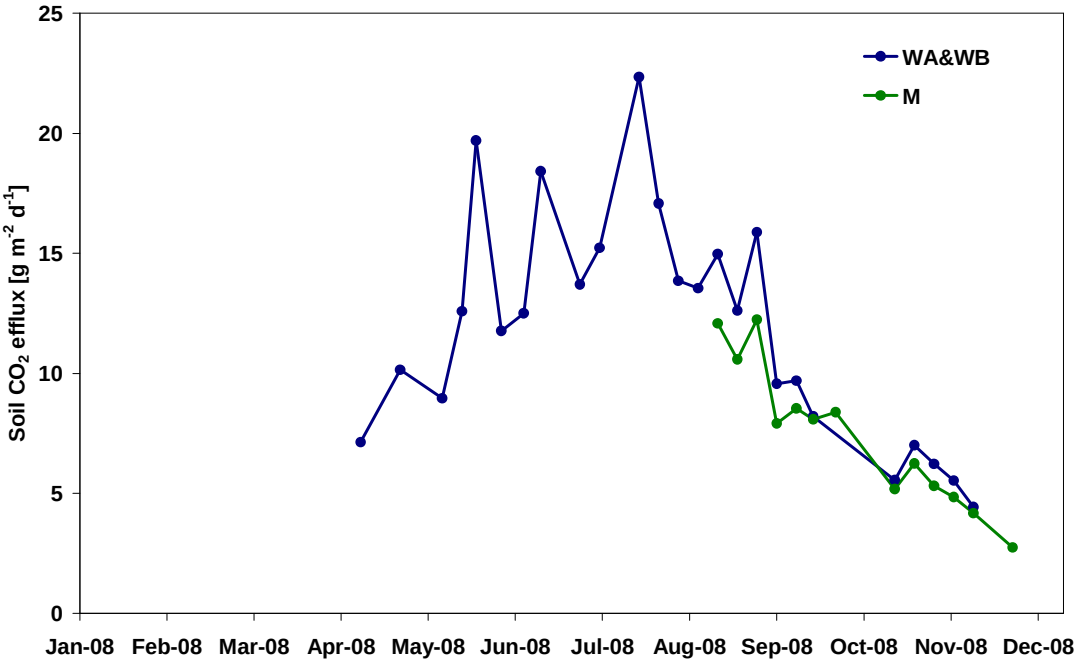

Figure 23a: Seasonal trend of soil CO_2 efflux measurements for transects WA/WB and grid M for the years 2008 (source: illustration of own data)

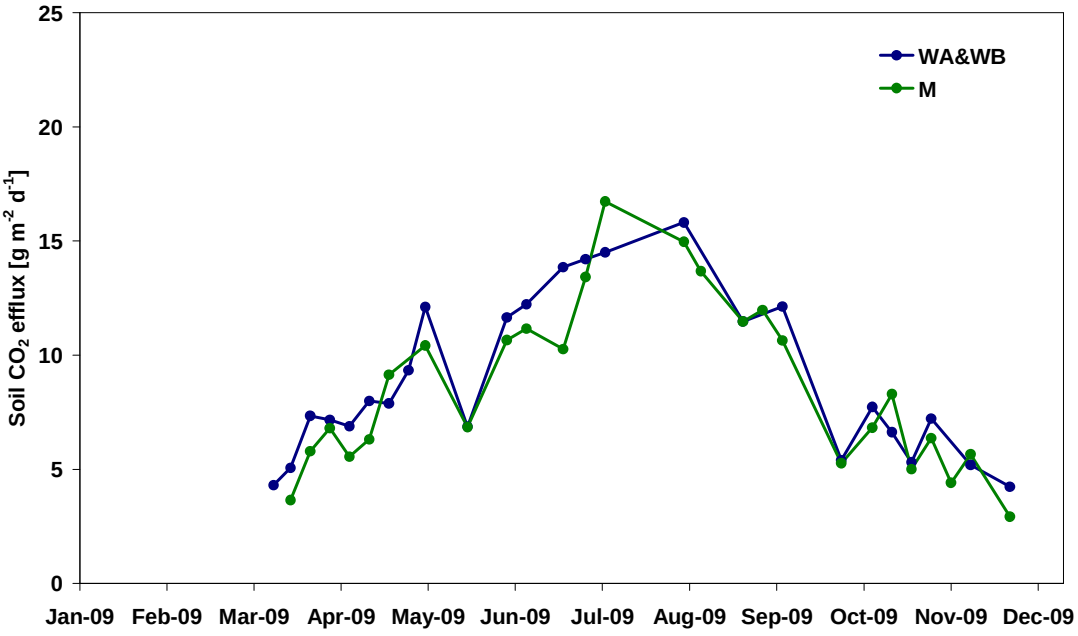

Figure 23b: Seasonal trend of soil CO_2 efflux measurements for transects WA/WB and grid M for the years 2009 (source: illustration of own data)

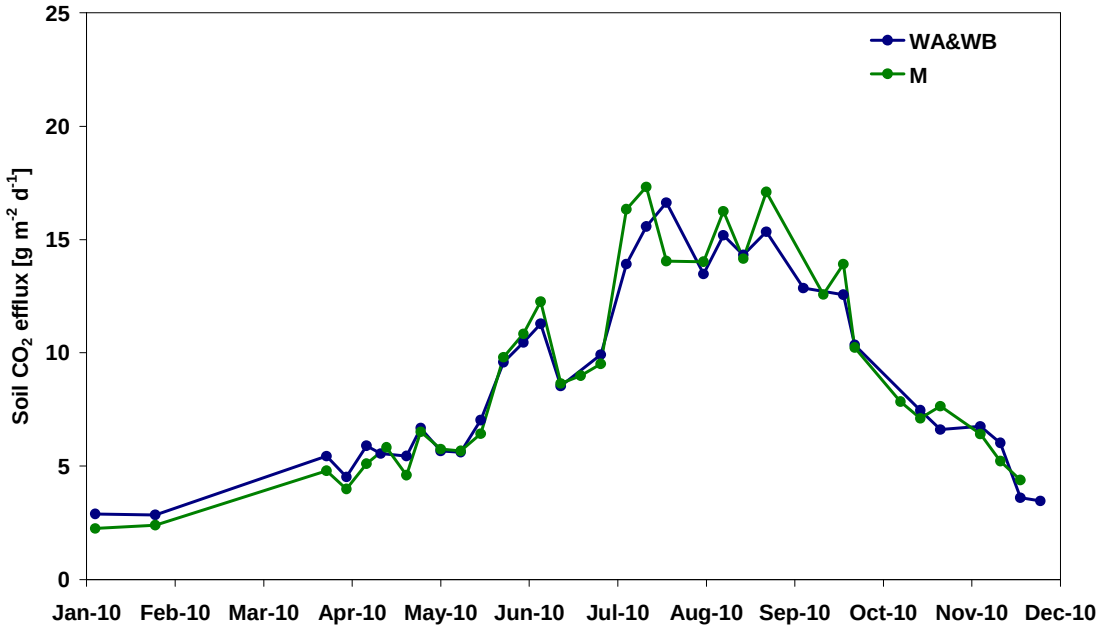

Figure 23c: Seasonal trend of soil CO_2 efflux measurements for transects WA/WB and grid M for the years 2009 (source: illustration of own data)

The growing season was defined from May to September, while the non-growing season was defined from October to April. Table 5 shows mean values of soil CO_2 efflux, standard deviation and coefficients of variation for transects WA and WB for all measurement years, while table 6 shows the same for measurement grid M.

Table 5: Mean values of soil CO_2 efflux (g/m^2d), standard deviation (SD) and coefficient of variation (CV) for transects WA and WB (n = number of measurements) (own data)

	Growing season (May – September) CO_2 efflux					Non-Growing-Season (October – April) CO_2 efflux				
	2006	2007	2008	2009	2010	2006	2007	2008	2009	2010
Mean	14.2	14.7	14.1	11.7	11.6	8.7	6.7	6.0	6.6	5.4
SD	5.2	5.0	6.1	5.8	6.2	3.8	3.4	2.7	3.1	3.0
CV[%]	37	34	43	50	53	44	50	45	48	56
n	351	378	620	380	740	323	386	200	387	492

The years 2006-2008 showed similar mean values of soil CO_2 efflux for the growing season for transects WA and WB, while 2009 and 2010 held much lower mean values. The year 2006 featured a mean value of 8.7 g m^{-2} d^{-1} for WA/WB for the non-growing season, which was high compared to the years 2007-2010 which can be explained by the fact that measurements started in October 2006. Values from January to April tend to be lower than the soil CO_2 efflux values from October to December. For measurement grid M soil CO_2 efflux mean were lower in general compared to transects WA/WB, at the same time the coefficients of variation were higher for grid M compared to WA/WB. This could be referred to the existence of outlier points in grid M, which showed constantly

low values throughout the year due to their position in a bog area (see file "point characteristics"on CD).

Table 6: Mean values of soil CO_2 efflux (g/m²d), standard deviation (SD) and coefficient of variation (CV) for grid M (n = number of measurements) (own data)

	Growing season (May – September) CO_2 efflux			Non-Growing Season (October – April) CO_2 efflux		
	2008	2009	2010	2008	2009	2010
Mean	10.0	11.7	10.4	5.3	5.6	3.3
SD	4.8	6.0	7.6	3.4	3.5	2.6
CV[%]	48	51	73	64	63	79
n	176	415	602	214	393	429

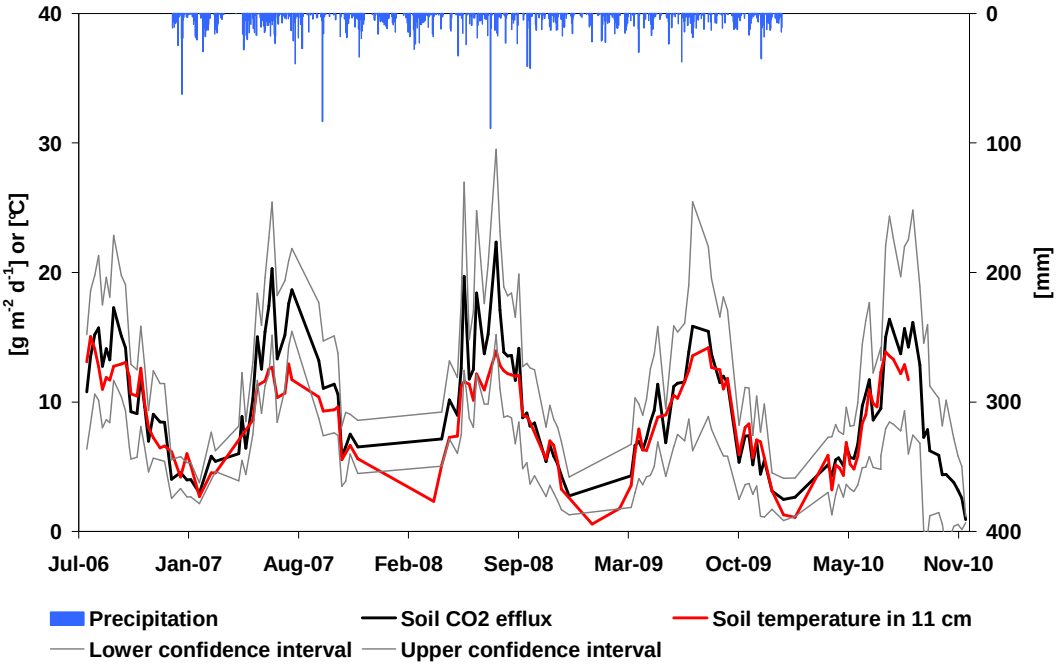

Figure 24: Mean measured soil CO_2 efflux of WA/WB and M with upper and lower confidence intervals (CO_2 efflux ± standard deviation), mean measured soil temperature in 11 cm depth of WA/WB and M and measured precipitation (source: illustration of own data)

Figure 24 illustrates the mean measured soil CO_2 efflux of all measurement points from 2006 to 2010 with confidence intervals (standard deviation). The years 2007 and 2008 showed the highest mean measured soil CO_2 efflux, with values around 20-22 g m^{-2} d^{-1}, while years 2006, 2009 and 2010 displayed lower maximum mean measured values during summer month (16-17 g m^{-2} d^{-1}). Standard deviation was highest during summer months leading to larger spatial variability. During 2006 and 2007 standard deviation values were low in compared to 2008 and especially 2009 and 2010. This can be attributed to the fact that that 2006 and 2007 only include data from transects WA and WB because grid M did not exist at that time. The addition of grid M to the total quantity of points leads to an increase in standard deviation and therefore an increase in spatial variability.

Soil temperatures at 5 and 11 cm depth showed the same seasonal course as the soil CO_2 efflux. Figure 25 shows the seasonal course of soil moisture, soil temperature and soil CO_2 efflux for transects WA and WB for the year 2008. Other years and measurement grid M contained similar seasonality for those three parameters (appendix, figures A3-A7). In contrast, soil moisture features a contrary seasonal course compared with soil temperature and soil CO_2 efflux.

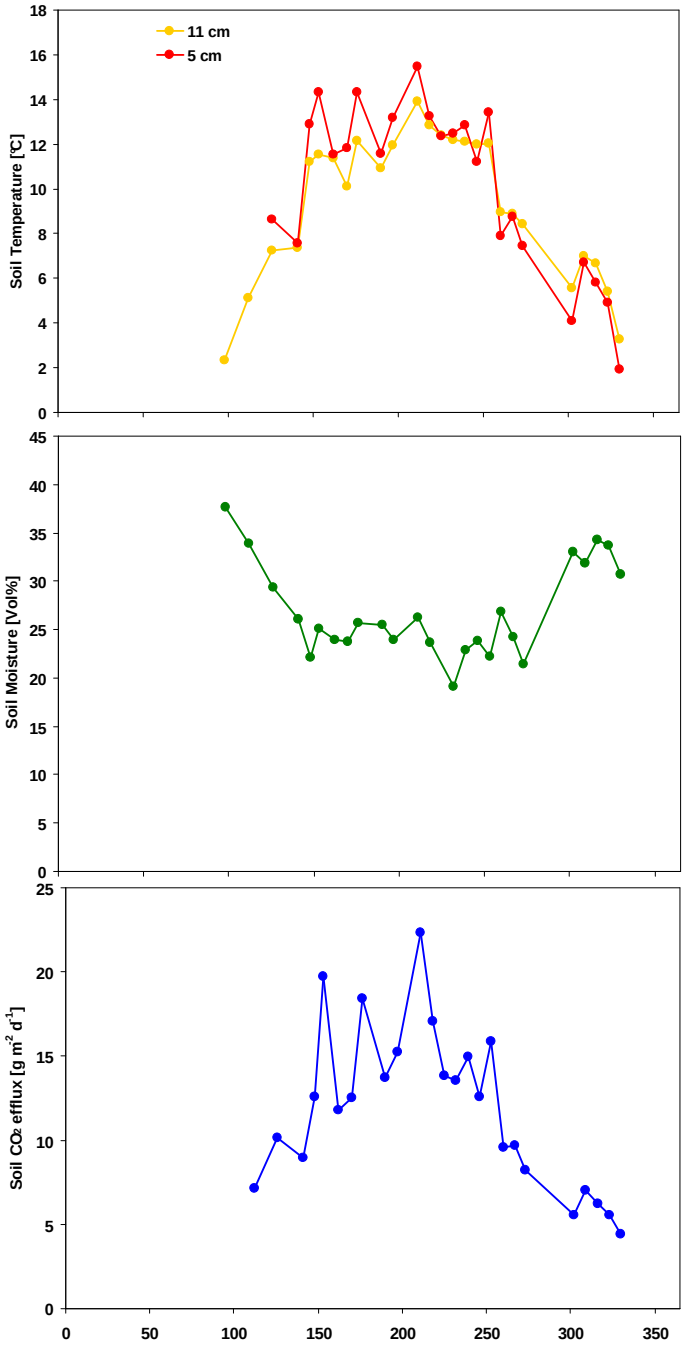

Figure 25: Seasonal course of measured soil temperature, soil moisture (over an integral of 15 cm) and soil CO_2 efflux for transects WA and WB for the year 2008 (source: illustration of own data)

Tables 5 and 6 show the coefficient of variation for all measurement values and all years. For each point the mean soil CO_2 efflux was calculated separately for the considered period of time and the coefficient of variation for all mean values from individual points was calculated in a second step. The coefficient of variation therefore includes spatial patterns. To exclude the impact of spatial variation, figures 26 and 27 show the temporal coefficient of variation for each year for the measurement grids by calculating the coefficient of variation as a mean of the single coefficients of variation for each of the measurement points. This results in lower coefficients of variation for the growing season and the non growing season compared to tables 5 and 6. Taking into account all seasons leads to higher coefficients of variation, in comparison to a separate season approach.

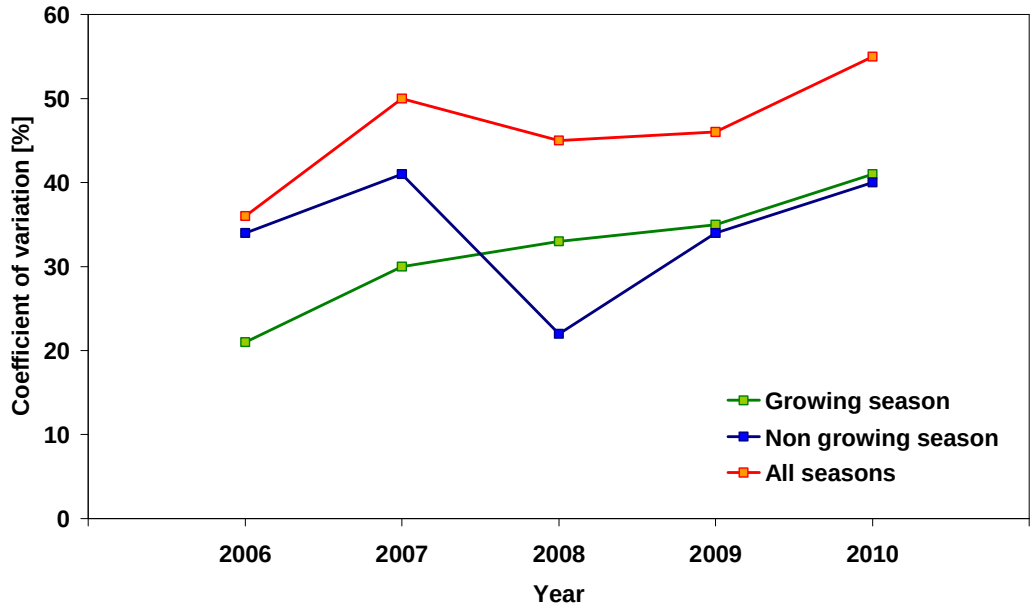

Figure 26: Temporal coefficient of variation (= mean of the single coefficients of variation for each measurement point for all measurement dates of one year) for measurement transects WA and WB (source: illustration of own data)

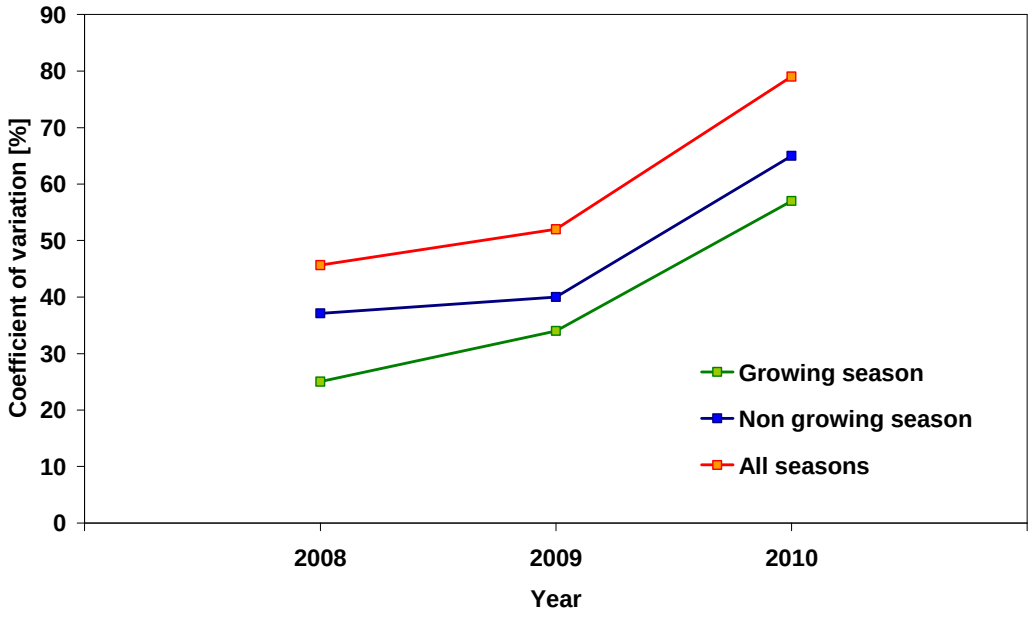

Figure 27: Temporal coefficient of variation (= mean of the single coefficients of variation for each measurement point for all measurement dates of one year) for measurement grid M (source: illustration of own data)

4.1.2 Diurnal variability in soil CO_2 efflux

The long term chamber measured hourly soil CO_2 efflux for individual days in September and October 2009. A weak diurnal pattern was visible. Some days showed a nearly constant course of soil CO_2 efflux, while others showed a trend towards a peak in the afternoon hours. Figure 28 shows the diurnal soil CO_2 efflux and soil temperature at 5 cm depth of three consecutive days from 17.09.2009 to 19.09.2009.

The diurnal course of soil CO_2 efflux roughly follows the course of soil temperature, apart from minor irregularities in soil CO_2 efflux rates. The irregularities were larger than the general measurement accuracy of the measurement chamber of ± 1.5%.

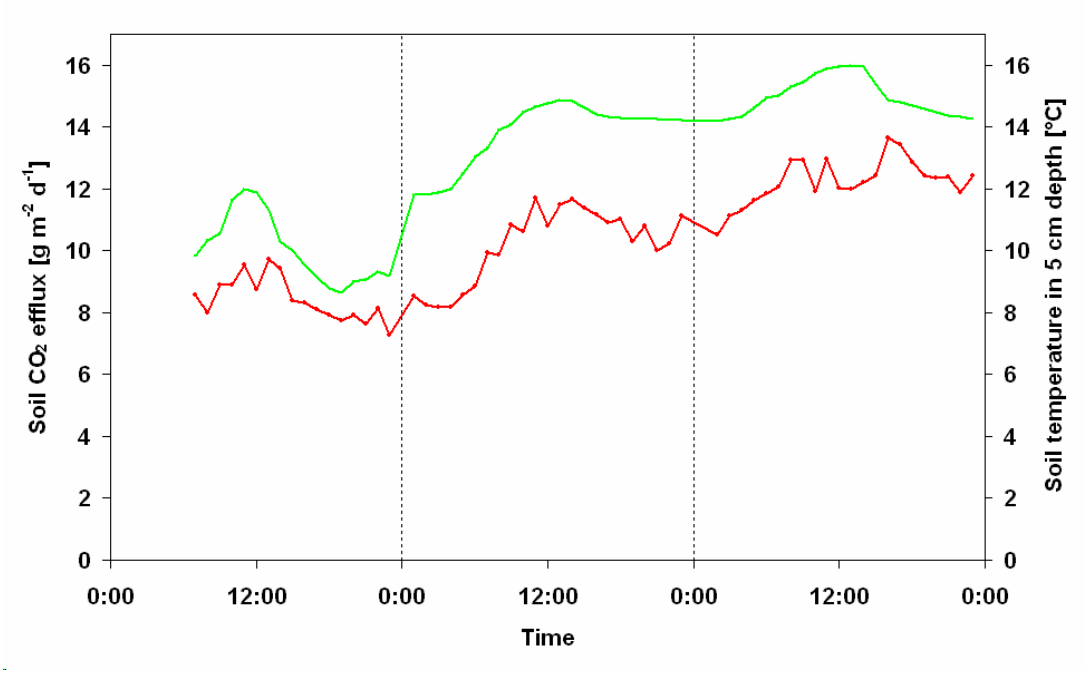

Figure 28: Diurnal course of soil CO_2 efflux (red) and soil temperature (5 cm depth; green) from 17/09/2009 to 19/09/2009, measured with the LICOR-8100-101 long-term chamber (source: illustration of own data)

4.1.3 The effects of root exclusion on soil CO_2 efflux

Exclusion of roots resulted in the exclusion of autotrophic respiration and therefore heterotrophic respiration was measured. Autotrophic respiration could be calculated by subtracting measured heterotrophic respiration from total soil respiration measured at the control plots. Heterotrophic respiration seems to be the dominant type of respiration in the Wüstebach catchment (see figure 29). Autotrophic respiration on average accounted for 21-59% for individual points. Literature values for the contribution of autotrophic respiration to total soil respiration range from 5...95% (Hanson et al. 2000). Díaz-Pinés et al. (2008) gained 25% autotrophic respiration of total soil respiration from their study in a spruce-dominated Austrian mountain forest, which is supported by studies from Buchmann (2000), Epron et al. (1999) and Lee et al. (2003). A direct correlation of the percentage of autotrophic respiration with the distance of the measurement point from the next tree was not visible. On the one hand measurement points M1 and M1a, M24, M24a and M24b (see figure 9 for position) are located very close to a tree (distance = 0.6 m) and show a high percentage of autotrophic respiration; on the other hand measurement points M7, M7a and M7b are located close to a tree as well (distance = 0.9 m) and show only a moderate contribution of autotrophic respiration to total soil respiration. Measurement points M29 and M29a are located far from a tree (distance = 2.6 m) and show only 21% of autotrophic respiration. Measurement point M16 lies very far from the next tree (distance = 4.6 m) but still shows a moderate amount of autotrophic respiration (36%).

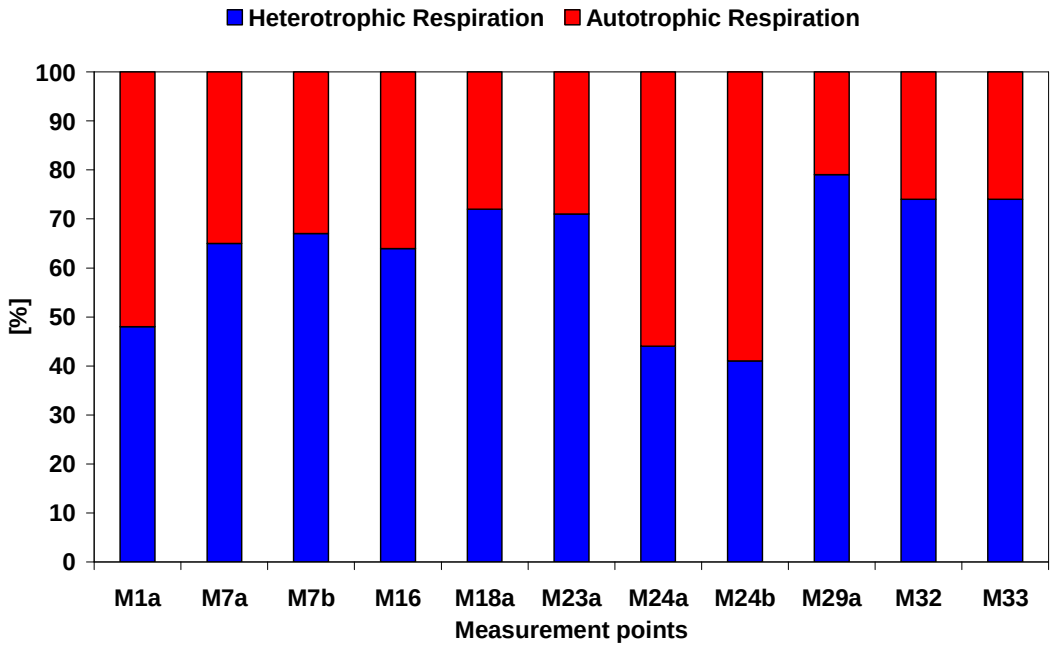

Figure 29: Percentage of heterotrophic and autotrophic respiration for rootless measurement points and their control points. (source: illustration of own data)

A great variability among single values for individual measurement dates hints at temporal variability in the proportion of heterotrophic respiration and autotrophic respiration (figure 30). The temporal course of the proportion of heterotrophic respiration to total soil respiration was similar for neighbouring points, e.g. M7a & M7b or M24a & M24b.

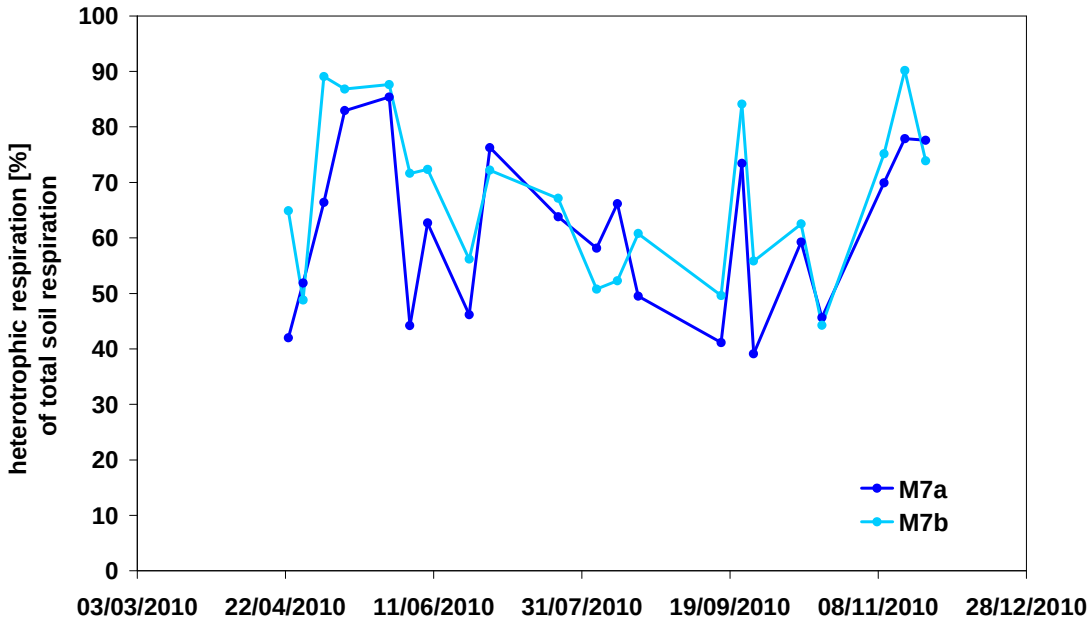

Figure 30: Temporal course of the percentage of heterotrophic respiration to total soil respiration for rootless neighbouring points M7a and M7b (source: illustration of own data)

With regard to the drawbacks of the used exclusion methods, uncertainties in the measurements must be taken into account. Temperature and soil moisture regimes within the collar can be different, since the used steel collars do not allow lateral flow of water and might heat up faster than the surrounding soil. Control samples were taken in September 2008 to compare soil temperature and soil moisture inside and outside the collars. A temperature increase of up to 0.5°C was noticed inside the collars at a depth of 5 cm (appendix, tables A1-A3). For a depth of 11 cm no significant temperature change was observable. Soil moisture showed a slight increase in the collars compared to the adjacent soil, but this increase was smaller than the general small-scale (~ 1 m) spatial variability in soil moisture.

For the trenched plots the degradation of dead roots can be an extra source of CO_2. This would lead to an underestimation of autotrophic respiration. This issue is generally acknowledged by scientists, but there is no consistent methodology for an implementation of corrections. Epron et al. (1999) investigated root decay of trenched plots by sampling root biomass at the time of trenching and after a period of 2 years. An average root biomass loss of 26% per year was determined. Published values for root decay average at around 34% per year, with considerably high ranges from 21-96% per year (Bowden et al. 1993, Lavigne et al. 2003, Nakane et al. 1986, Saiz et al. 2006). Vogt et al. (1996) found no consistent trend of root turnover or soil organic matter accumulation among different forest types or soil orders. Therefore it is likely that root degradation itself is also site-specific and therefore the application of literature values for root decay is not advisable.

For the plots where root exclusion was used, soil layers were disturbed greatly and due to compression the original properties of the soil layers might have been changed.

From October 2008 the measurement point M19 showed a water column in the collar (5cm above the soil surface) due to its placement in the bog area and the oversaturated soil. Therefore it was not included in the above figure 29.

4.1.4 The effects of soil horizons removal on soil CO_2 efflux

The removal of litter and organic layers generally resulted in a decrease of soil CO_2 efflux. Soil CO_2 efflux was reduced by 34-39% on average after removal of the needle litter layer and by 43-46% after removal of needle litter layer and organic layers (figure 31). Similar results were reported by Buchmann (2000) for a spruce forest in Eastern Germany with a decrease in soil CO_2 efflux by 10-20%, when needle litter was removed, and a decrease by 30-40% when needle litter and the organic layers were removed. Saiz

et al. (2007) detected a 40% decrease in soil CO_2 efflux from litter and organic layer removal in a 15-year old Sitka spruce stand.

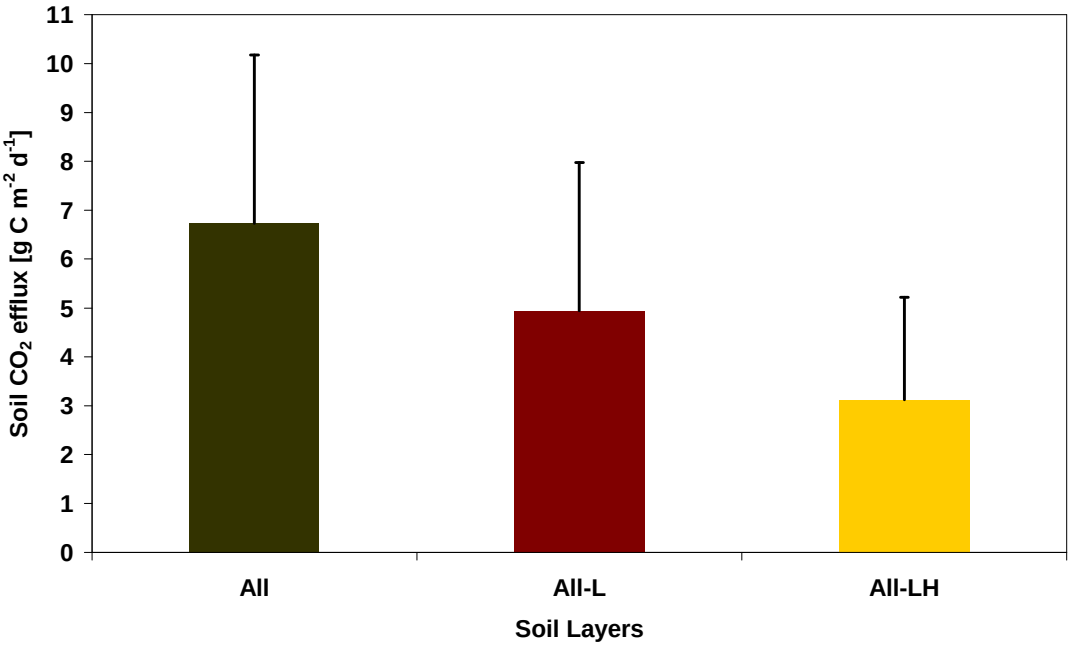

Figure 31: Effects of soil layer removal on measured soil CO_2 efflux. ***All***: mean values of all control points (n=4) for all measurement dates and standard deviation (whisker). ***All-L***: mean values of all points with removed litter layer (n=2) for all measurement dates and standard deviation (whisker). ***All-LH***: mean values of all points with removed litter and organic layers (n=2) for all measurement dates and standard deviation (whisker). 57 measurement days were included in the calculation. (source: illustration of own data)

The considered points showed a very low litter layer density; therefore the removal of needle litter might have partially led to a removal of organic soil, too. Data could be biased because the points were only irregularly cleared from fallen needle litter during 2009 and 2010

4.1.5 Relationship between soil temperature and soil CO_2 efflux

An exponential equation (eq. 38) was used to describe the relationship between soil temperature at various depths (5 cm and 11 cm) and soil CO_2 efflux.

Transects WA/WB and measurement grid M were considered separately, because of their different characteristics with regard to soil types and distances from point to point and from surrounding trees.

Soil temperature values for transects WA and WB ranged from 0°C to 19.3°C for a depth of 5 cm (median: 8.5°C; n=70), and from 0.4°C to 18.1°C for a depth of 11 cm (median: 8.7°C; n=127) over the complete measurement period. Spatial variability was very low.

Soil temperature values for grid M ranged from 0°C to 19.6°C for a depth of 5 cm (median: 8.3°C; n=63), and from 0°C to 15.5°C for a depth of 11 cm (median: 8.1°C;

n=63) over the complete measurement period. Spatial variability was similar to transects WA and WB.

Transects WA and WB

The coefficients of determination of the exponential regression of soil temperature and soil CO_2 efflux were between 50% and 82% for single measurement points over the whole measurement period with median values of 64% in 5 cm depth and 69% in 11 cm depth. A separate consideration of each measurement year for a depth of 5 cm resulted in high coefficients of determination for the year 2008 compared to the years 2009 and 2010 (table 7).

Table 7: Coefficients of determination [%] of the relationship between soil temperature and soil CO_2 efflux for transects WA and WB for individual years. Minimum values and maximum values among all measurement points are given, as well as median values for the whole measurement transects. (own data)

	2008	**2009**	**2010**
R^2 (minimum)	61	21	37
R^2 (maximum)	96	88	86
R^2 (median)	82	62	69

An examination of individual seasons (spring, summer, autumn, winter) was difficult due to a lack of data. With such a low data volume (low number of measurement dates) each measurement date was accorded a high impact on the regression, resulting in uncertain regression equations. Nevertheless the separation of the measurement years in growing season (May-September) and non-growing season (October-April) featured enough data ($n > 10$). A high variability of R^2 among the individual measurement points was visible with high ranges, as displayed in table 8.

Table 8: Coefficients of determination [%] of the relationship between soil temperature and soil CO_2 efflux for transects WA and WB for individual seasons (growing season vs. non-growing season). Minimum values and maximum values among all measurement points are given, as well as median values for the whole measurement transects. (own data)

	Growing Season			**Non-Growing Season**	
	2008	**2009**	**2008-2010**	**2009**	**2008-2010**
R^2 (minimum)	12	6	30	1	3
R^2 (maximum)	91	78	77	87	69
R^2 (median)	61	57	51	55	43

A regression of all measurement points and all measurement dates (figure 32) results in a coefficient of determination of 50% and highly scattered data, which hints at different temperature – soil CO_2 efflux relationships for individual points.

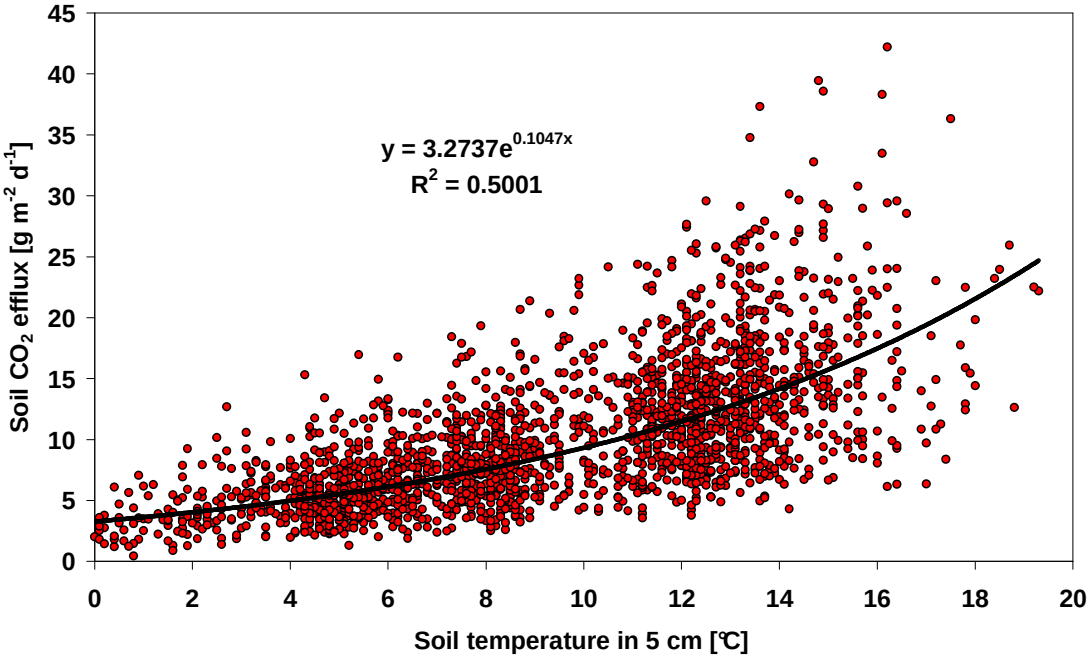

Figure 32: Exponential regression of soil temperature in 5 cm depth and soil CO_2 efflux for all measurement points of transects WA and WB and for all measurement dates (level of significance: $\alpha = 0.01$) (source: illustration of own data)

The use of mean values for each measurement day (field average) on the other hand results in a high coefficient of determination of 92% (figure 33).

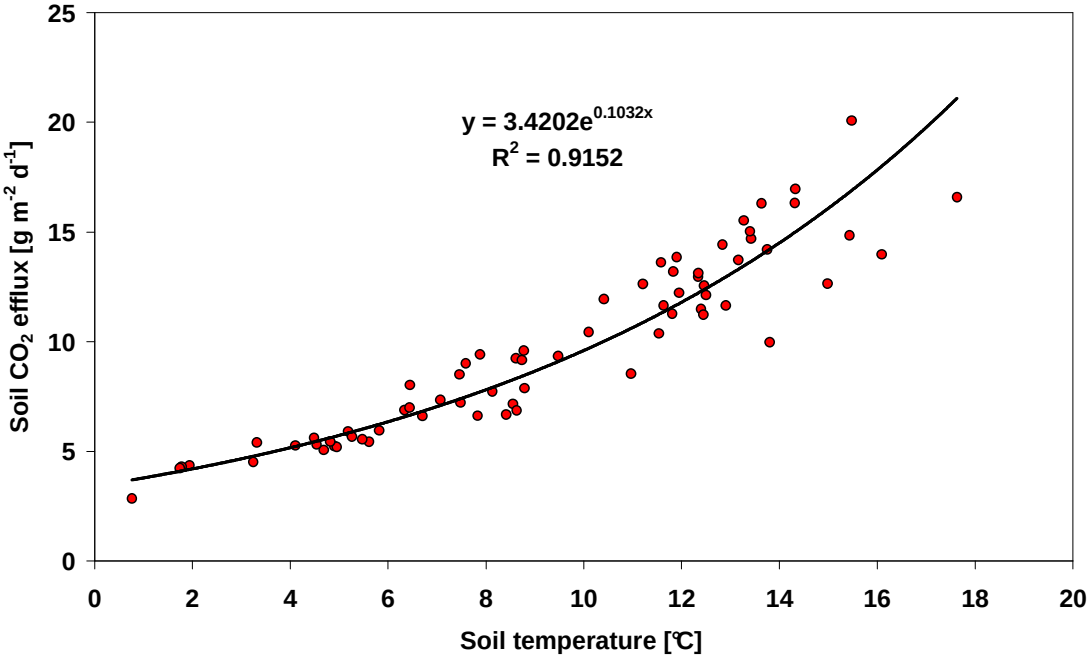

Figure 33: Exponential regression of field average values for soil temperature in 5 cm depth and soil CO_2 efflux of transects WA and WB for all measurement dates (level of significance: $\alpha = 0.01$) (source: illustration of own data)

The correlation with temperature in 11 cm depth shows a similar picture. A regression of all measurement points and all measurement dates (figure 34) results in a coefficient of determination of 49%, while the use of mean values for each measurement day (field average) on the other hand results in a high coefficient of determination of 85% (figure 35). All regressions were highly significant ($p < 0.01\%$, Student's t-test).

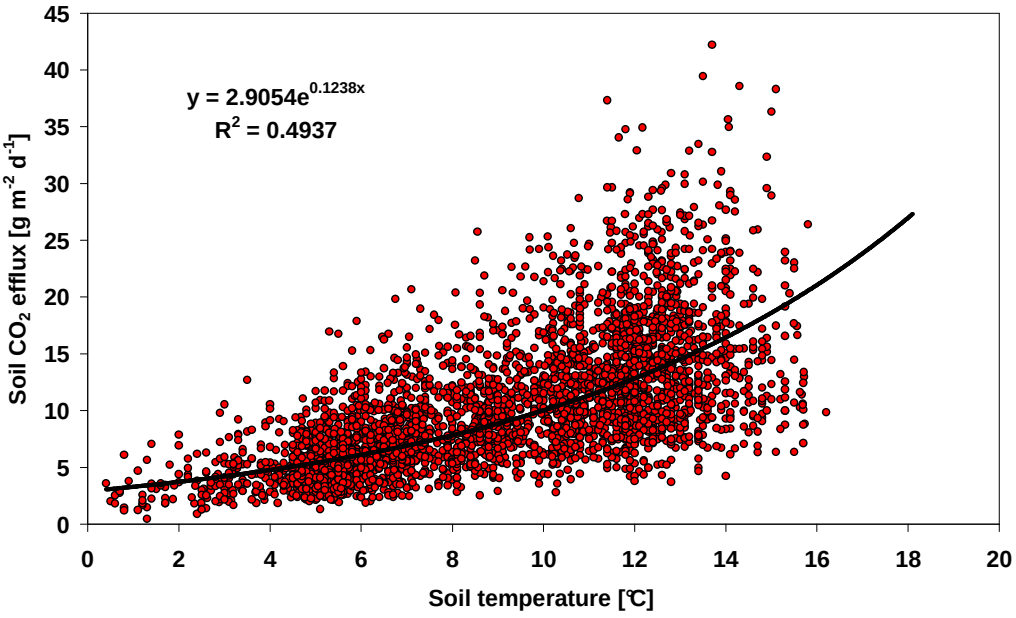

Figure 34: Exponential regression of soil temperature in 11 cm depth and soil CO_2 efflux for all measurement points of transects WA and WB and for all measurement dates (level of significance: $\alpha = 0.01$) (source: illustration of own data)

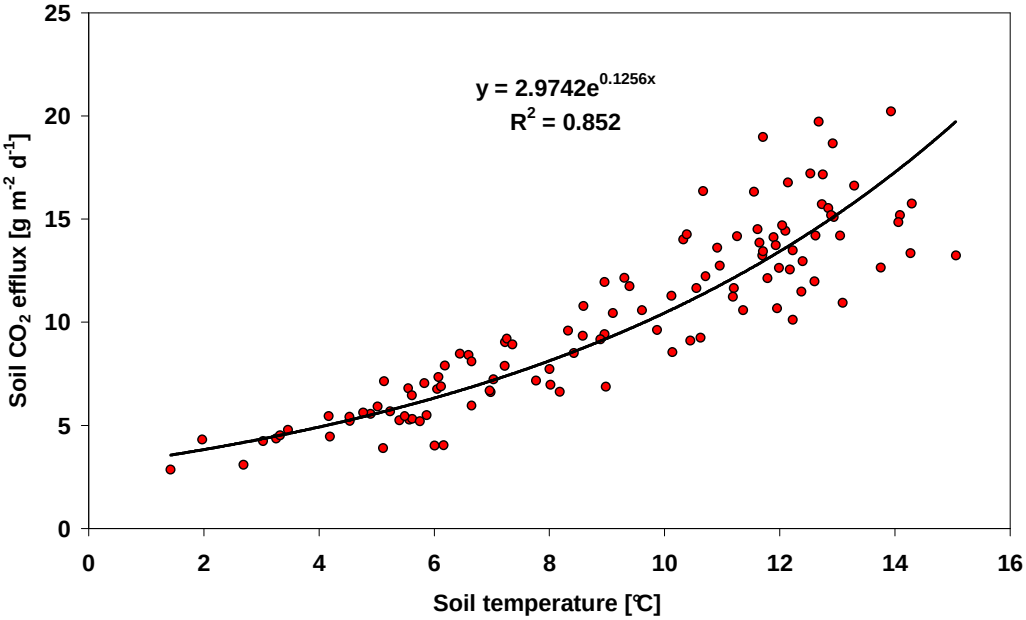

Figure 35: Exponential regression of field average values for soil temperature in 11 cm depth and soil CO_2 efflux of transects WA and WB for all measurement dates (level of significance: $\alpha = 0.01$) (source: illustration of own data)

Q_{10} values for growing seasons and non-growing seasons for individual points varied between 1.1 and 7.4, with median values between 2.5 and 3.0 for all measurement points (table 9).

Table 9: Q_{10} values for individual seasons for transects WA and WB. Minimum values and maximum values among all measurement points are given, as well as median values for the whole measurement transects. (own data)

	Growing Season			Non-Growing Season	
	2008	**2009**	**2008-2010**	**2009**	**2008-2010**
Q_{10} (minimum)	1.4	1.4	1.8	1.1	1.3
Q_{10} (maximum)	6.8	7.2	5.5	4.8	7.4
Q_{10} (median)	2.7	2.5	2.5	2.5	3.0

The typical range of Q_{10} for European and North American forest systems lies between 2 and 6.3 (Davidson 1998). It has to be taken into account that short-term temperature dependence may differ greatly from annual timescales (Janssens & Pilegaard 2003). A comparison of Q_{10} values determined in different studies is difficult, since some studies are based on measured field data, while others take into account simulations of fitted Q_{10} relationships (Fang & Moncrieff 2001). The Q_{10} value over the whole measurement period taking into account all measurement points for a depth of 5 cm was 2.8, while the Q_{10} value for a depth of 11 cm was 3.4. Q_{10} values for field averages were 2.8 for a depth of 5 cm and 3.5 for a depth of 11 cm, respectively. This confirms the assumption that Q_{10} values increase with the depths of the temperature measurements (Davidson et al. 2006). As pointed out by Graf et al. (2008) the fact that temperature measurements of single measurement depths are correlated with total soil CO_2 efflux, which is a sum of efflux from various depths, is mostly not considered.

Grid M

The coefficients of determination were between 0.21 and 0.91 for single measurement points over the whole measurement period with median values of 71% in 5 cm depth and 72% in 11 cm depth. A separate consideration of each measurement year for a depth of 5 cm resulted in high coefficients of determination for the year 2008 compared to the years 2009 and 2010 (table 10). This resembles data for transects WA and WB.

Table 10: : Coefficients of determination [%] of the relationship between soil temperature and soil CO_2 efflux for grid M for individual years. Minimum values and maximum values among all measurement points are given, as well as median values for the whole measurement grid. (own data)

	2008	**2009**	**2010**
R^2 (minimum)	56	1	30
R^2 (maximum)	98	91	93
R^2 (median)	90	70	74

Values for growing season (2008-2010) and non-growing season (2008-2010) are comparable to those from transects WA and WB, with slightly higher ranges (table 11). Median coefficients of determination are 44% for the growing season and 49% for the non-growing season.

Table 11: C Coefficients of determination [%] of the relationship between soil temperature and soil CO_2 efflux for grid M for individual seasons (growing season vs. non-growing season). Minimum values and maximum values among all measurement points are given, as well as median values for the whole measurement grid. (own data)

	Growing Season 2008-2010	**Non-Growing Season 2008-2010**
R^2 (minimum)	5	1
R^2 (maximum)	79	83
R^2 (median)	44	49

A regression of all measurement points and all measurement dates for a temperature measurement depth of 5 cm (figure 36) results in a coefficient of determination of 43% and highly scattered data, comparable to transects WA and WB.

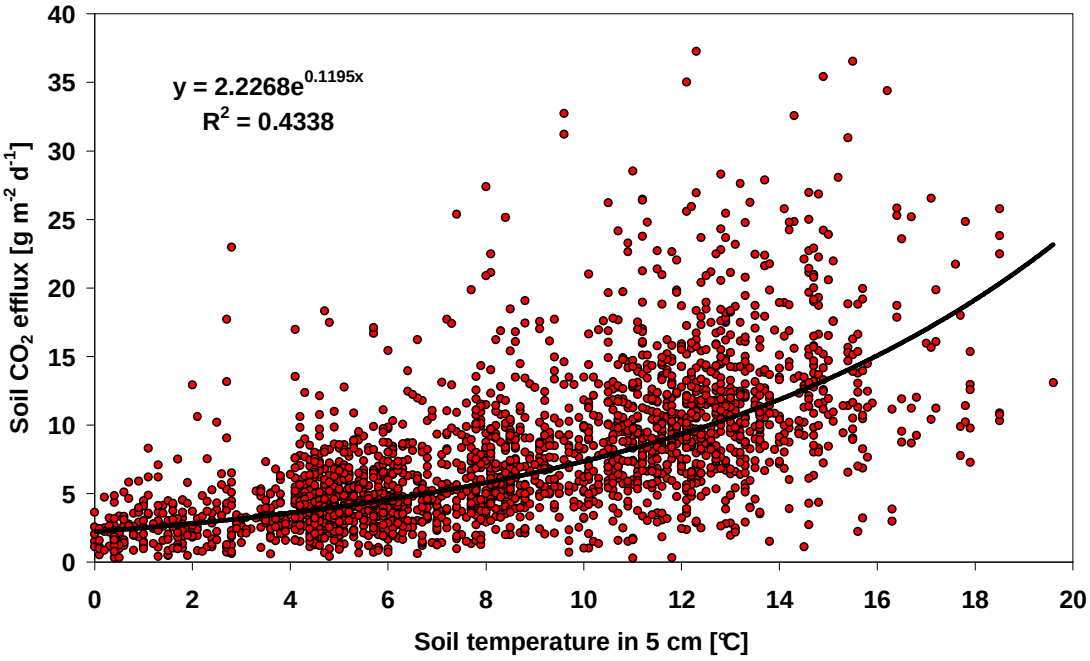

Figure 36: Exponential regression of soil temperature in 5 cm depth and soil CO_2 efflux for all measurement points of grid M and for all measurement dates (level of significance: $\alpha = 0.01$) (source: illustration of own data)

The use of mean values for each measurement day (field average) on the other hand results in a high coefficient of determination of 92% (figure 37).

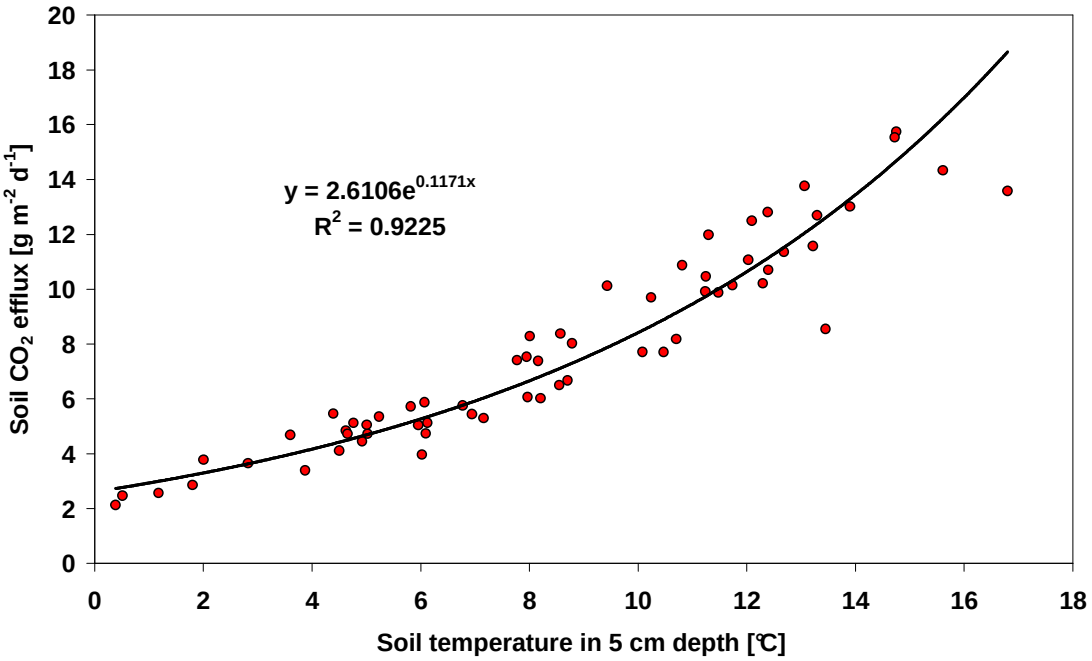

Figure 37: Exponential regression of field average values for soil temperature in 5 cm depth and soil CO_2 efflux of grid M for all measurement dates (level of significance: $\alpha = 0.01$) (source: illustration of own data)

Q_{10} values for growing seasons, non-growing seasons and all measurement years for individual points varied between 1.3 and 8.5, with median values between 2.4 and 3.4 for all measurement points (table 12).

Table 12: Q_{10} values for individual seasons for grid M. Minimum values and maximum values among all measurement points are given, as well as median values for the whole measurement grid. (own data)

	All measurements 2008-2010	**Growing Season 2008-2010**	**Non-Growing Season 2008-2010**
Q_{10} (minimum)	2.2	1.4	1.3
Q_{10} (maximum)	4.7	4.2	8.5
Q_{10} (median)	3.4	2.4	3.3

Q_{10} values for the non-growing season are mostly higher than Q_{10} values for the growing season; the median value for the non-growing season is 3.3 compared to 2.4 for the growing season. This is approved by Janssens et al. (2003) who found out that winter Q_{10} is always higher than summer Q_{10}. The high winter values are probably connected to low basal respiration rates. The increase in soil CO_2 efflux per temperature unit is smaller at low fluxes in winter, than at high fluxes in summer, despite higher Q_{10} values. The relative nature of Q_{10} leads to many different Q_{10} values produced by a given absolute increase in soil CO_2 efflux, depending on the magnitude of the flux.

The Q_{10} value over the whole measurement period taking into account all measurement points for a depth of 5 cm was 3.3, while the Q_{10} value for a depth of 11 cm was 4.1. Q_{10} values for field averages were 3.2 for a depth of 5 cm and 3.9 for a depth of 11 cm, respectively.

However, the Q_{10} values calculated here represent a combination of autotrophic and heterotrophic respiration, and both can exhibit different Q_{10} values. Boone et al. (1998) found that autotrophic respiration showed significantly higher Q_{10} values (4.6) than heterotrophic respiration (3.5). A comparison of Q_{10} values for measurement points M1, M7, M18, M23 and M24 with their rootless counterparts M1a, M7a/b, M18a, M23a and M24a/b resulted in higher Q_{10} values for the points including heterotrophic and autotrophic respiration (M1, M7, M18, M23, M24) compared to points with heterotrophic respiration only (M1a, M7a/b, M18a, M23a, M24a/b; figure 38).

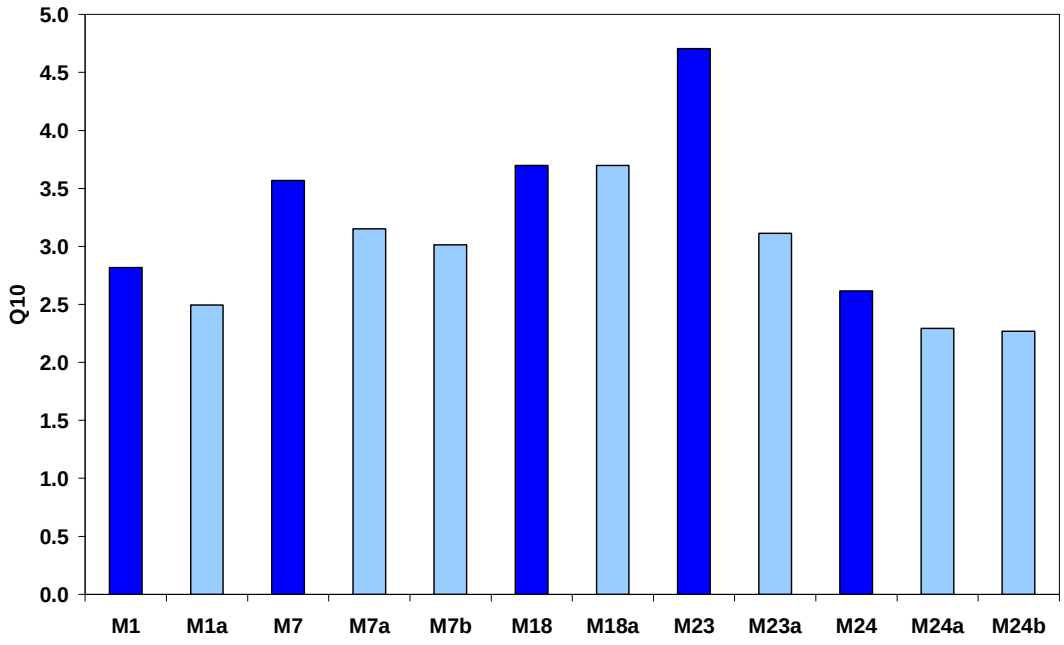

Figure 38: Q_{10} values for rootless points and control points (dark blue: control point; light blue: rootless point) (source: illustration of own data)

4.1.6 Relationship between soil moisture and soil CO_2 efflux

Soil moisture values for transects WA and WB ranged from 3 Vol% to 81 Vol% for single measurements (median: 30.7 Vol%; n=77), and from 4 Vol% to 100 Vol% for measurement grid M (median: 30.2 Vol%; n=44) over the complete measurement period. Spatial variability was high, with a coefficient of variation ranging from 7 Vol% to 47 Vol % (median: 27 Vol%) for transects WA and WB and a coefficient of variation ranging from 23 Vol% to 86 Vol% (median: 38 Vol%) for measurement grid M. The comparably higher spatial variability for grid M can be attributed to the presence of bog

soil for two of the measurement points which showed permanently saturated soil conditions.

Soil moisture data featured several gaps due to broken instruments. None of the measurement years holds a complete data set over a period of 12 months. For the year 2008 data is available from April to November for transects WA and WB. Figure 39 shows the mean monthly soil moisture for WA/WB for this time period and the cumulative monthly precipitation.

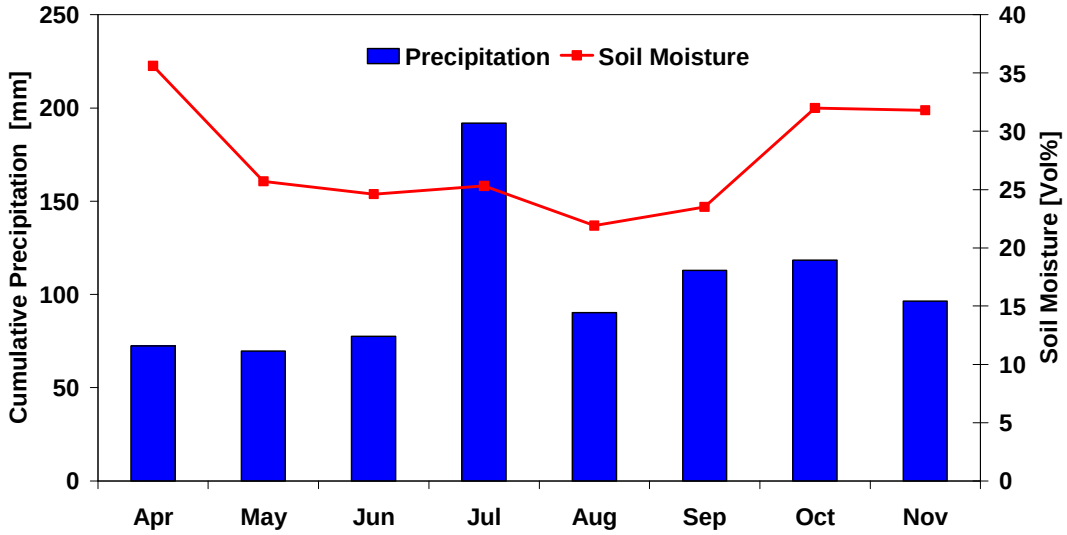

Figure 39: Mean monthly soil moisture and cumulative precipitation of transects WA and WB for 2008 (source: illustration of own data)

The coefficients of determination of the exponential regression of soil moisture and soil CO_2 efflux were between 0% and 47% for single measurement points over the whole measurement period, with a median value of 27% for transects WA and WB. For measurement grid M the coefficients of determination were between 3% and 64% for single measurement points, with a median value of 22 %.

An exponential regression of mean values for each measurement day (field average) with soil moisture (figures 40 and 41) results in a coefficient of determination of 55% for transects WA and WB and in a coefficient of determination of 40% for measurement grid M.

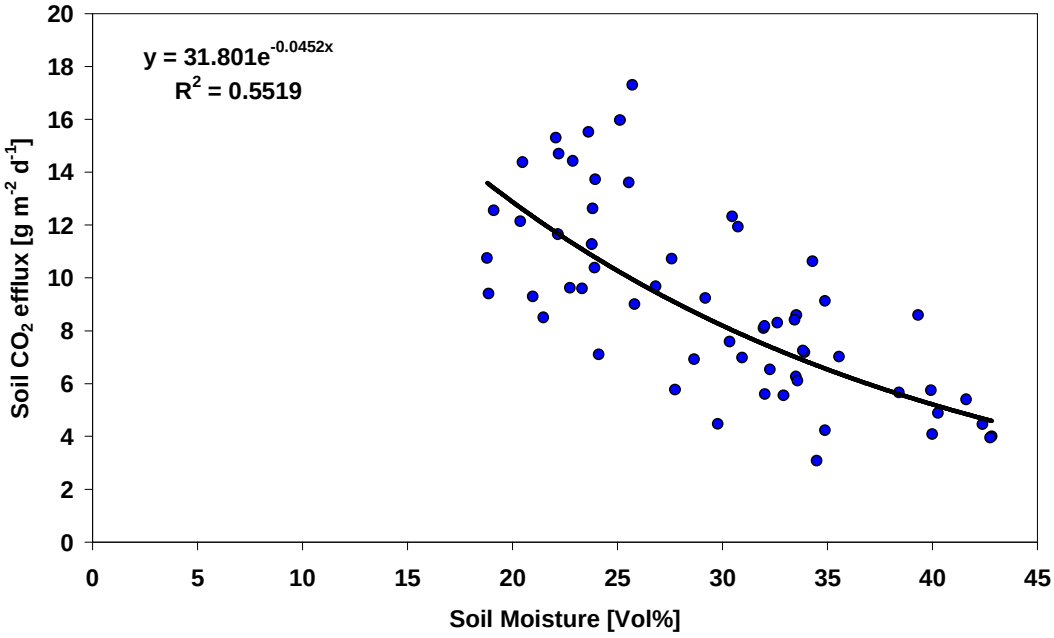

Figure 40: Exponential regression of field average values for soil moisture and soil CO_2 efflux of transects WA and WB for all measurement dates. The relationship is significant (level of significance: $\alpha = 0.01$). (source: illustration of own data)

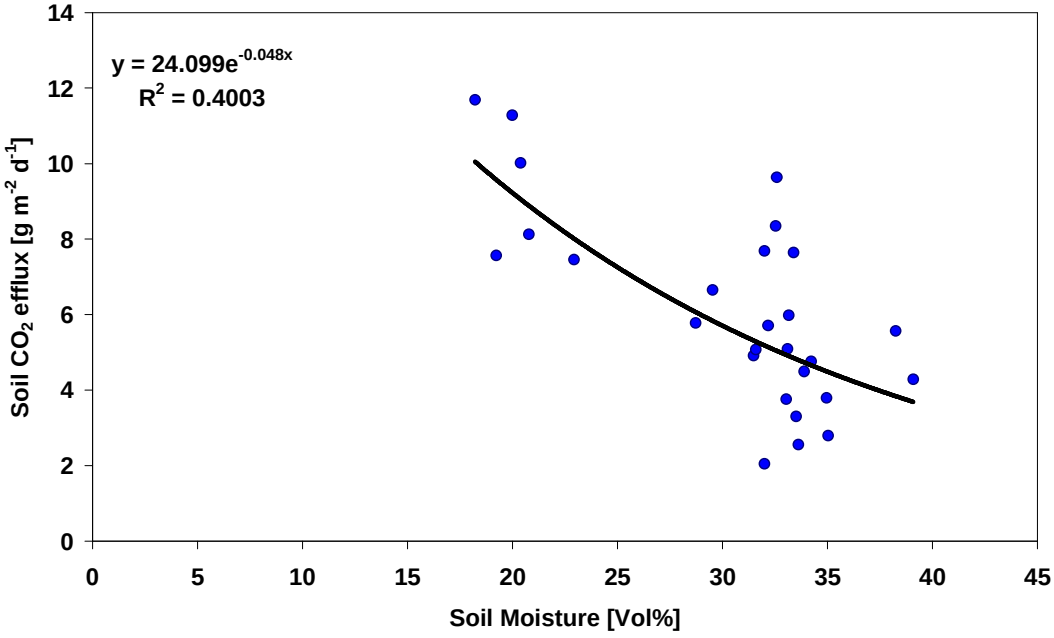

Figure 41: Exponential regression of field average values for soil moisture and soil CO_2 efflux of grid M for all measurement dates. The relationship is significant ((level of significance: $\alpha = 0.01$)). (source: illustration of own data)

Soil moisture and soil CO_2 efflux showed a negative correlation, for individual points a bimodal correlation, as found by Davidson (1998) or Xu and Qi (2001), resulted in a better fit, when values below 10 Vol% were present (figure 42). This did not relate to all points. Especially when soil moisture values were low in general (figure 43), lower soil water contents were connected with a higher soil CO_2 efflux.

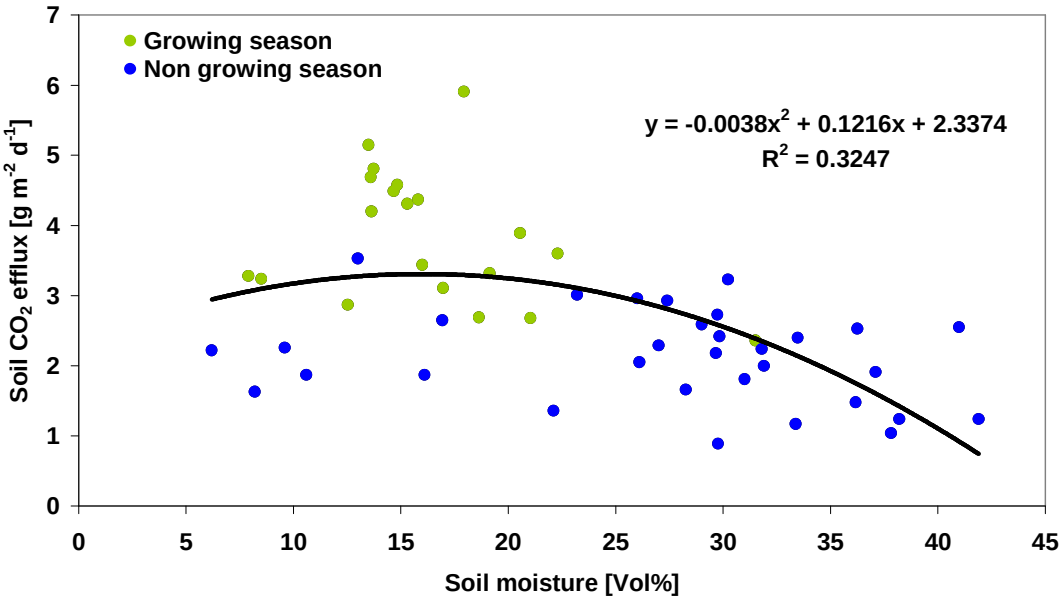

Figure 42: Polynomial (bimodal) regression of measurement point WA10 for soil moisture and soil CO_2 efflux for all measurement dates (growing season = green, non growing season = blue). The relationship was significant (level of significance: $\alpha = 0.01$) (source: illustration of own data)

.

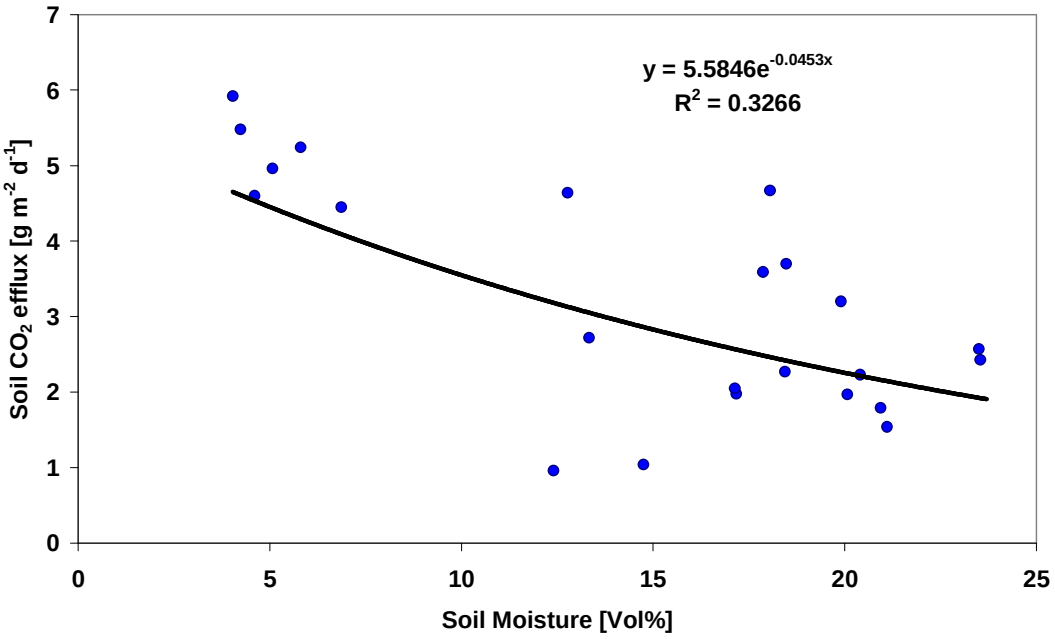

Figure 43: Exponential regression of measurement point M1 for soil moisture and soil CO_2 efflux for all measurement dates. The relationship was significant (level of significance: $\alpha = 0.01$) (source: illustration of own data)

4.1.7 Temporal stability

In order to understand spatial patterns it is useful to know whether the data are time persistent. The Pearson correlation coefficient of consecutive days (calculated after

Vachaud et al. 1985) gives information about data persistence and can be found in table 13 for soil CO_2 efflux, soil water content and soil temperature for transects WA and WB for years 2006 and 2008 and in table 14 for M for 2008 to 2010. A table for the years 2007, 2009 and 2010 for WA and WB can be found in the appendix (table A4.

High correlation coefficients between consecutive measurement dates indicate temporal persistence. The highest temporal stability was detected for soil water content (Θ_{15}), with most values above 90%. This resembles findings by Vachaud et al. (1985). Soil CO_2 efflux (CO_2) – with some exceptions - showed high values for most of the time intervals. The correlation coefficients did not seem to depend on the length of the interval between consecutive measurement dates.

High correlation coefficients were present for short intervals, as well as for long intervals. Low correlations coefficients could be found for both as well.

Negative values were detected for soil temperature (T_{11}), which can be accounted to the low variability of temperature throughout the plot and the accuracy of the soil temperature measurements. Similar observations were made by Herbst et al. (2009), who conducted a study on bare soil. Highest correlation coefficients were detected for soil moisture, followed by soil respiration and soil temperature. In general correlation coefficients were mostly lower compared to results from our study.

Table 13: Pearson Correlation Coefficients for soil CO_2 efflux (CO_2), soil temperature in 11 cm depth (T_{11}; 11 cm was chosen because the temperature data for 5 cm was not available over such a long period of time) and soil water content over an interval of 15 cm (θ_{15}) for transects WA and WB. The Pearson Correlation Coefficients were highly significant for coefficients > 0.7 ($p < 0.01$). (own data)

Year	Date	Interval [d]	Pearson Correlation Coefficient		
			CO_2	T_{11}	θ_{15}
2006	**18.09**				
	25.09	7	0.82	0.92	0.92
	02.10	7	0.68	0.88	0.91
	05.10	3	0.85	0.65	0.89
	16.10	11	0.60	0.39	0.78
	23.10	7	0.08	-0.24	0.66
	30.10	7	0.34	0.44	0.75
	06.11	7	0.69	0.08	0.70
	15.11	9	0.66	0.74	0.36
	27.11	12	0.76	0.69	0.61
	05.12	8	0.67	0.74	0.31
	18.12	13	0.71	0.70	0.26
2008	**21.5**	181	0.75	0.07	0.62
	28.5	7	0.78	0.26	0.91
	2.6	5	0.55	0.73	0.89
	11.6	9	0.56	0.85	0.91
	19.6	8	0.81	0.77	0.94
	25.6	6	0.76	0.65	0.92
	9.7	14	0.80	0.53	0.89
	16.7	7	0.87	0.78	0.94
	30.7	14	0.81	0.69	0.96
	6.8	7	0.65	0.64	0.94
	20.8	14	0.69	0.80	0.92
	27.8	7	0.86	0.78	0.91
	3.9	7	0.90	0.85	0.91
	10.9	7	0.80	0.69	0.95
	17.9	7	0.67	0.47	0.94
	24.9	7	0.87	0.69	0.91
	30.9	6	0.88	0.52	0.98
	29.10	29	0.89	0.51	0.91
	5.11	7	0.96	0.74	0.89
	12.11	7	0.95	0.78	0.85
	19.11	7	0.94	0.68	0.78
	26.11	7	0.92	0.74	0.61

Table 14: Pearson Correlation Coefficients for soil respiration (R_s), soil temperature in 11 cm depth (T_{11}) and soil water content (θ_{15}) for grid M. The Pearson Correlation Coefficients were highly significant for coefficients > 0.7 ($p < 0.01$). (own data)

Year	Date	Interval [d]	Pearson Correlation Coefficient		
			R_s	T_{11}	θ_{15}
2008	**27.8**				
	3.9	7	0.90	0.62	0.92
	10.9	7	0.93	0.64	0.94
	17.9	7	0.97	0.39	0.95
	24.9	7	0.96	0.82	0.94
	30.9	6	0.91	0.92	0.94
	8.10	8	0.85	0.33	0.88
	29.10	21	0.87	0.13	0.93
	5.11	7	0.94	0.84	0.87
	12.11	7	0.89	0.74	0.85
	19.11	7	0.95	0.83	0.93
	26.11	7	0.93	0.70	0.92
	10.12	14	0.89	0.69	0.95
2009	**2.4**	113	0.59	0.38	0.96
	9.4	7	0.37	0.50	0.91
	16.4	7	0.38	0.79	0.93
	23.4	7	0.60	0.33	0.96
	30.4	7	0.81	0.85	0.96
	7.5	7	0.80	0.68	0.96
	20.5	13	0.70	0.66	0.94
	2.11	166	0.59	0.17	0.92
	9.11	7	0.87	-0.03	0.95
	23.11	14	0.74	-0.19	0.96
	30.11	7	0.81	0.80	0.93
	14.12	14	0.83	0.71	0.98
2010	**4.1**	21	0.83	0.27	0.96
	26.3	81	0.83	0.73	0.96
	2.4	7	0.80	0.13	0.95
	9.4	7	0.32	0.42	0.90
	16.4	7	0.79	0.77	0.82
	23.4	7	0.86	0.89	0.61
	28.4	5	0.56	0.55	0.61
	5.5	7	0.33	0.30	0.98
	12.5	7	0.59	0.86	0.93
	19.5	7	0.56	0.82	0.95
	27.5	8	0.70	0.53	0.96
	3.6	7	0.87	0.73	0.98
	16.6	13	0.70	0.76	0.97
	23.6	7	0.63	0.64	0.98
	30.6	7	0.47	0.23	0.97
	9.7	9	0.52	0.59	0.98

4.2 Spatial variability in soil CO_2 efflux measurements

Coefficients of variation for single measurement days were calculated for soil CO_2 efflux, soil temperature and soil moisture to show spatial variability. For soil CO_2 efflux coefficients of variation were high and ranged from 15% to 65% for transects WA/WB and from 35% to 103% for grid M, with median coefficients of variation of 37% and 53% respectively. Lower values were detected for soil moisture, ranging between 7% and 53%

for transects WA/WB and between 22% and 79% for grid M, with median values of 31% and 35%. Lowest spatial variability was found for soil temperature with ranges between 2-50% for transects WA/WB and between 2-68% for grid M. Median values were 5% for WA/WB and 4% for M.

4.2.1 Spatial distribution of soil CO_2 efflux

Spatial variability of soil CO_2 efflux for individual days could be high; by looking at median values the spatial variability in the research area was moderate (figures 44 and 45). Median values were used to exclude the influence of extreme values. Distinct spatial patterns with regard to morphology or distance to the stream were not visible. Nevertheless single measurement points showed a constant behaviour over time by displaying either higher or lower values compared to all other measurement points. Apart from those extreme values the measurement points showed median values between 5.1 and 13.4 g m^{-2} d^{-1}. Several measurement points showed median values between 5.1 and 10 g m^{-2} d^{-1} (figures 44 and 45). Low values of less than 5 g m^{-2} d^{-1} could mainly be found in measurement grid M, where points were affected by litter removal or root exclusion or were situated in the bog area.

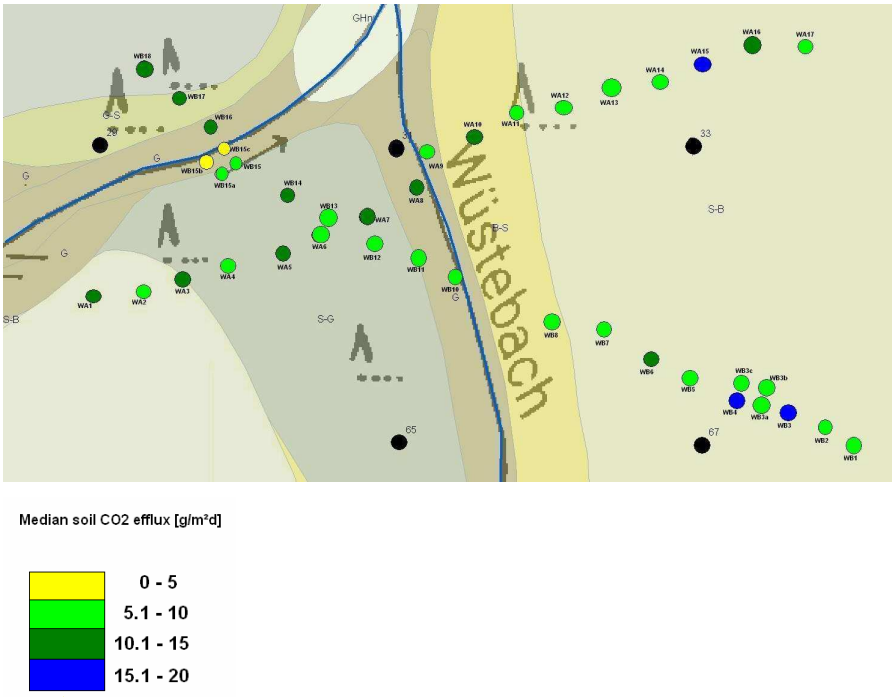

Figure 44: Median soil CO_2 efflux rates over the whole measurement period for transects WA and WB (black dots are not relevant) (source: illustration of own data)

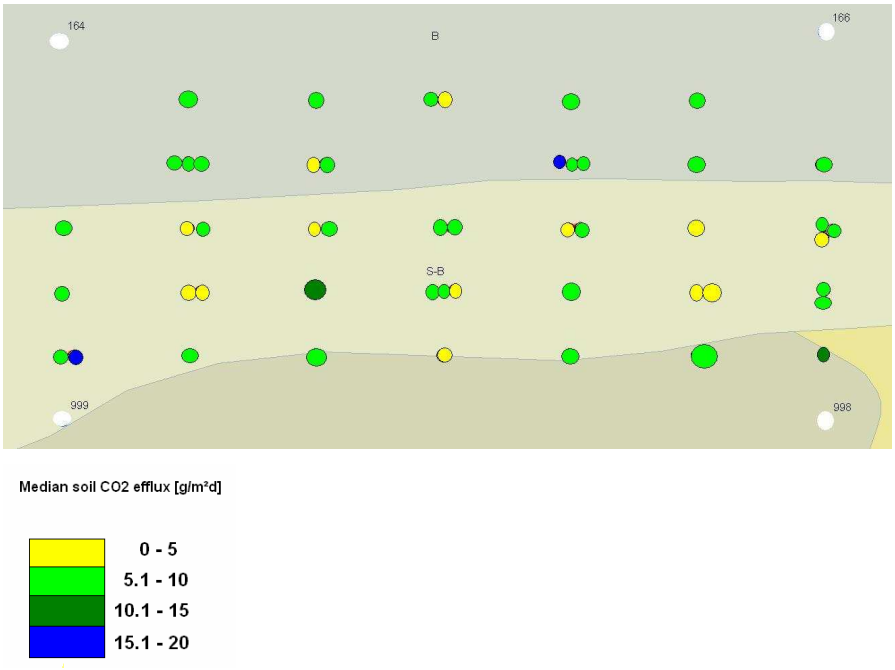

Figure 45: Median soil CO_2 efflux rates over the whole measurement period for grid M (black dots are not relevant) (source: illustration of own data)

4.2.2 Relationship between vegetation parameters and soil CO_2 efflux

Soil CO_2 efflux and the thickness of the litter layer partly showed some consistency (figures 46 and 47). Especially some of the extreme values were well explained by the thickness of the litter layer. Points WB3, M1 and M31 showed comparably high soil CO_2 efflux rates, which went along with thick litter layers. A thick litter layer can either mean a good supply with fresh decomposable litter, needed for microbial respiration or constricted microbial respiration rates which limit the decomposition of litter.

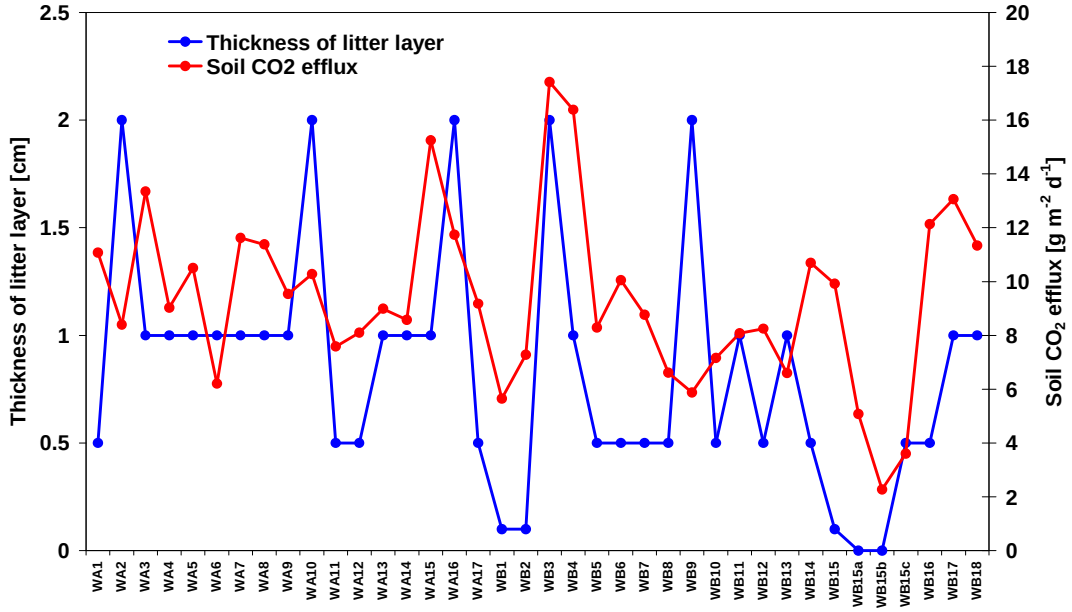

Figure 46: Median soil CO_2 efflux and thickness of litter layer for transects WA and WB (source: illustration of own data)

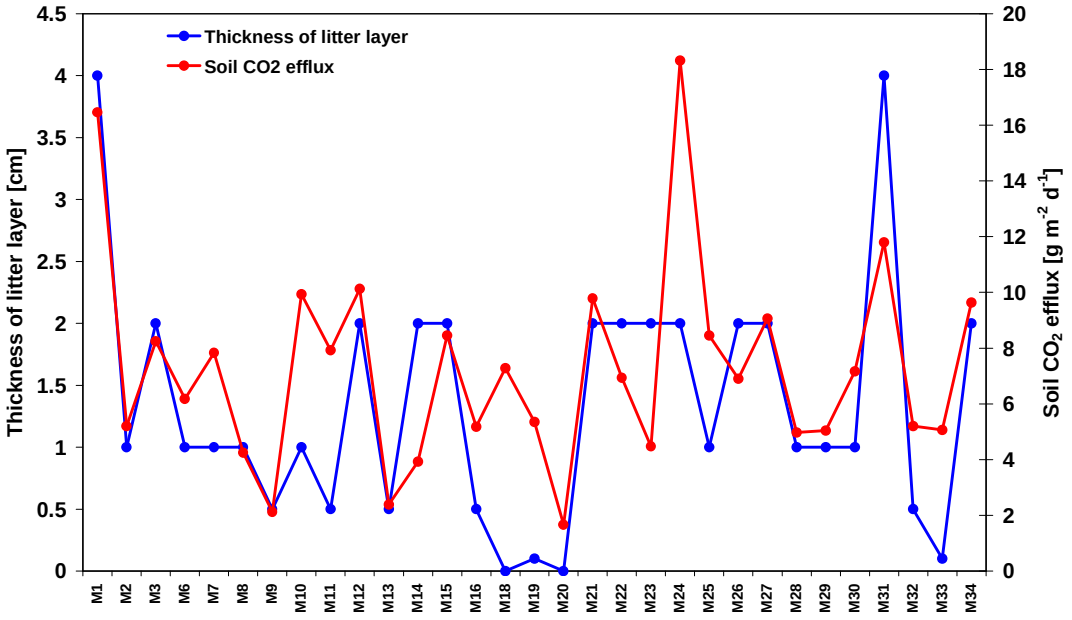

Figure 47: Median soil CO_2 efflux and thickness of litter layer for grid M (source: illustration of own data)

A correlation of soil CO_2 efflux with the distance from the nearest tree showed a weak correlation for WA and WB (figure 48) and a good correlation for grid M (figure 49). Several outliers were excluded from these regression calculations (points from young stands, bog-affected points, and points with very high values of soil CO_2 efflux).

A negative correlation was detected for all measurement grids. With an increase of distance between a measurement point and the nearest tree soil CO_2 efflux decreased. This might hint at a decrease of root density with an increase of distance from a tree and at a decrease of litter layer density with an increase of distance from a tree. Therefore heterotrophic as well as autotrophic respiration would be affected.

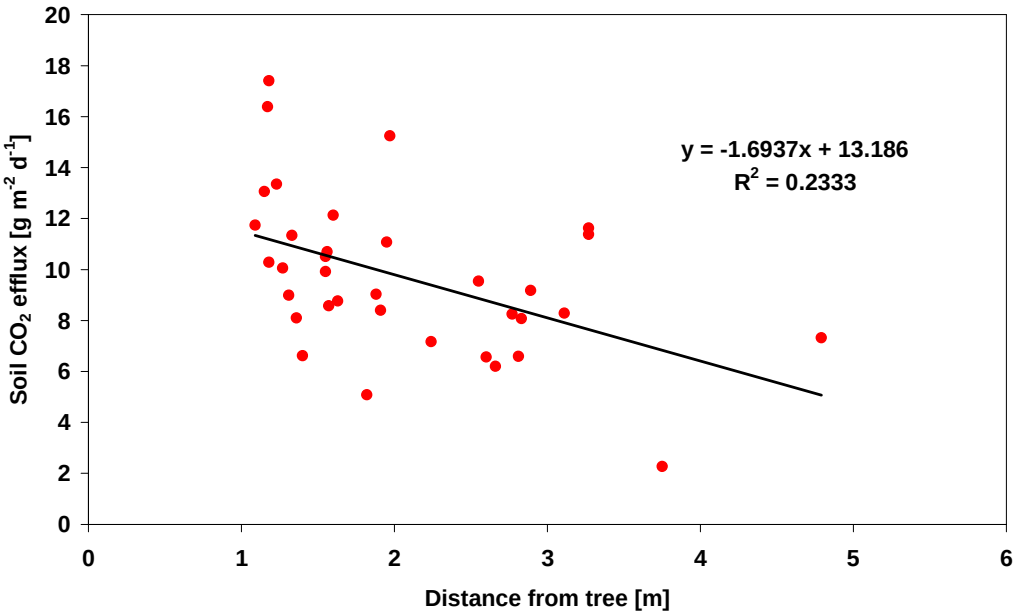

Figure 48: Linear regression of median soil CO_2 efflux and distance from the next tree for transects WA and WB for the whole measurement period (n = 131 dates). The relationship is not significant ($p > 0.05$). (source: illustration of own data)

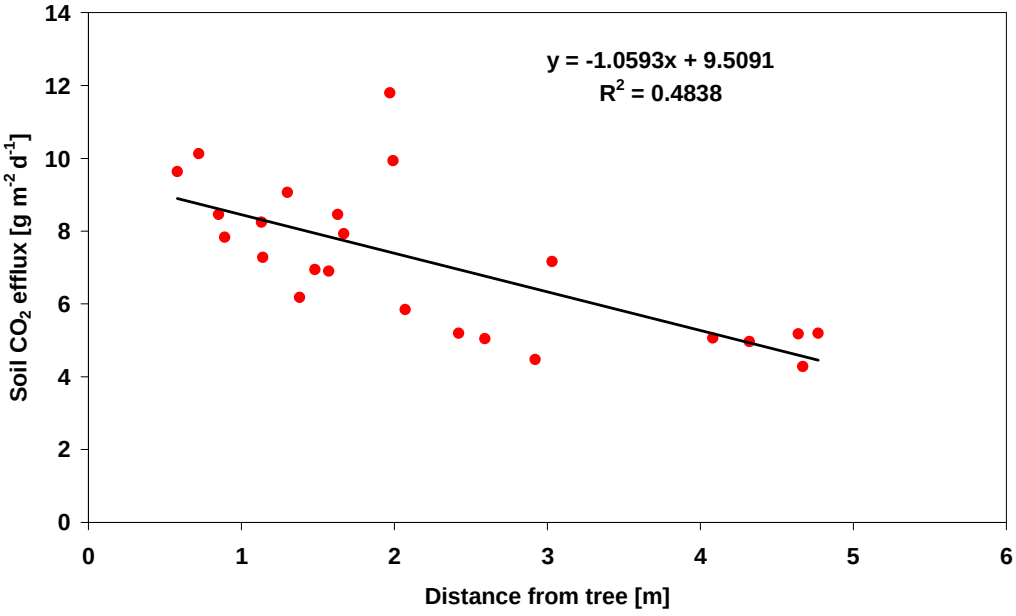

Figure 49: Linear regression of median soil CO_2 efflux and distance from the next tree for grid M for the whole measurement period (n = 73 dates). The relationship is significant ($p < 0.05$). (source: illustration of own data)

The mean relative root biomass was calculated after Ammer and Wagner (2005) for six measurement points (WA10, WB3, WB15, M20, M23 and M25) and compared to measured root biomass (see Chapter 3.6). Figure 50 shows no correlation. Particularly the measurement points from measurement grid M did not fit in due to their low measured root biomass. Exclusion of those points would lead to a coefficient of determination of 96%. Since the correlation would then be based on three points only, the outcome has to be considered with caution.

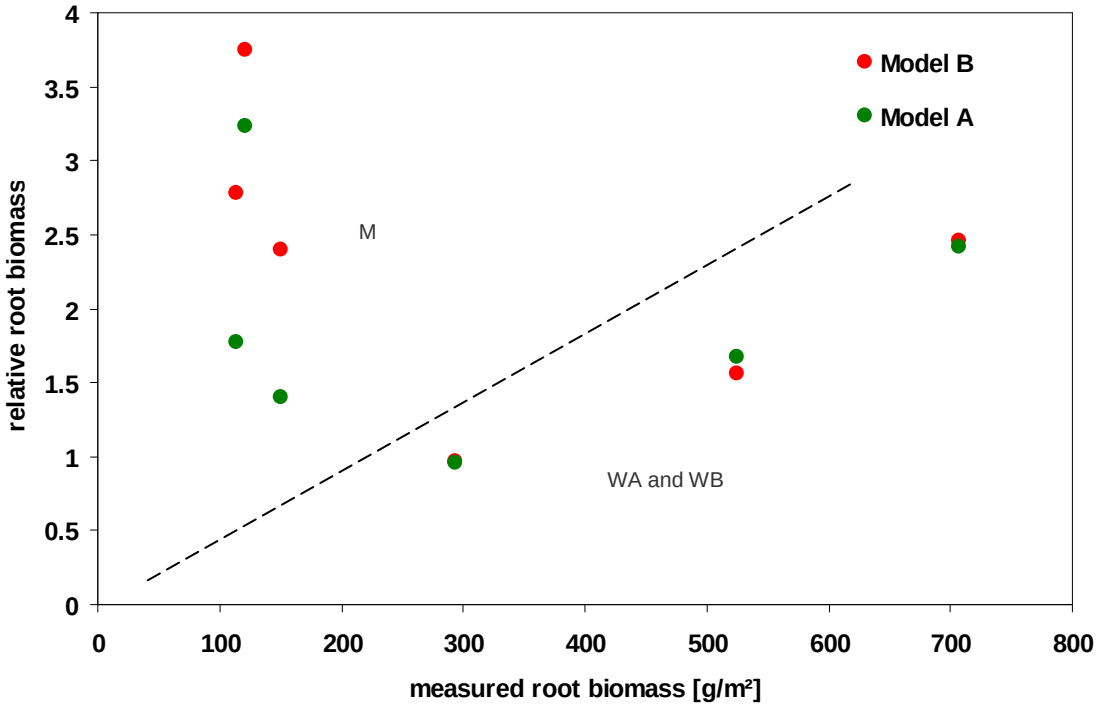

Figure 50: Comparison of measured root biomass versus calculated mean relative root biomass for model A and model B after Ammer & Wagner (2005) (source: illustration of own data)

Measurement point M20 of grid M is situated in the bog area with a grass cover instead of the common needle litter cover. Roots detected through the soil analysis were thin grass roots, which could be a possible reason for the low measured biomass values.

4.2.3 Variogram analysis

Semivariograms were used to examine spatial patterns. Figure 51 shows selected variograms of soil CO_2 efflux, soil temperature and soil water content. For soil CO_2 efflux no spatial correlation was visible for most of the measurement dates (c) with one exception (d). On the 09th of April a range of 31 m was given for soil CO_2 efflux. This value should be used with care due to the high nugget effect and the uniqueness of this event. It is likely that no spatial correlation was present on this scale (distance of points:

5-10 m) referring to research by Herbst et al. (2009). Their study revealed a spatial correlation with a maximum range of 5.4 m for a relatively homogenous bare field.

Soil water content showed good spatial correlation for some measurement dates (figure 51b). Due to low spatial variability of soil temperature, the semivariance for transects WA and WB was exiguous with a tendency towards 0, showing a high spatial dependency (figure 51a). Soil water content displayed a good spatial correlation for most measurement dates for transects WA/WB, while well correlated measurement days were scarce for grid M. Ranges varied from 26.1 m to 135 m, with a median range of 62.3 m for WA/WB and a median range of 44 m for measurement grid M (table 15).

The analysis of variograms has shown that soil CO_2 efflux had no spatial correlation across this measurement setup; ranges were probably lower and could therefore not be detected.

Table 15: VESPER variogram parameters C_0, C_1 and A_1 for individual dates for soil moisture. C_0 = nugget effect; C_1 = sample variance; A_1 = range. (own data)

		C_0	C_1	A_1
M	29.10.2008	0.002	0.003	26.5
	05.11.2008	0.000	0.010	35.5
	02.04.2009	0.001	0.003	36.6
	07.05.2009	0.001	0.008	44.0
	09.04.2010	0.001	0.011	56.9
	23.06.2010	0.016	0.030	53.8
	30.06.2010	0.026	0.041	48.4
WA & WB	15.11.2006	11.2	20.7	51.8
	27.11.2006	36.8	76.6	39.3
	24.10.2007	45.9	30.4	55.0
	21.05.2008	13.0	58.3	46.8
	28.05.2008	19.5	39.1	29.3
	02.06.2008	5.1	55.6	26.1
	09.07.2008	37.8	47.5	46.1
	16.07.2008	22.4	40.0	33.5
	26.11.2008	14.5	17.8	123.4
	19.03.2009	10.5	14.6	71.8
	23.04.2009	0	27.4	27.1
	02.11.2009	29.0	23.2	62.3
	26.03.2010	46.5	42.7	92.0
	02.04.2010	34.6	90.3	135.0
	28.04.2010	28.6	50.2	85.2
	19.05.2010	28.0	38.1	77.7
	27.05.2010	45.9	46.4	90.6
	03.06.2010	21.9	56.9	71.5
	16.06.2010	41.0	61.7	88.8

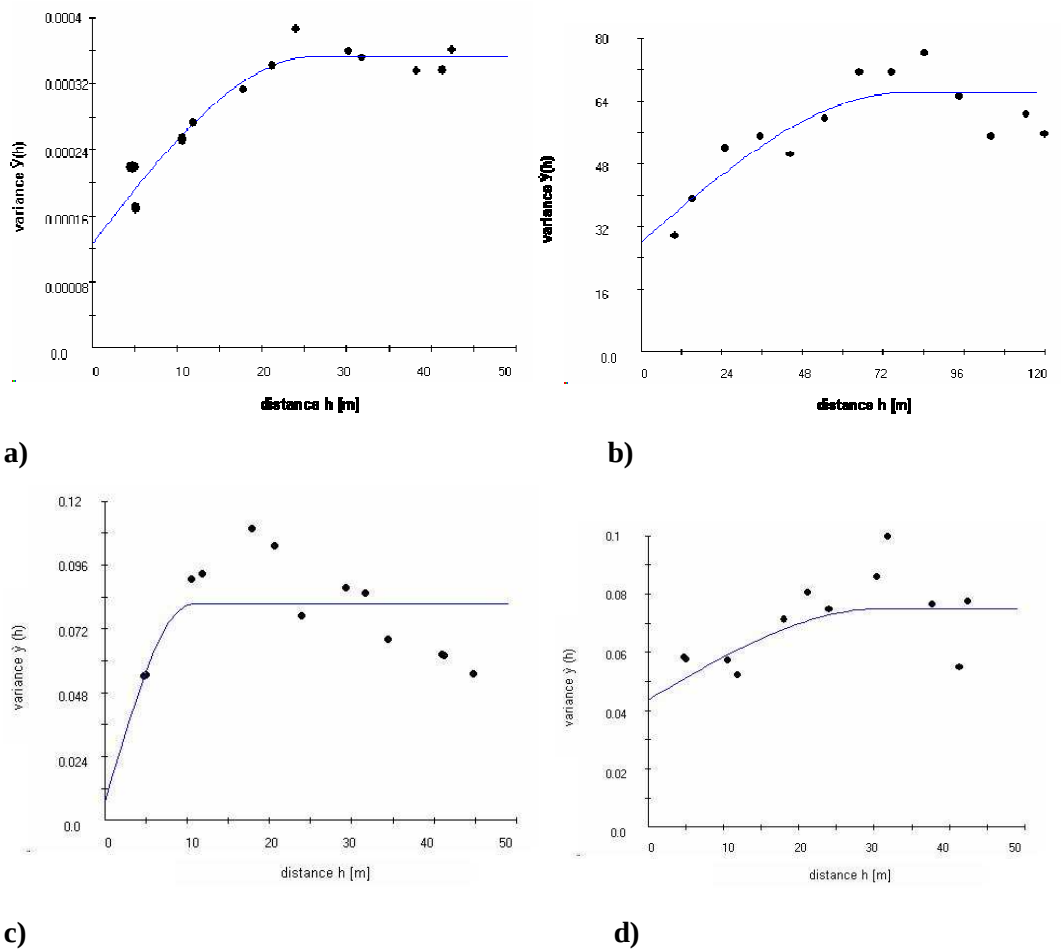

Figure 51: Selected variograms of measurement grid M for soil temperature (a), soil moisture (b) and soil CO_2 efflux (c) for the 23.11.2009. Figure 5(d) shows the variogram for soil CO_2 efflux for the 09.04.2009. (source: illustration of own data)

4.2.4 Analysis of Mean Relative Differences (MRD)

To characterize soil CO_2 efflux on a larger scale (e.g. on the scale of the river catchment), it is useful to calculate field averages or to use representative test sites. A representative test site could be that site which always shows a mean behaviour over time. This can be determined using the mean relative differences method (MRD), first applied by Vachaud et al. (1985). Calculating mean relative differences can otherwise be helpful to identify outliers and characterize spatial patterns.

Figures 52(a-c) and 53(a-c) show the ranked MRD of the transects WA/WB and measurement grid M respectively, for soil CO_2 efflux, soil temperature and soil moisture over the complete measurement period. Mean relative differences were sorted into classes, which were defined individually for each of the parameters due to great

differences in range. Equally sized classes among the individual ranges for soil respiration, soil moisture or soil temperature were aimed at, with red and dark blue signs characterizing extreme values and green signs characterizing points which can be seen as representative field averages. For the soil water content of grid M median values were used instead of mean values due to high outliers present, e.g. points located in the bog area. Additional figures of ranked MRD for individual measurement years can be found in the appendix (CD).

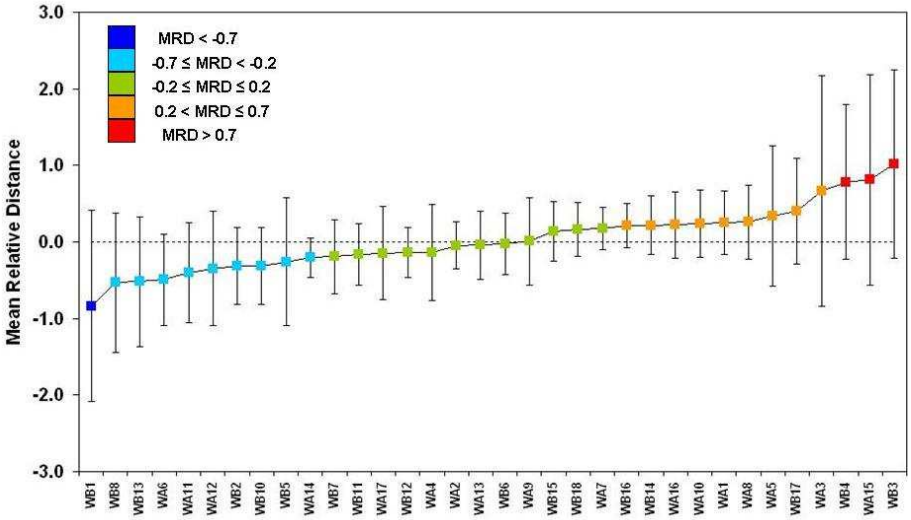

a)

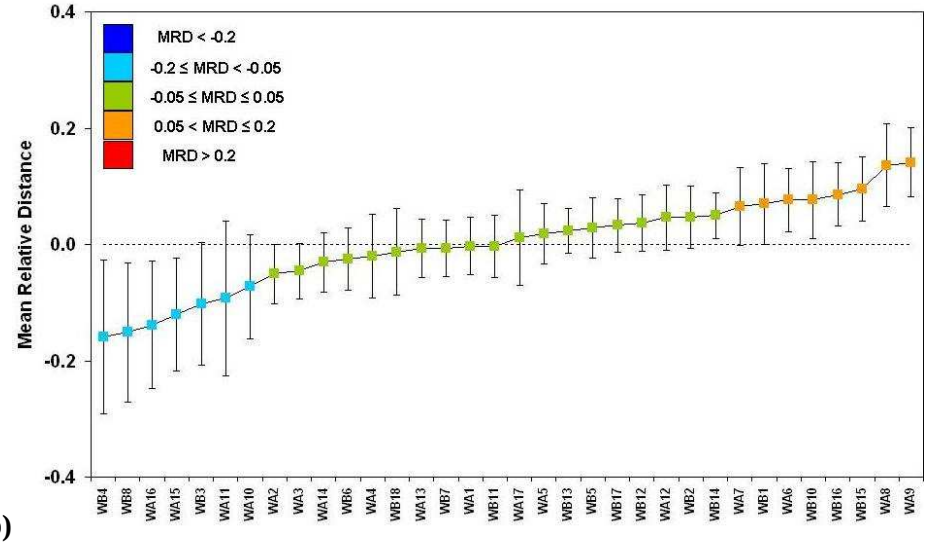

b)

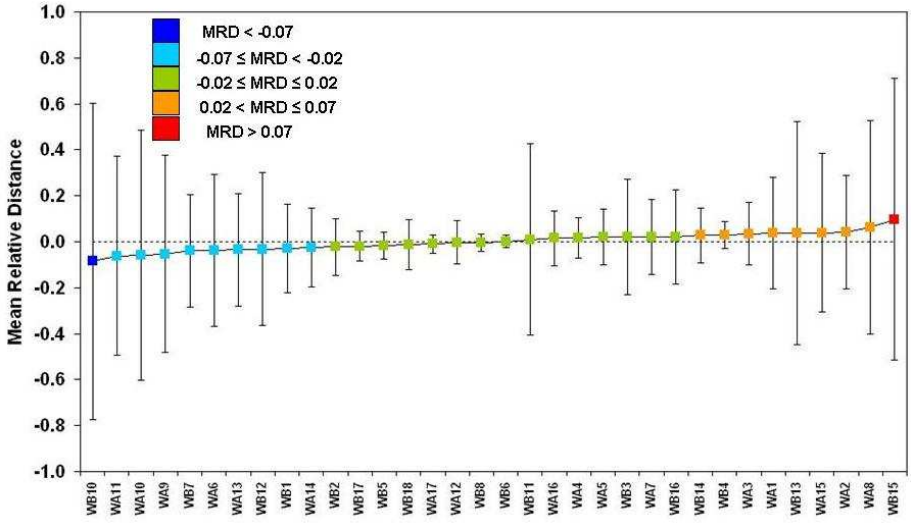

c)

Figure 52a-c: Ranked mean relative differences of soil CO_2 efflux (a), soil moisture (b) and soil temperature (c) for transects WA and WB over the whole measurement period (source: illustration of own data)

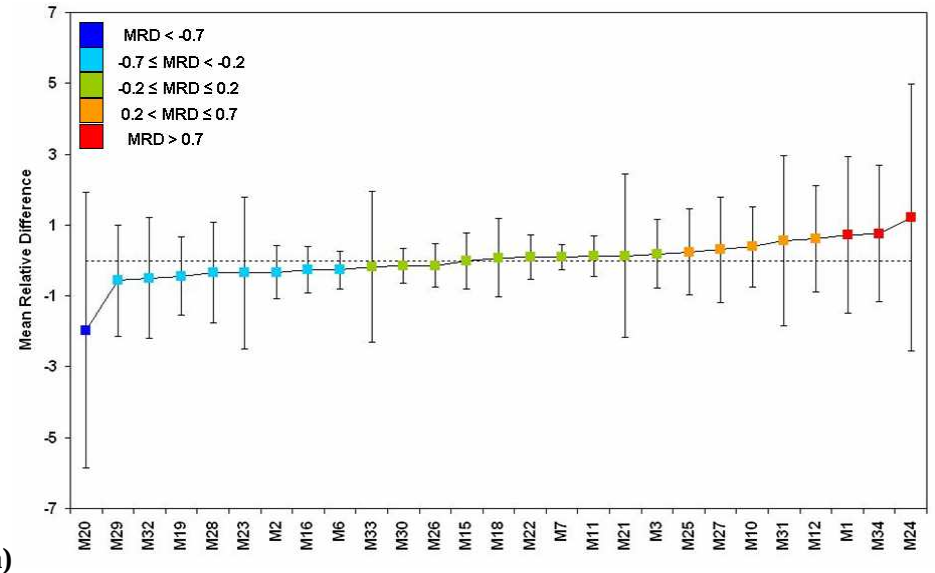

a)

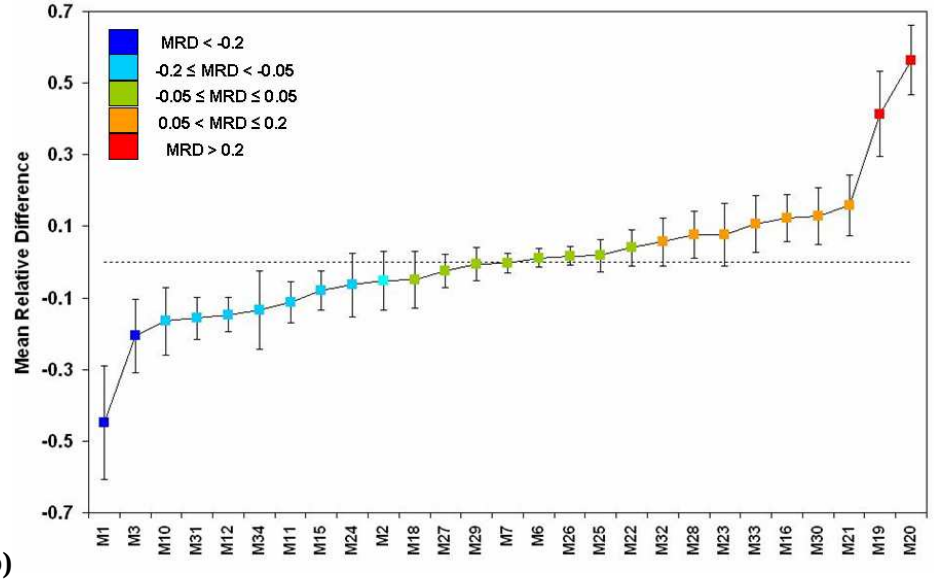

b)

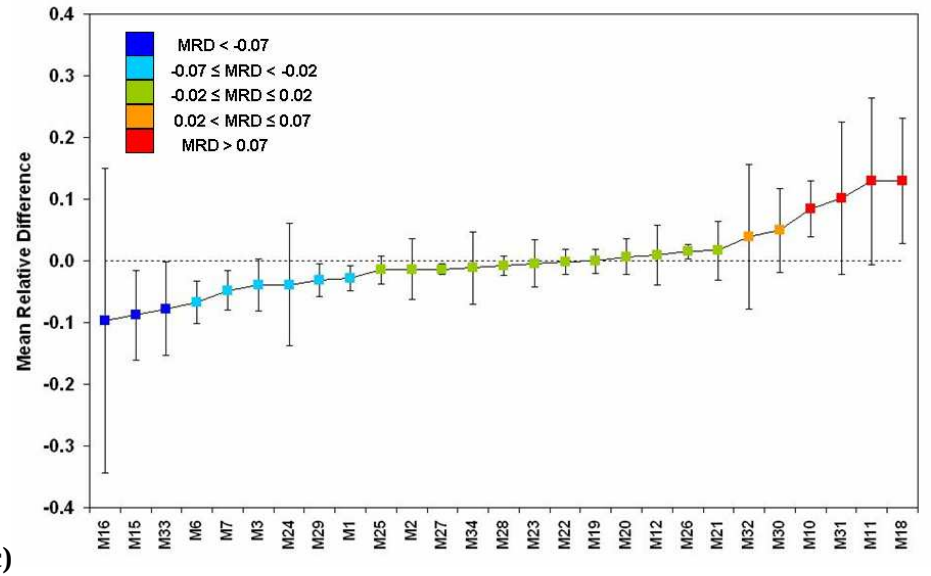

c)

Figure 53a-c: Ranked mean relative differences of soil CO_2 efflux (a), soil moisture (b) and soil temperature (c) for grid M over the whole measurement period (source: illustration of own data)

When the MRD is close to zero and the standard deviation is small, the point can be said to characterize the field average. Soil CO_2 efflux showed higher MRD values compared to soil temperature and soil water content. This can be attributed to a general higher spatial variability. Mean relative differences for soil temperature were very low, most values showed an MRD < 0.05. For soil CO_2 efflux in each case only one or two measurement points showed an MRD value below 0.05, MRD values for most measurement points exceeded 0.1.

The point WB6 for transects WA/WB could be identified characterizing the field average, having a MRD less than 0.05 for all three parameters and low standard deviation. For grid M no point could be identified showing a MRD less than 0.05 for all three parameters, the MRD for soil CO_2 efflux exceeded 0.05. The points M22 and M26 showed low MRD for temperature and soil moisture (< 0.05) and adequate MRD for soil CO_2 efflux (0.09 and 0.14 respectively). Mean soil CO_2 efflux over the whole measurement period for WB6 was 10.8 g/m²d with a range from 2.6 g/m²d to 22.8 g/m²d. This value is comparable to the calculated mean value of 10.3 g/m²d for all measurement points of WA and WB.

Mean soil CO_2 efflux rates for points M22 and M26 were 8.2 g/m²d with a range from 1.5 g/m²d to 27 g/m²d and 7.5 g/m²d with a range from 1.5 g/m²d to 17.6 g/m²d respectively. This corresponds to the calculated mean value of 7.9 g/m²d for soil CO_2 efflux.

Graphical visualization was used to help detecting spatial patterns in soil CO_2 efflux in combination with soil temperature and soil moisture (figures 54 and 55).

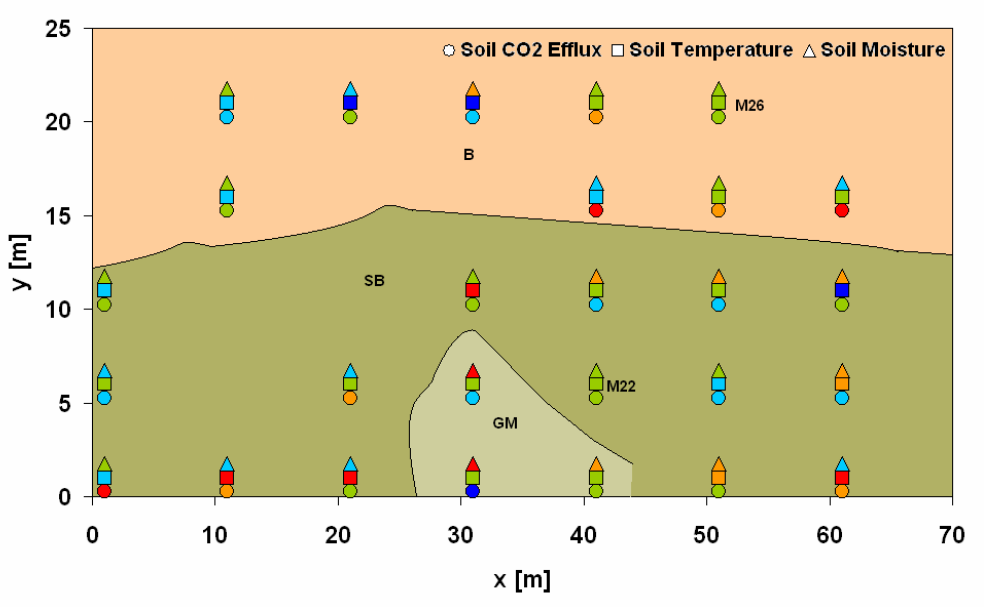

Figure 54: Areal distribution of MRD groups for soil CO_2 efflux (*dark blue*: MRD < -0.7, *light blue*: -0.7 ≤ MRD < -0.2, *green*: -0.2 ≤ MRD ≤ 0.2, *orange*: 0.2 < MRD ≤ 0.7, *red*: MRD > 0.7), soil temperature (*dark blue*: MRD < -0.07, *light blue*: -0.07 ≤ MRD < -0.02, *green*: -0.02 ≤ MRD ≤ 0.02, *orange*: 0.02 < MRD ≤ 0.07, *red*: MRD > 0.07) and soil moisture (*dark blue*: MRD < -0.2, *light blue*: -0.2 ≤ MRD < -0.05, *green*: -0.05 ≤ MRD ≤ 0.05, *orange*: 0.05 < MRD ≤ 0.2, *red*: MRD > 0.2). Soil types: B (Cambisol), SB (Planosol-Cambisol) and GM (Histosol-Gleysol; Niedermoorgley) (source: illustration of own data)

For measurement grid M (figure 54) a trend was visible of slightly decreased soil temperature values among the northern points of the measurement plot and slightly increased soil temperature values among the bottom points. For soil CO_2 efflux the occurrence of extreme values seemed to be randomly distributed over the measurement plot. Extreme values for soil moisture were mostly restricted to lower parts of the measurement plot, where bog is present.

Analyzing other environmental factors such as substrate availability or root distribution might help to find out whether similar soil temperature and soil moisture values are responsible for similar soil CO_2 efflux or whether other factors play an important role. The graphical visualization helps to understand that patterns of soil CO_2 efflux did not follow patterns of soil temperature. High soil temperatures did not necessarily lead to high soil CO_2 efflux. Slightly elevated soil temperatures and slightly decreased soil moisture could lead to slightly elevated soil CO_2 efflux as well as slightly decreased soil CO_2 efflux. To conclude some other factor beside soil temperature and soil moisture must be the reason for the spatial variability in soil CO_2 efflux, at least for this special case. In a study of spatial patterns in two stands of Douglas fir (*Pseudotsuga menziesii*) and beech (*Fagus sylvatica*) Longdoz et al. (2000) detected horizontal heterogeneity in root density, SOM (soil organic matter) biomass, C:N and lignin:N ratios, soil acidity and soil texture as possible causes for spatial variability in soil CO_2 efflux. Raich and Tufekcioglu (2000) set a focus on tree species composition as a main driver for spatial patterns in soil respiration. Soe and Buchmann (2005) took up the hypothesis by Longdoz et al. (2000) and assumed that stand characteristics could explain some of the spatial variation. Their study showed that the combination of root, soil and stand structure measurements might help to understand mechanisms underlying soil respiration and the role of soil respiration itself in the global carbon budget.

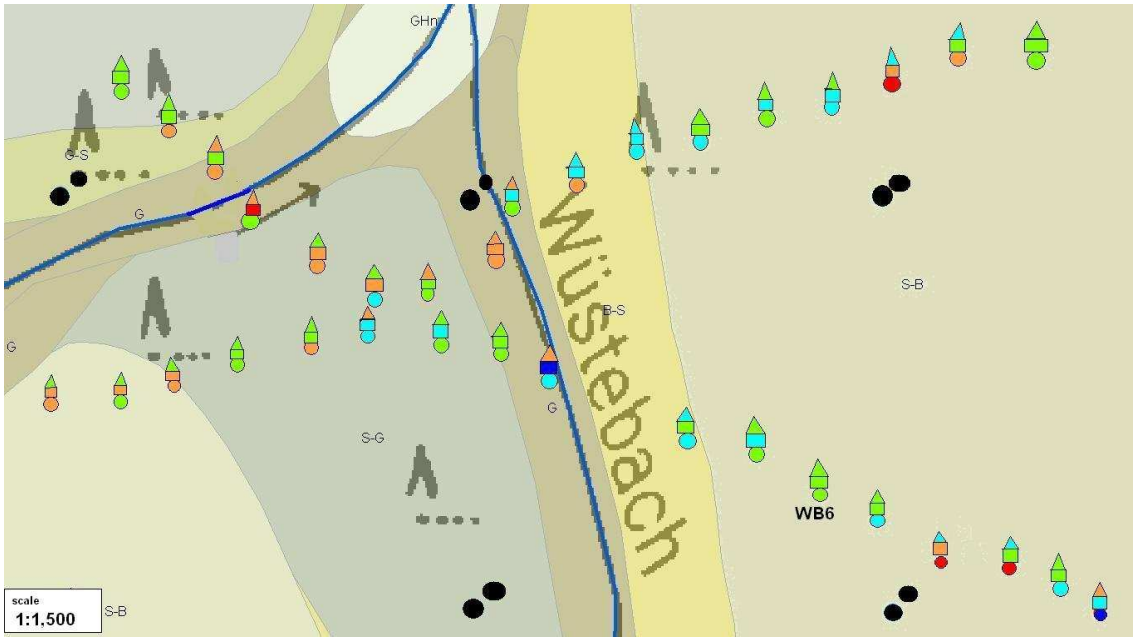

Figure 55: Areal distribution of MRD groups for soil CO_2 efflux (circle, *dark blue*: MRD < -0.7, *light blue*: -0.7 ≤ MRD < -0.2, *green*: -0.2 ≤ MRD ≤ 0.2, *orange*: 0.2 < MRD ≤ 0.7, *red*: MRD > 0.7), soil temperature (square, *dark blue*: MRD < -0.07, *light blue*: -0.07 ≤ MRD < -0.02, *green*: -0.02 ≤ MRD ≤ 0.02, *orange*: 0.02 < MRD ≤ 0.07, *red*: MRD > 0.07) and soil moisture (triangle, *dark blue*: MRD < -0.2, *light blue*: -0.2 ≤ MRD < -0.05, *green*: -0.05 ≤ MRD ≤ 0.05, *orange*: 0.05 < MRD ≤ 0.2, *red*: MRD > 0.2) (source: illustration of own data)

A similar picture was visible for transects WA and WB (figure 55), but some structures can be detected. Extreme values for soil CO_2 efflux could be found on the eastern slope, together with mostly lower efflux rates for the rest of the points. Soil CO_2 efflux rates in the western region tended to be elevated for several points. Soil moisture was higher with high MRD for points close to the stream. For a number of measurement points in WA/WB or in M it was visible that soil CO_2 efflux and soil moisture were opposed to each other. High soil moisture values were found in connection with low soil CO_2 efflux, while high soil CO_2 efflux rates were found in connection with low soil moisture.

5 Modelling soil CO_2 efflux and environmental parameters

5.1 Simulation of soil temperature and soil moisture as a modelling basis for PATCIS

To obtain continuous soil temperature and soil moisture data as input for the soil respiration model PATCIS, the model SIMULAT 1d was applied. The simulated period begins on the 1st of January 2007 and ends on the 31st of December 2009. The use of hourly values for the simulation results in 8760 time steps per year (the 29th of February 2008 was neglected). The model was calibrated for soil heat parameters, since measured soil temperature values were of sufficient quality for comparison with simulated soil temperature values. Measured soil moisture data included numerous gaps and characterized a value measured over an interval of 15 cm or less, depending on the insertion depth of the moisture probe. Error in measurements was high, depending on insertion depth, removal of litter and high spatial variability on a small scale. Therefore soil moisture was not used for model validation and parameters connected solely to soil moisture were not calibrated. The annual sum of precipitation for 2007 was comparably high with 1600 mm, while annual sums for 2008 and 2009 were 1318 mm and 1224 mm respectively. Only 29% of the precipitation evaporated according to the simulation, while discharge accounted for 70.9%. Figure 56 exemplary illustrates the amount of precipitation, simulated discharge and simulated actual evapotranspiration for the year 2007.

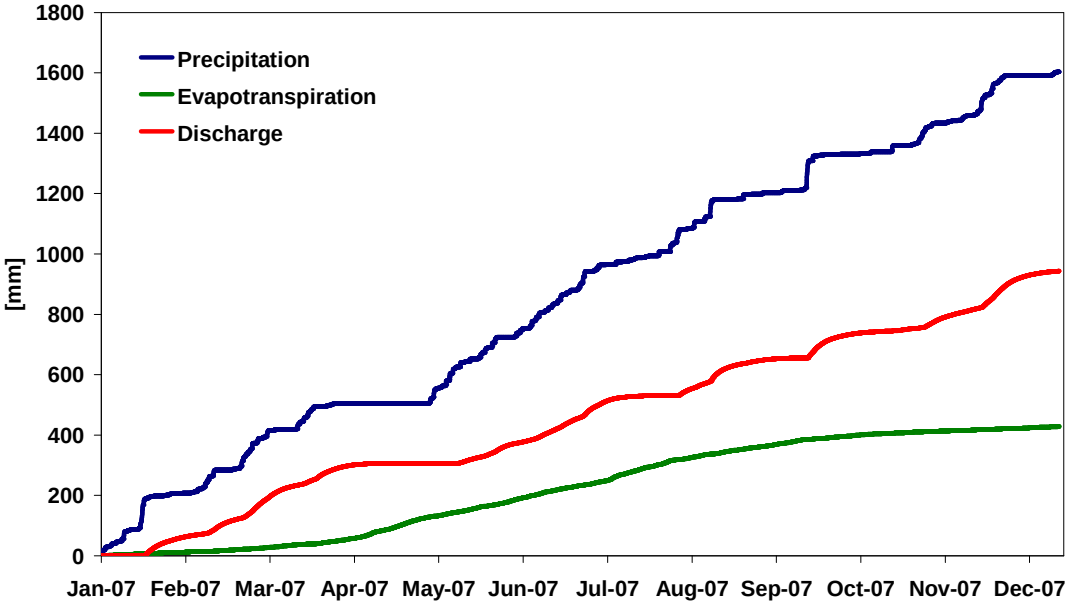

Figure 56: Cumulative precipitation and simulated actual evapotranspiration and discharge for the year 2007 (mean values of all measurement points)

Potential and actual evapotranspiration showed similar features with regard to peak height (figure 57), apart from smaller differences towards the beginning of the year 2007. Elevated discharge values follow intense precipitation events.

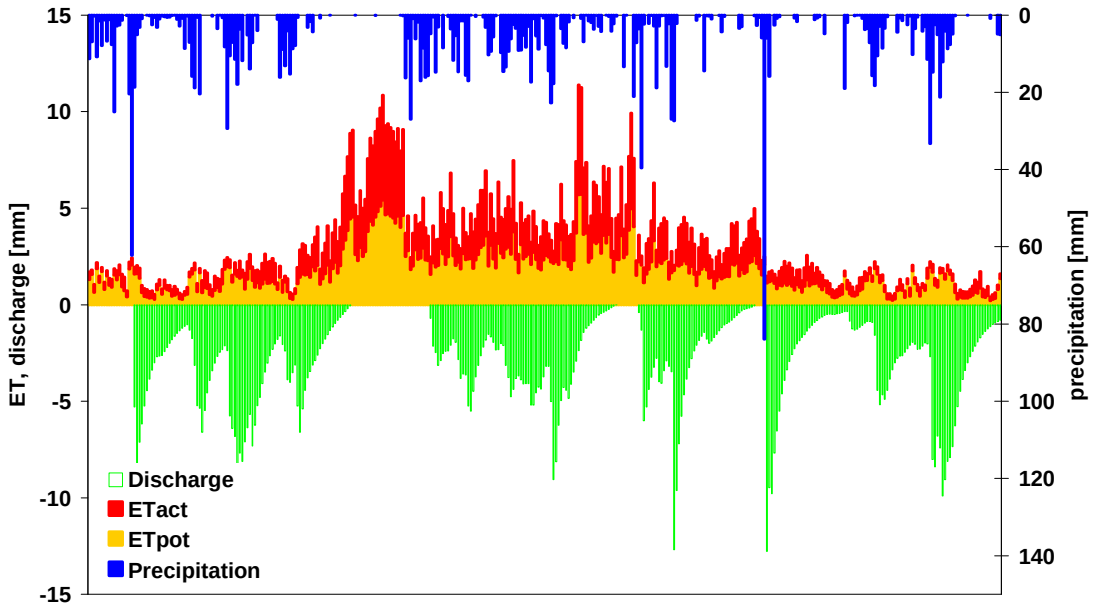

Figure 57: Simulated potential and actual evapotranspiration, discharge and precipitation for 2007 (mean values of all measurement points of WA/WB)

Soil moisture and soil temperature were simulated for all measurement points from 2007 to 2009. The year 2007 was used for manual calibration (values of the saturated water conductivity and the heat capacity coefficient were calibrated), while 2008 and 2009 served as validation years.

Measured soil temperature values in 11 cm depth were compared to simulated soil temperature values (figure 58). Coefficients of determination were between 86% and 99%, with a mean of 95%. All relationships were highly significant with $p < 0.001$.

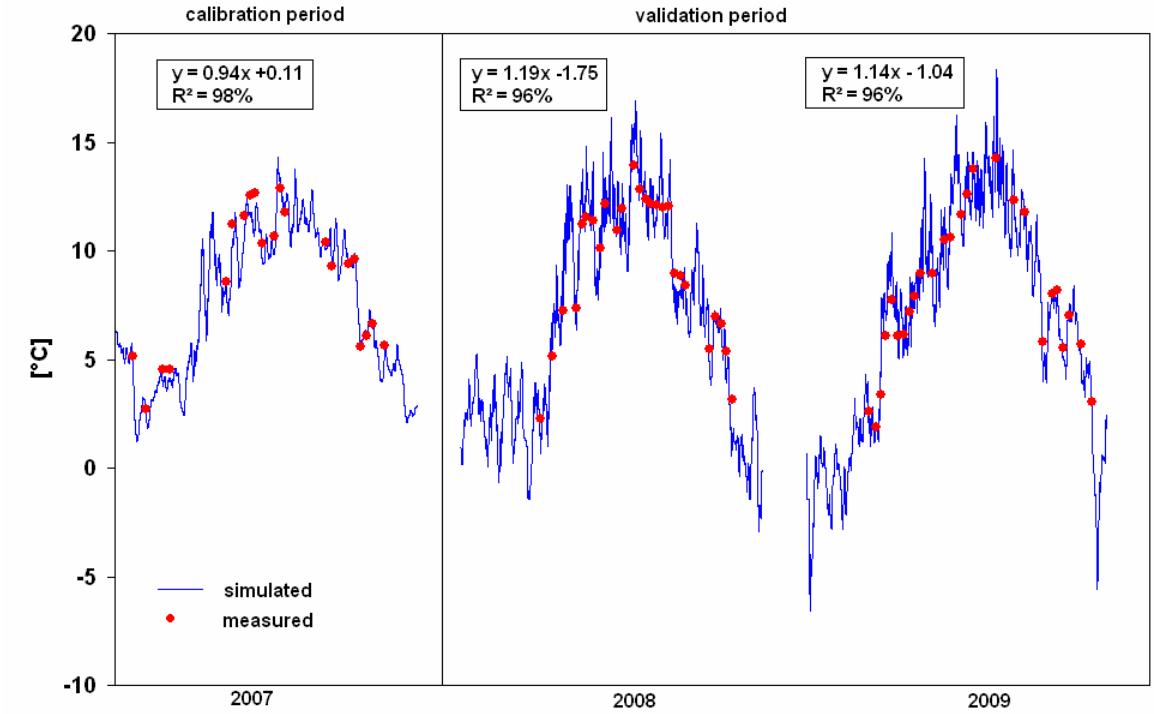

Figure 58: Simulated and measured soil temperature as a mean of all measurement points (11 cm depth) from 2007-2009. 2007 was used as calibration period (calibrated for saturated hydraulic conductivity and heat capacity), while 2008 and 2009 were used as validation periods with parameterization after 2007. All relationships were highly significant ($p < 0.001$). Gaps occur due to the removal of initial values (discontinuous simulation).

The comparison of simulated soil moisture values to measured soil moisture values was difficult. Soil moisture was measured over an integral of 15 cm, including needle litter. In some cases needle litter was removed, in other cases the moisture probe could not be totally immerged into the soil due to skeleton content. The measurements took place at different spots each time, due to the disturbance of the soil by the moisture probe. For each measurement point 2-3 soil moisture measurements were undertaken, from which a mean value was calculated to reduce small-scale spatial variability. Results of soil moisture measurements for the organic layers of the bog area need to be taken with care because the moisture probe was not calibrated for bog area as would be required. The litter layer density used in the model equals the litter layer density within the collar, while soil moisture measurements took place at spots where litter layer densities might differ (or might have been removed completely). Comparisons between simulated and measured soil moisture values were done for a couple of points from the measurement grid M for the year 2009. Figure 59a shows measured soil moisture values for measurement point M1, which displays a thick litter layer of 4 cm, and mean simulated soil moisture values of the top 15 cm. Measurement point M2 does not show a thick litter layer and therefore a higher measured soil moisture (figure 59b). Simulated soil moisture values of the top 15 cm tend to underestimate the measured soil moisture, while simulated soil moisture

values at a depth of 15 cm show an overestimation. Points of the bog area could not be simulated sufficiently (figure 59c). Soil moisture values were largely underestimated.

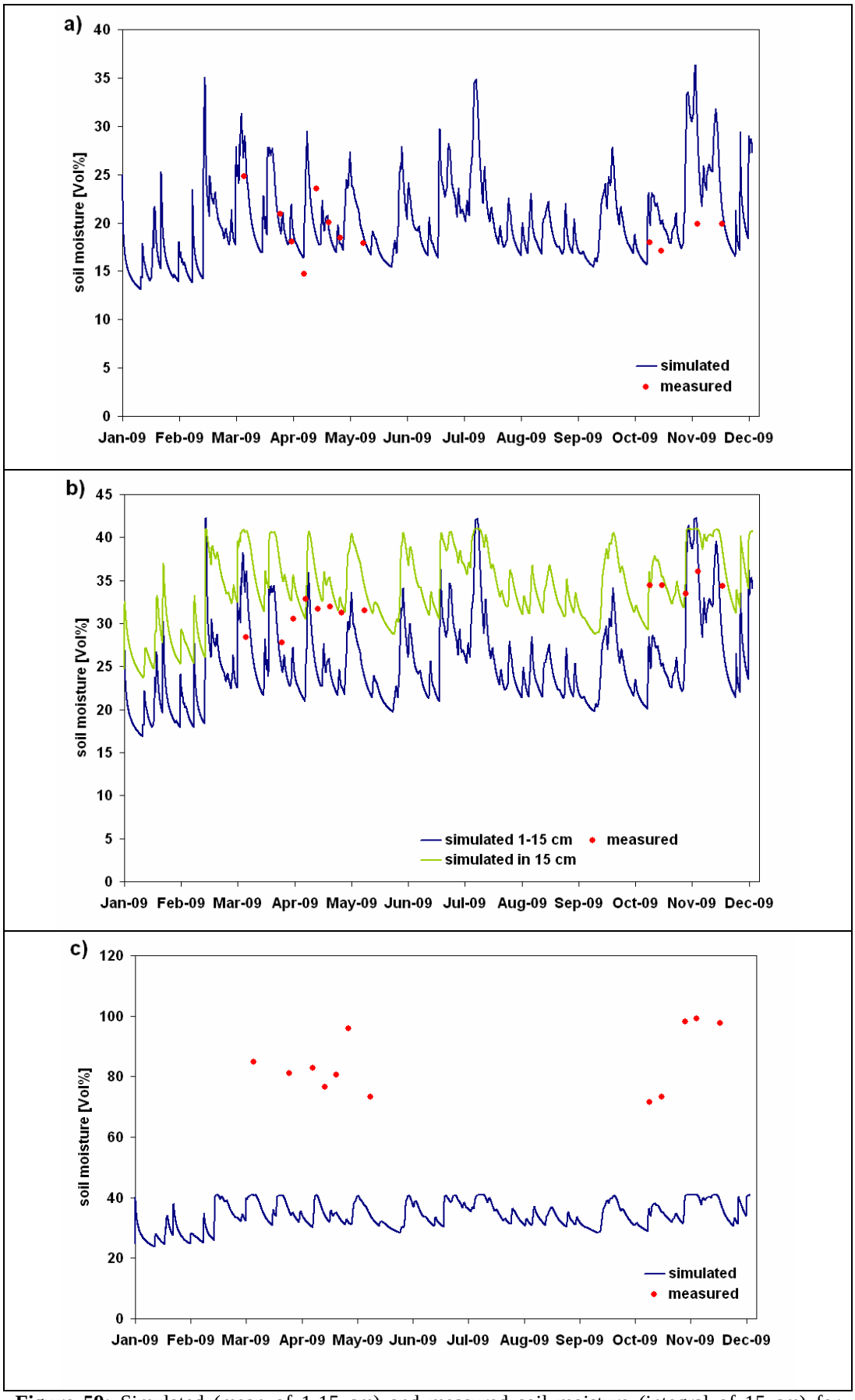

Figure 59: Simulated (mean of 1-15 cm) and measured soil moisture (integral of 15 cm) for measurement point M1 (a), M2 (b) and M20 (c) for the year 2009

Figure 60 shows simulated soil moisture values for each layer of measurement point WA1 for the year 2007 and precipitation values. Soil moisture values of the upper litter layer (0-2 cm) showed greater fluctuations during the year, in accordance to the course of precipitation. These fluctuations were reduced with decreasing simulation depth. A simulation depth of 40-60 cm displayed an almost constant level of soil moisture during the year.

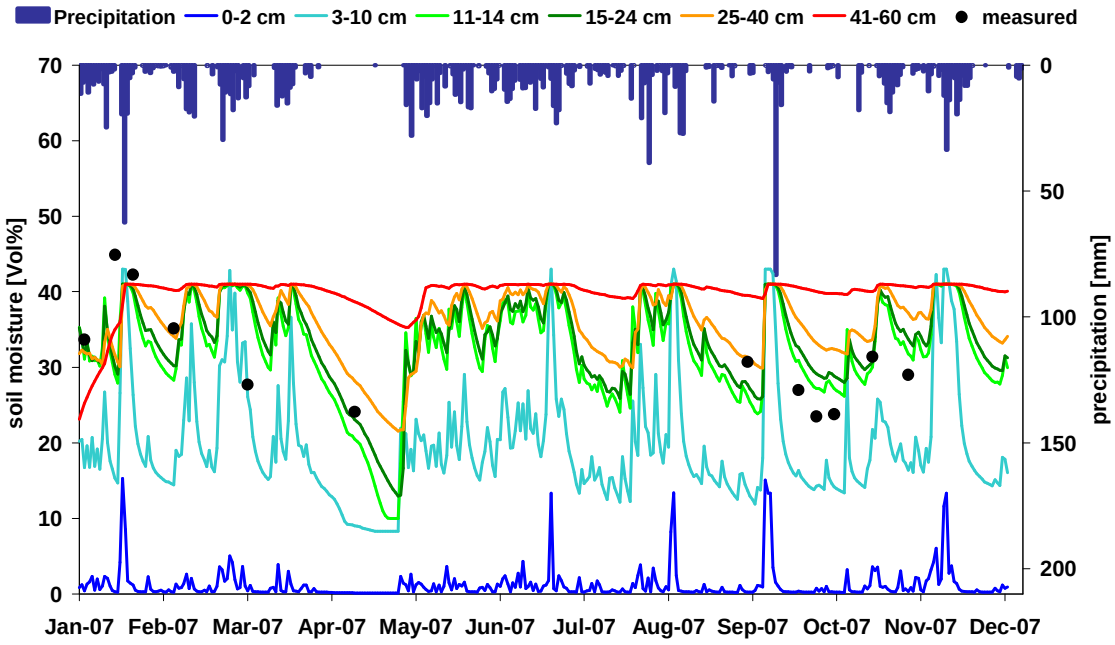

Figure 60: Simulated soil moisture values for each layer of WA1, measured soil moisture and measured precipitation for the year 2007

5.2 Simulation of soil CO_2 efflux

5.2.1 Parameterization of PATCIS

Before simulation of soil CO_2 efflux could take place, the model needed to be parameterized, using the Latin Hypercube analysis. In addition to this the model was calibrated for some points with insufficient quality of model results. For the calibration the parameter organic matter content was changed. The model PATCIS features a parameterization file with several parameters used for model parameterization (see table 16).

Table 16: Parameters used for Latin Hypercube parameterization

parameter	name / unit	range	equation
activation energy at < 10°C	E / [kJ mol^{-1}]	$6*10^5$-$1*10^6$	(20)
activation energy at 10-20°C	E / [kJ mol^{-1}]	$6*10^5$-$1*10^6$	(20)
activation energy at > 20°C	E / [kJ mol^{-1}]	$6*10^5$-$1*10^6$	(20)
moisture parameter a for mineral soil	a / --	5-30	(22)
moisture parameter c for mineral soil	c / --	0.02-0.2	(22)
moisture parameter a for forest soil	a / --	5-10	(22)
moisture parameter c for forest soil	c / --	0.02-0.2	(22)
Michaelis Menten constant	K_m / [mg O_2 m^{-3}]	$4*10^4$-$1*10^5$	(23)
optimal organic matter decay rate	λ_{lab} / mg CO_2 g^{-1} s^{-1}	$3*10^{-6}$-$7*10^{-6}$	(12)
optimal litter decay rate	λ_{res} / mg CO_2 g^{-1} s^{-1}	0.01-0.2	(12)
microbial respiration rate parameter	γ_m / mg CO_2 g^{-1} s^{-1}	1-2	(13)
optimal root respiration rate for roots Ø 5-10 mm	γ_{ri} / mg CO_2 g^{-1} s^{-1}	$3*10^{-5}$-$6*10^{-5}$	(14)
optimal root respiration rate for roots Ø > 10 mm	γ_{ri} / mg CO_2 g^{-1} s^{-1}	0.05-0.5	(14)
root respiration constant	γ_r / mg CO_2 g^{-1} s^{-1}	0.01-0.02	(16)

Instead of using an automatic calibration procedure, the model was parameterized with the Latin Hypercube method, which uses stratified sampling without replacement (see chapter 3.52). The probability distribution is split into *n* intervals of equal probability, where *n* is the number of samples that are to be performed on the model. As the simulation progresses each of the *n* intervals is sampled once. The sum of squares of the residual between estimated and measured CO_2 effluxes is used as an indicator to find parameter values which produce the best estimate of soil CO_2 efflux.

For parameterization, PATCIS was run 150 times with different model parameter combination sets. Results, as well as the quality of simulation for each parameter set, were displayed in the output. Each year was calibrated individually for transects WA/WB and measurement grid M. The five best parameter combinations for each measurement point and year were selected. For grid WA/WB the model was validated for the years 2008 and 2009 by using parameter values of the best parameter combination from 2007 and for grid M the model was validated for the year 2009 by using parameter values of the best parameter combination from 2008, respectively.

Parameterization of individual years for individual points resulted in several good fits of parameter combinations with totally different character (see figures 61 and 62 for point M1), which resembles the concept of equifinality (Beven 2006).

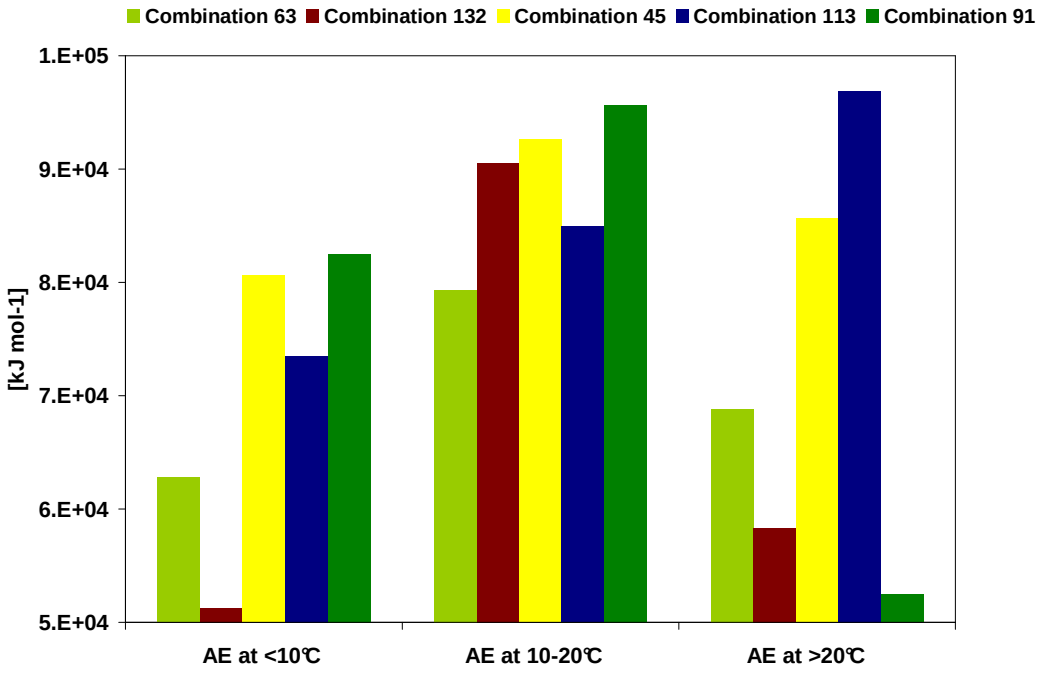

Figure 61: Values of activation energy for the five best parameter combinations for point M1 for 2008. Note that temperature > 20°C are rarely been measured and therefore not representative for the simulation.

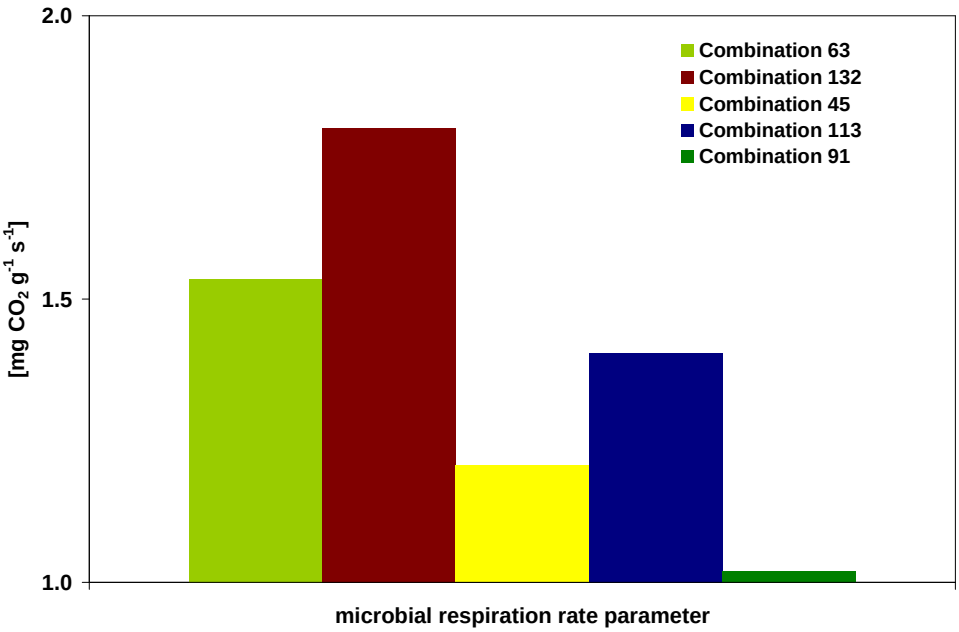

Figure 62: Values of optimal organic matter decay rate for the five best parameter combinations of M1 for 2008

Only 35 of the 150 different parameter combinations were among the five best fits for all measurement points of WA/WB for the calibration year 2007, while in 2008 74 and for 2009 100 different parameter combinations were among the best five (figures 63-65).

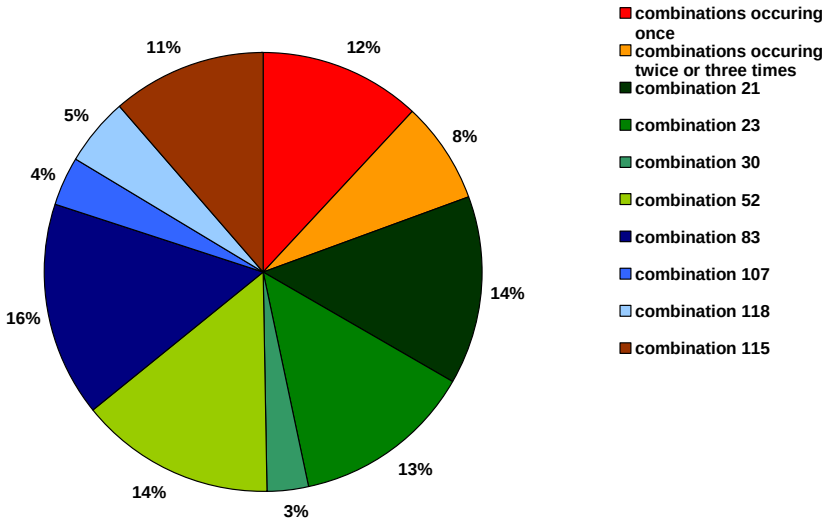

Figure 63: Occurrence of parameter combinations among the five best fits of WA/WB for 2007

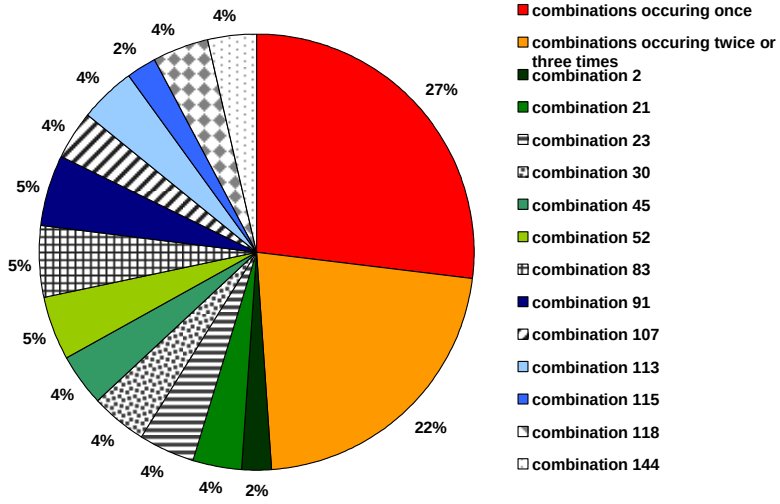

Figure 64: Occurrence of parameter combinations among the five best fits of WA/WB for 2008

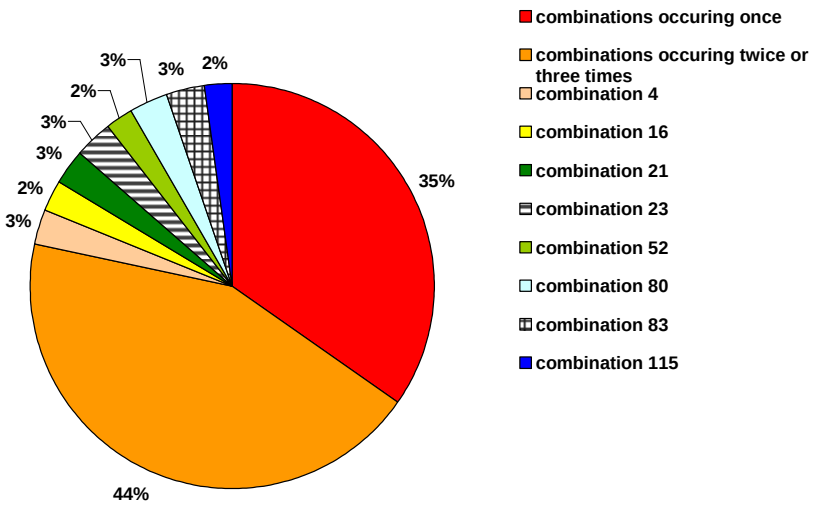

Figure 65: Occurrence of parameter combinations among the five best fits of WA/WB for 2009

For measurement grid M the year 2008 features 106 different parameter combinations, while year 2009 shows 71 different parameter combinations (figures 66 & 67).

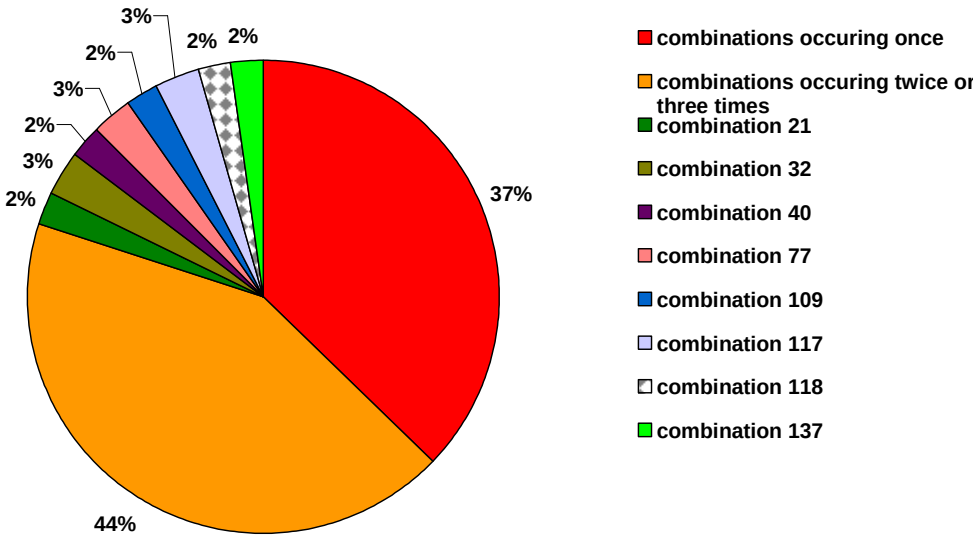

Figure 66: Occurrence of parameter combinations among the five best fits of M for 2008

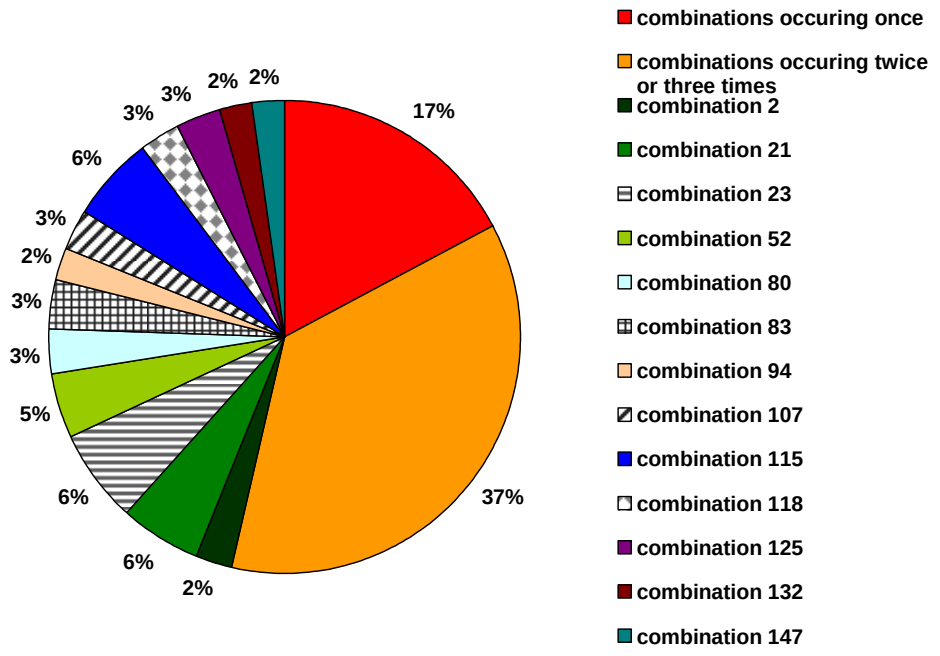

Figure 67: Occurrence of parameter combinations among the five best fits of M for 2009

The calibration year 2007 exhibited 27 out of 34 measurement points with an identical parameter set for the five best fits. Therefore, spatial variability concerning model parameters was low. For 2008 (2nd calibration year of WA/WB) a maximum of 7 measurement points out of 34 shared the same parameter set among the five best fits, while for 2009 (3rd calibration year of WA/WB) only a maximum of 5 measurement points out of 34 shared the same parameter set among the best fits. The spatial variability of calibration parameters was high during those years.

For grid M only two identical parameter sets of the five best fits were present for 2008, for 2009 no identical parameter set existed. The results from the validation of the 2007 parameter combinations for the years 2008 and 2009 for transects WA/WB were of moderate quality. The coefficient of determination was similar, but values were generally overestimated for both years.

Each year displayed one measurement date, which held an outlier position. For the year 2007 it was the 25th of April, for 2008 the 28th of May and for 2009 the 20th of August. Excluding these days improved the fit, except for 2009 for transects WA and WB. The year 2009 generally showed low coefficients of determination for the calibration, as well as for the validation. The validation of 2009 mostly brought about an underestimation of measured values. The model was calibrated using measured soil organic matter for some points. Where measurement values of soil organic matter were not available, they were transferred from other points, which may cause larger uncertainties in the model output.

5.2.2 Sensitivity Analysis

A sensitivity analysis was performed on parameters and factors driving soil respiration by applying a +/-10% change on each parameter separately. Results can be found in table 17; parameters are ranked by their order of influence on soil CO_2 efflux. The evaluation of the sensitivity is based on Lenhart et al. (2002) for each parameter (eq 42); results can be found in table 18.

$$SI_{10} = \frac{output_{+10\%} - output_{-10\%}}{output_{ref}} \quad (42)$$

in which

SI_{10} = sensitivity index with 10% change of input parameter

$output_{+10\%}$ = model output with input parameter increased by 10%

$output_{-10\%}$ = model output with input parameter decreased by 10%

$output_{ref}$ = model output with original input parameter

Table 17: Sensitivity analysis of model parameters

Variable or Parameter	% change in output for a 10% increase of model parameter	% change in output for a 10% decrease of model parameter
Soil temperature	+9.81	-7.71
Soil organic matter	+8.75	-7.63
Microbial respiration constant	+8.60	-7.53
Activation energy	-2.70	+4.33
Soil Moisture	+2.48	-1.77
Moisture parameters for roots and microbes	+2.4	-1.80
Root respiration constant	+2.37	-1.24
Live fine root biomass	+2.36	+0.38
Oxygen concentration constant	-0.60	+1.77
Optimal specific organic matter decomposition rate	+1.44	-0.32
Soil bulk density	+1.20	+0.55
Optimal specific fine root respiratory rate	+0.67	-0.45
Aboveground litter fall	+0.63	+0.49
Soil particle density	+0.53	+0.56

An increase in temperature of 1°C resulted in an increase of soil CO_2 efflux by 9.7%, while a decrease in temperature of -1°C resulted in a decrease of soil CO_2 efflux by 7.1%.

Table 18: Sensitivity index of model parameters and ranking after Lenhart et al. (2002)

Variable or Parameter	SI-Index	
Soil temperature	0.23	high
Soil organic matter	0.17	average
Microbial respiration constant	0.16	average
Activation energy	0.01	negligible to low
Soil moisture	0.01	negligible to low
Moisture parameters for roots and microbes	0.04	negligible to low
Root respiration constant	0.03	negligible to low
Live fine root biomass	0.02	negligible to low
Oxygen concentration constant	0.02	negligible to low
Optimal specific organic matter decomposition rate	0.02	negligible to low
Soil bulk density	0.002	negligible to low
Optimal specific fine root respiratory rate	0.002	negligible to low
Aboveground litter fall	0.002	negligible to low
Soil particle density	0.000006	negligible to low

The most important parameter controlling soil CO_2 efflux was soil temperature, which had the greatest impact during summer months. This is shown in figure 68 in which simulated temperature was decreased and increased by 10%. This agrees well with previous studies (Moncrieff & Fang 1999, Hui & Luo 2004, Saiz et al 2007). Considering the high quality of simulations, this results in a low uncertainty concerning soil temperature.

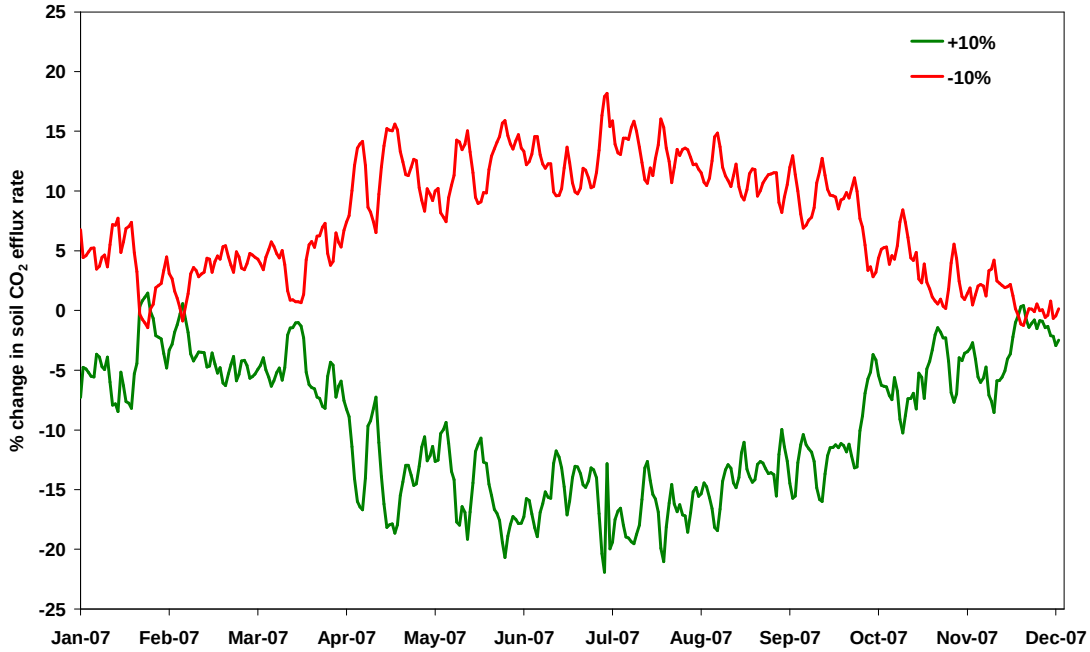

Figure 68: Sensitivity of modelled soil CO_2 efflux to a ±10% change in soil temperature for measurement point WA2 for 2007.

The seasonal trend for the influence of soil moisture on soil CO_2 efflux was more variable than that of soil temperature throughout the year, nevertheless a decrease or increase of

10% resulted in a high impact on soil moisture during months, where precipitation and soil moisture were low (figure 69). The introduced greater pressure on soil moisture conditions through an increase or decrease provided limiting conditions for soil respiration.

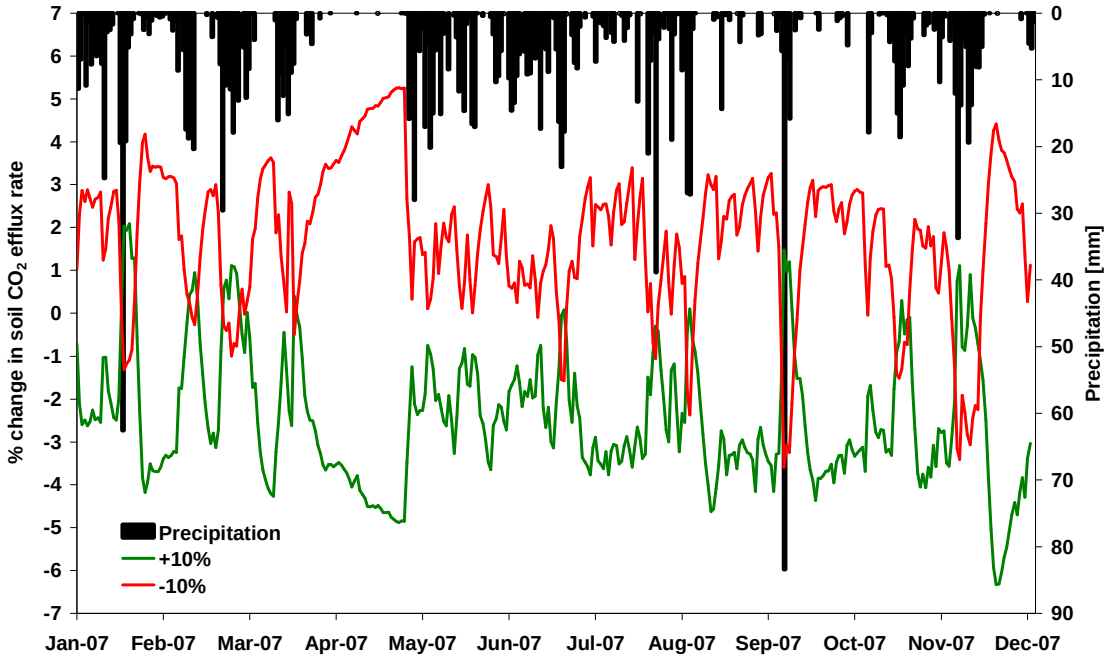

Figure 69: Sensitivity of modelled soil CO_2 efflux to a ±10% change in soil moisture for WA2 for 2007

Another important factor controlling soil respiration was soil organic matter. The sensitivity of the efflux to organic matter present in the soil profile and the comparably smaller sensitivity to live root biomass confirmed the heterotrophic component as a larger contributor to soil respiration as compared to autotrophic respiration. Previous studies (Hui & Luo 2004, Saiz et al. 2007) detected autotrophic respiration as a larger contributor to soil respiration as compared to heterotrophic respiration, which resulted in a higher sensitivity of model results to changes in parameters connected to autotrophic respiration. On the other hand the sensitivity analysis showed other factors such as soil particle density, moisture parameters and aboveground litter fall with a much more limited role on soil CO_2 efflux (table 17).

5.2.3 Seasonal variation of soil CO_2 efflux and soil respiration

Simulated mean daily total soil CO_2 efflux rates simulated with the process-based model PATCIS increased from 1.3 g CO_2 $m^{-2}d^{-1}$ in spring to the maximum value of 31.5 g CO_2 $m^{-2}d^{-1}$ in summer and decreased to 1.2 g CO_2 $m^{-2}d^{-1}$ in winter. The total annual CO_2 efflux for simulated years ranged from 2528 g CO_2 $m^{-2}a^{-1}$ to 3590 g CO_2 $m^{-2}a^{-1}$. Transects WA and WB showed higher annual efflux rates compared to measurement grid M (figure 70). Moncrieff and Fang (1999) reported an annual efflux of 5136 g CO_2 $m^{-2}a^{-1}$, while other studies with PATCIS resulted in comparably lower values of 691 g CO_2 $m^{-2}a^{-1}$ (Saiz et al. 2007) or 1211 g CO_2 $m^{-2}a^{-1}$ (Hui & Luo 2004). The global annual soil respiration database of Raich and Schlesinger (1992) show a range of annual soil respiration rates from 250-1255 g CO_2 m^{-2} a^{-1} for temperate coniferous forest systems.

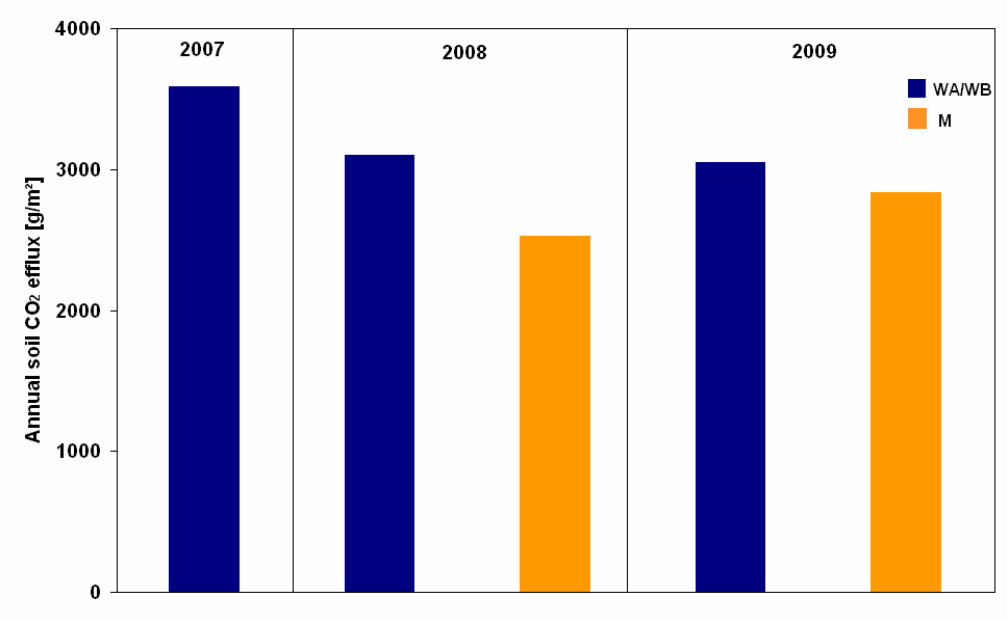

Figure 70: Simulated mean annual soil CO_2 efflux rates of transect WA/WB and grid M

The simulated seasonal trend of soil CO_2 efflux in transects WA and WB (figure 71) and for grid M (figure 72) was similar for all simulated years, as it is driven by the same climate. Soil CO_2 efflux increased during spring and summer, and reached mean maximum values of 31.5 g CO_2 m^{-2} d^{-1} in July 2007. Similar to measured values (chapter 4.1.1) soil CO_2 efflux rates declined again during fall (September/October), reaching values close to those in spring (April).

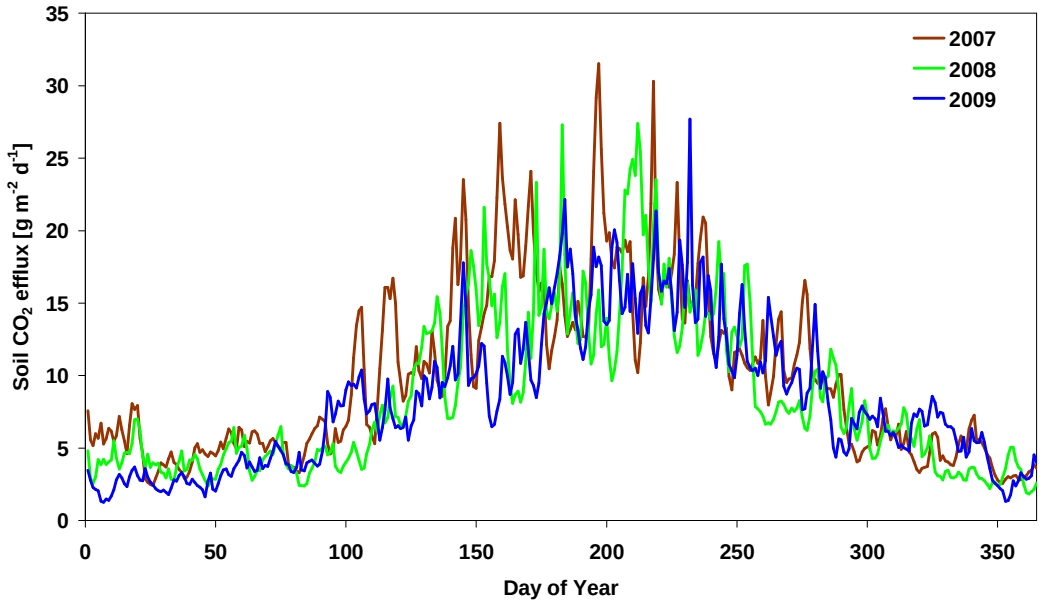

Figure 71: Simulated mean seasonal soil CO_2 efflux rates of transects WA/WB for the years 2007-2009

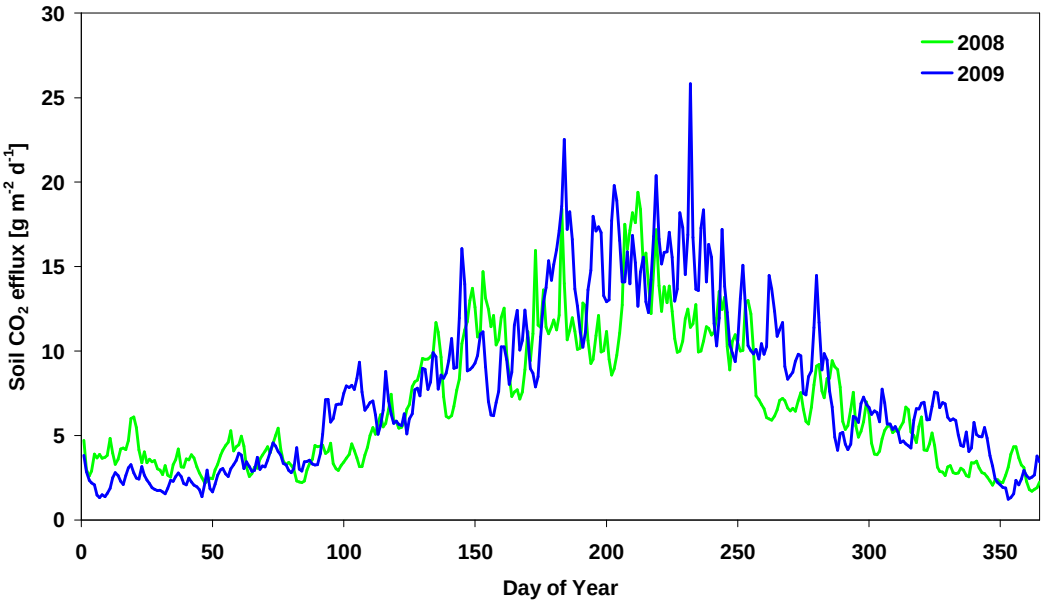

Figure 72: Simulated mean seasonal soil CO_2 efflux rates of grid M for the years 2008-2009

Soil temperatures in layer 2 (organic layer) of transect WA showed the same seasonal course as the soil CO_2 efflux (figure 74) for the year 2007. In some cases soil moisture featured a contrary seasonal course compared to soil temperature and soil CO_2 efflux, in other cases high soil moisture came along with soil temperature and soil CO_2 efflux. Sudden increases in soil moisture conditions during summer lead to a subsequent major increase in soil CO_2 efflux. This corresponds to findings of Hanson et al. (2003), who

pointed out the effects of drought periods on microbial respiration. While dry periods cause cumulative death of microbial cells and therefore a decrease in microbial soil respiration, even a small precipitation event shortly after this period leads to a significant increase in soil respiration due to the sudden substrate availability. High precipitation events during colder months on the other hand did not cause this effect (figure 73). Here the low soil temperature was the crucial factor.

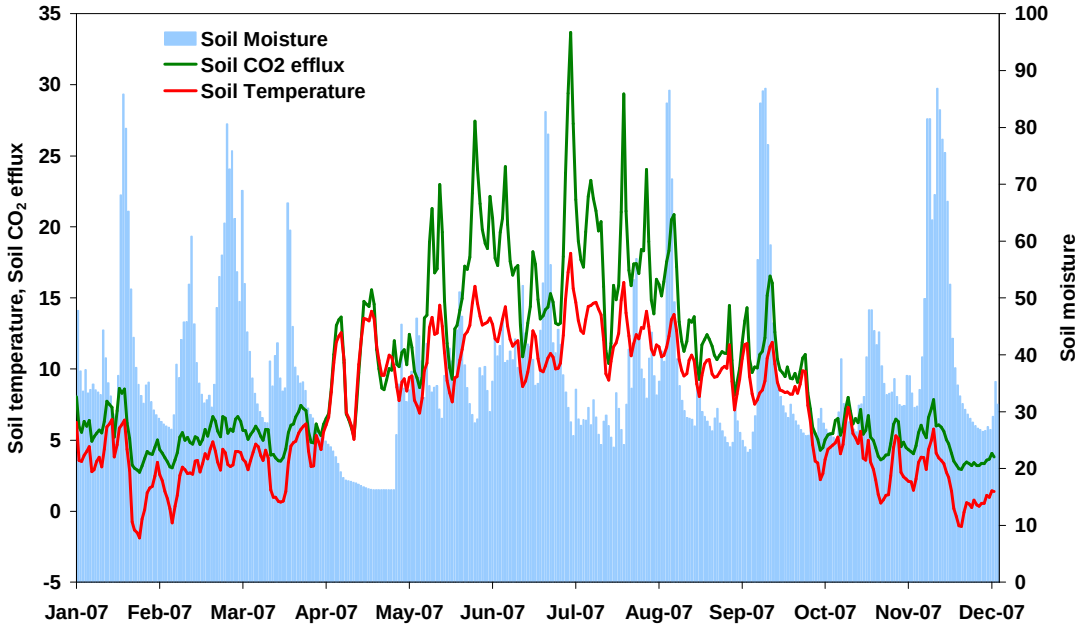

Figure 73: Seasonal mean course of soil moisture [Vol%], soil temperature [°C] in layer 2 and simulated soil CO_2 efflux [g m^{-2} d^{-1}] for the year 2007 for measurement grid WA/WB

PATCIS differentiates between soil respiration, which includes heterotrophic and autotrophic respiration, and soil CO_2 efflux, which describes the total amount of CO_2 emitted by soil, including soil respiration and CO_2 transported by gas and water.

The difference between soil CO_2 efflux and soil respiration simulated with PATCIS was minimal (Figure 74). The largest difference coincided with major rainfall events, as displayed in figure 74 for measurement year 2007 (other years showed similar results). The observed minimal difference between soil CO_2 efflux and soil respiration refers to little restriction on gas transport within the soil, which is supported by the fact that most CO_2 is produced in the highly porous upper soil layers (Figure 75).

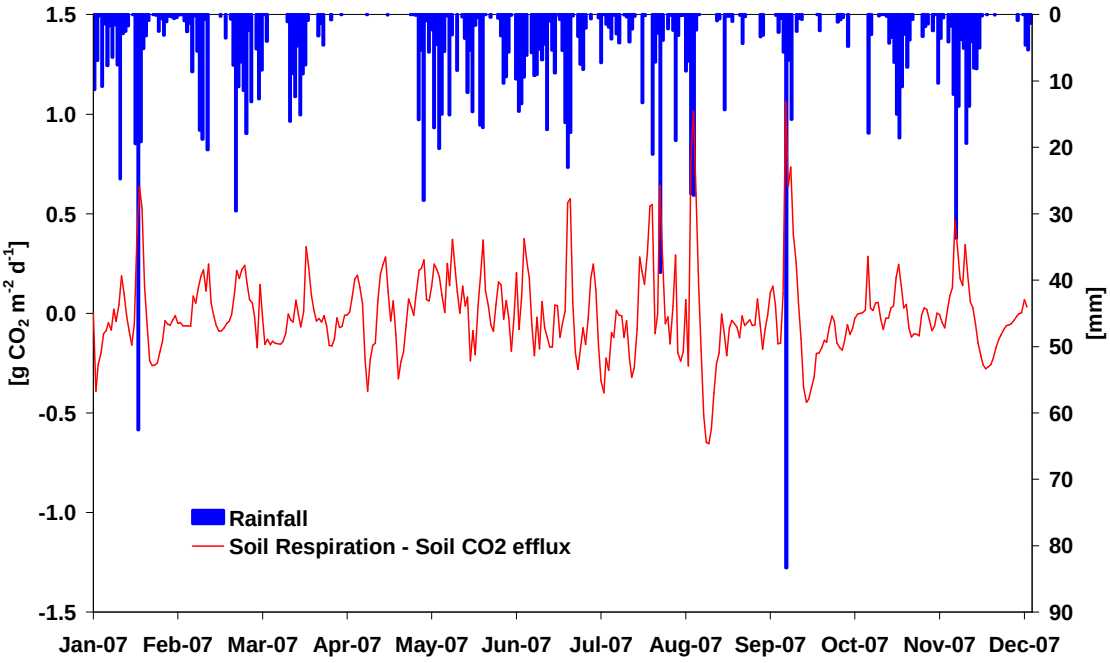

Figure 74: Difference between simulated soil CO_2 efflux and soil respiration of WA/WB for 2007

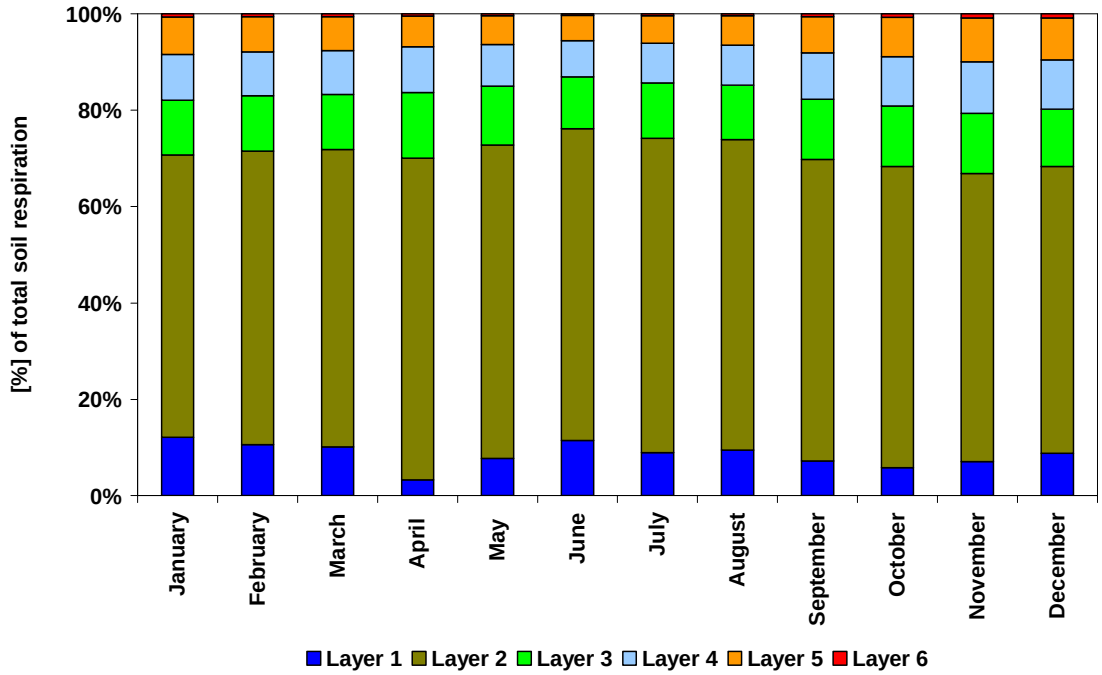

Figure 75: Simulated monthly soil respiration for individual layers of WA/WB (mean of all points) for 2007

Seasonal coefficients of variation, mean values of soil CO_2 efflux and standard deviation can be found in table 19 for transects WA and WB for all simulated years, relevant for the days where field measurements were done simultaneously.

Simulated mean values of soil CO_2 efflux for the growing season were similar to measured mean values, while simulated mean values for the non-growing season were slightly lower compared to mean measured values. The seasonal coefficients of variation were slightly lower for simulated values compared to measured values.

Table 19: Mean values, standard deviation and coefficients of variation for simulated and measured soil CO_2 efflux rates of WA/WB for individual seasons

		Growing season (May – September) CO_2 efflux			Non-Growing-Season (October – April) CO_2 efflux		
		2007	2008	2009	2007	2008	2009
Simulated	Mean	14.3	14.1	14.1	6.1	5.1	6.6
	SD	4.5	5.0	5.5	2.1	1.1	1.8
	CV(%)	32	36	39	35	21	27
Measured	Mean	14.7	14.1	11.7	6.7	6.0	6.6
	SD	5.0	6.1	5.8	3.4	2.7	3.1
	CV(%)	34	43	50	50	45	48

In general modelled soil CO_2 efflux using the PATCIS model compared well with observed measurements. Coefficients of determination were between 0% and 99%, with a median value of 73% (table 20 & 21; most relationships were significant with $p < 0.05$).

Table 20: Linear regression results of measured and simulated soil CO_2 efflux for transects WA and WB

	2007			2008			2009		
	gradient	***intersection with y-axis***	***R²***	***gradient***	***intersection with y-axis***	***R²***	***gradient***	***intersection with y-axis***	***R²***
WA1	1.02	0.00	81	0.99	0.01	88	1.02	-0.01	61
WA2	0.99	0.00	93	0.99	0.02	83	1.00	-0.01	63
WA3	0.81	0.01	85	0.98	-0.01	88	0.97	0.00	69
WA4	1.00	0.00	93	1.01	0.01	87	1.00	0.01	65
WA5	0.99	0.00	83	1.00	0.00	83	1.00	0.01	76
WA6	1.01	0.03	90	1.02	0.06	56	0.99	0.00	45
WA7	1.00	0.01	82	0.99	-0.01	76	0.85	0.05	30
WA8	0.83	0.03	80	0.82	0.04	81	0.99	0.04	88
WA9	1.02	0.01	92	0.88	0.06	74	1.01	0.01	79
WA10	1.00	0.00	79	1.01	0.00	83	0.99	0.00	58
WA11	0.97	0.01	79	1.01	0.01	66	1.00	0.00	84
WA12	1.02	0.00	88	1.01	0.01	73	1.00	0.01	68
WA13	0.94	0.01	83	1.01	0.01	75	0.98	0.00	57
WA14	0.94	0.01	81	1.00	0.00	77	1.00	0.00	57
WA15	0.68	0.00	82	0.90	0.03	69	0.67	0.03	24
WA16	0.89	0.00	90	0.99	0.00	96	1.02	0.00	67
WA17	0.97	0.02	87	1.00	-0.01	94	1.01	0.00	55
WB1	1.03	0.01	81	1.00	0.01	72	1.01	0.03	60
WB2	0.99	0.00	82	1.02	0.01	72	1.00	0.03	49
WB3	0.75	0.00	68	1.00	-0.06	85	1.00	-0.02	56
WB4	0.97	-0.03	84	1.00	-0.06	85	0.98	-0.01	55
WB5	1.01	-0.01	89	1.00	0.00	77	1.00	0.00	46
WB6	0.97	0.01	74	1.00	0.01	92	0.98	0.00	75
WB7	0.93	0.01	87	1.01	0.01	83	1.01	0.03	60
WB8	0.99	0.00	95	0.99	0.01	75	1.02	0.00	46
WB10	1.00	0.01	88	1.03	0.00	53	1.00	0.03	29
WB11	1.02	0.00	75	1.00	0.00	72	1.00	0.00	37
WB12	0.98	0.00	93	0.98	0.01	73	0.99	0.00	37
WB13	0.98	0.00	82	1.00	0.00	70	1.00	0.04	29
WB14	0.98	-0.01	91	0.97	0.00	77	1.03	-0.01	56
WB15	1.02	-0.01	68	1.00	0.01	86	1.00	0.04	64
WB16	1.02	0.01	86	0.99	0.00	92	1.03	0.00	65
WB17	1.00	-0.01	86	0.98	-0.01	95	0.90	0.02	43
WB18	0.97	0.00	77	0.99	0.01	92	1.02	0.00	43

Table 21: Linear regression results of measured and simulated soil CO_2 efflux for transects WA and WB (na = no data available)

	2007			2008		
	gradient	***intersection with y-axis***	***R²***	***gradient***	***intersection with y-axis***	***R²***
M1	0.76	0.00	85	0.77	0.00	51
M2	0.99	0.00	92	1.00	0.00	50
M3	1.01	-0.01	79	1.00	0.00	50
M6	1.00	0.00	84	0.98	0.01	69
M7	1.00	0.00	91	1.00	0.01	70
M8	1.00	-0.01	92	0.99	0.02	73
M9	1.00	0.01	60	0.99	0.02	35
M10	0.99	0.01	97	0.97	0.00	74
M11	1.01	-0.01	86	0.99	0.00	80
M12	1.03	-0.01	85	0.98	0.00	53
M13	1.00	0.00	51	1.00	0.01	19
M14	0.84	0.02	84	1.04	0.01	83
M15	1.03	0.01	79	1.01	0.08	49
M16	0.99	0.00	99	1.01	0.00	69
M16metal	0.99	0.00	81	0.99	0.03	65
M18	1.01	0.00	86	1.00	0.05	26
M19	1.30	0.00	92	1.01	0.05	47
M19metal	1.00	0.05	74	0.99	0.08	4
M20	1.20	0.03	64	na	na	na
M21	0.97	0.00	73	1.01	0.02	68
M22	1.01	0.00	92	1.00	0.04	47
M23	0.94	0.01	85	0.97	0.01	59
M24	0.99	-0.03	65	0.56	0.09	33
M25	1.02	0.00	97	1.00	0.01	74
M26	1.00	0.00	78	1.02	0.01	63
M27	1.01	-0.01	64	1.02	0.05	42
M28	1.01	0.00	92	1.00	0.05	74
M29	1.00	0.00	85	1.00	0.01	35
M30	1.00	0.00	91	0.98	0.00	85
M31	0.99	-0.06	80	1.00	0.00	71
M32	1.00	0.01	84	0.99	0.00	67
M32metal	1.00	0.01	88	0.99	0.01	74
M33	1.00	0.01	86	1.02	0.03	70
M33metal	1.00	0.04	71	1.00	0.02	66
M34	0.99	0.02	72	0.99	0.07	57

Mean simulated and mean measured soil CO_2 efflux values are illustrated in figures 76-84 for different years and measurement grids.

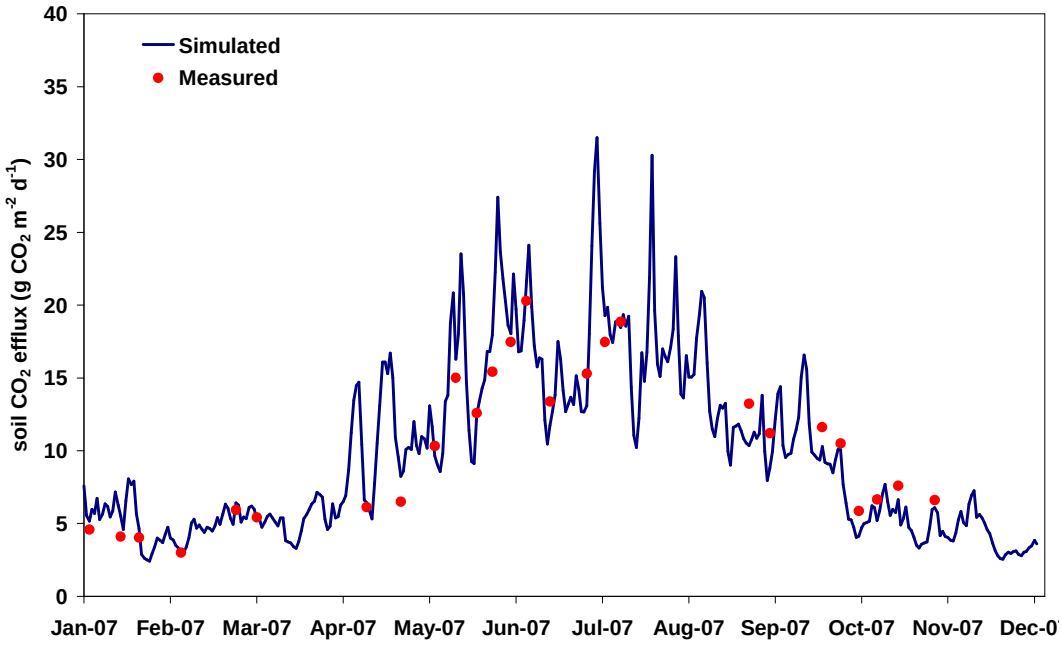

Figure 76: Mean simulated and mean measured values of soil CO_2 efflux for the year 2007 for transects WA and WB

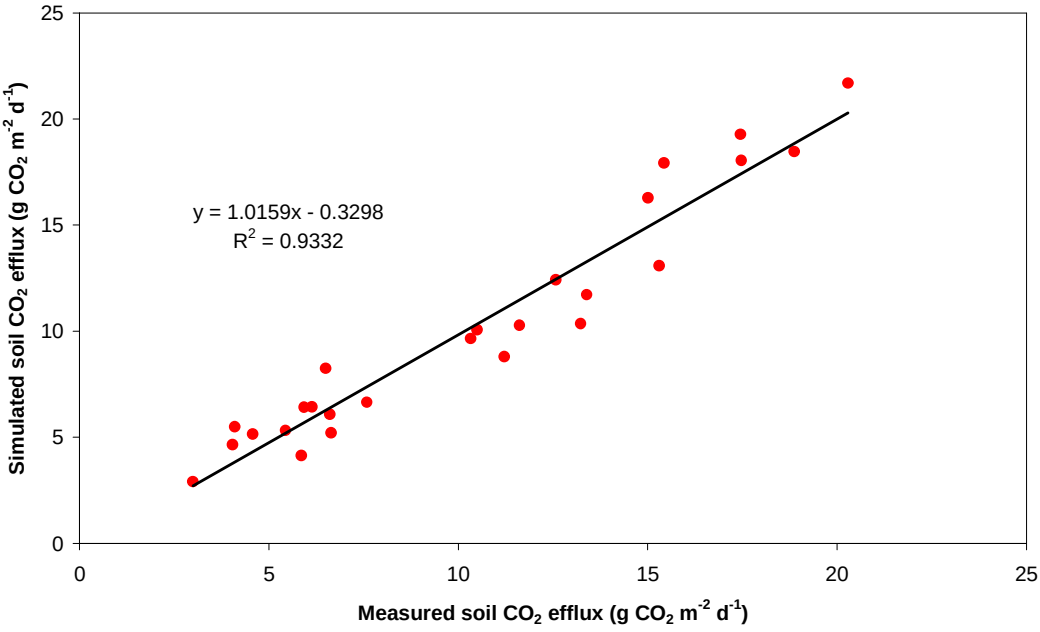

Figure 77: Mean measured soil CO_2 efflux versus mean simulated soil CO_2 efflux for 2007 for WA and WB

As shown in figures 76 and 77 mean measured values fit well with mean simulated values for the year 2007, with a high coefficient of determination of 93%.

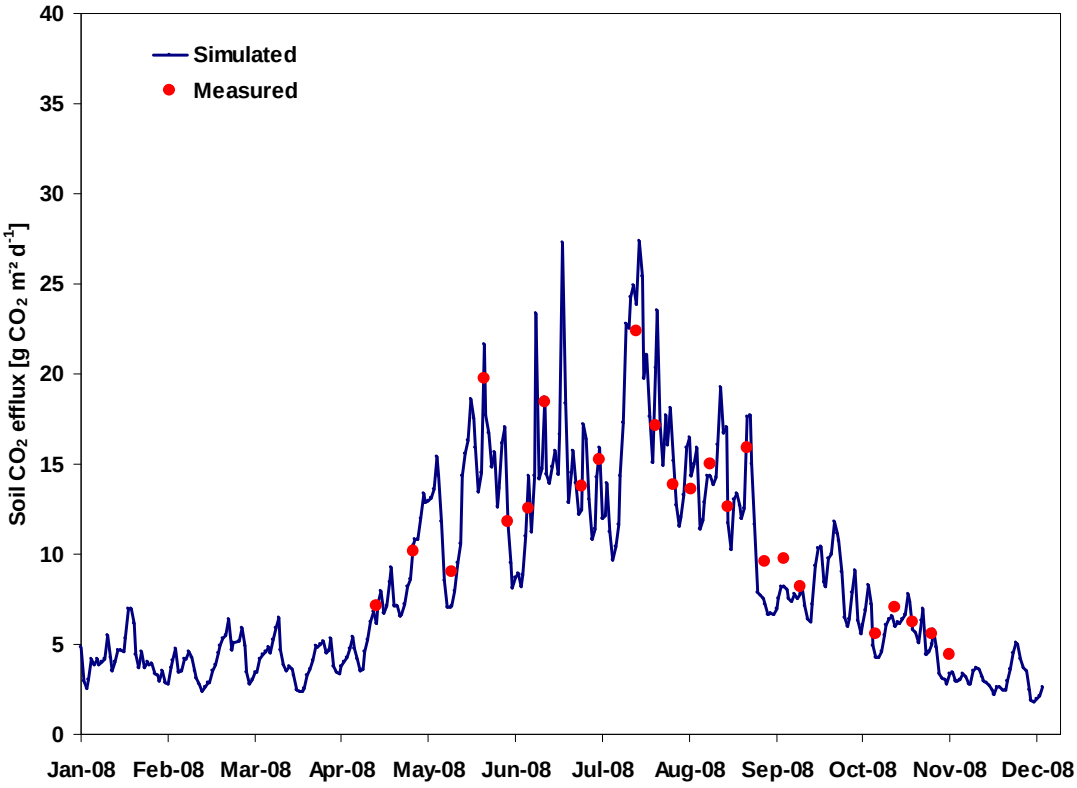

Figure 78: Mean simulated and mean measured values of soil CO_2 efflux for the year 2008 for transects WA and WB (new calibration of 2008, R^2 = 97%)

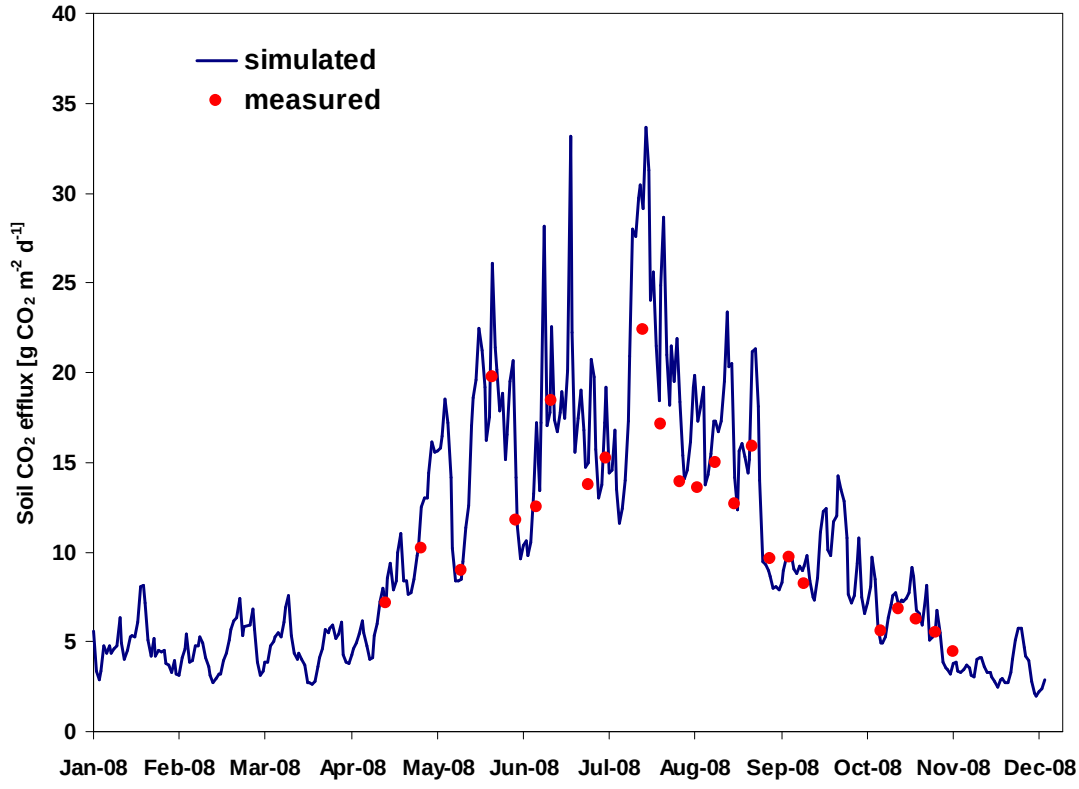

Figure 79: Mean simulated and mean measured values of soil CO_2 efflux for the year 2008 for transects WA and WB (validation of 2007 parameter combinations, R^2 = 97%)

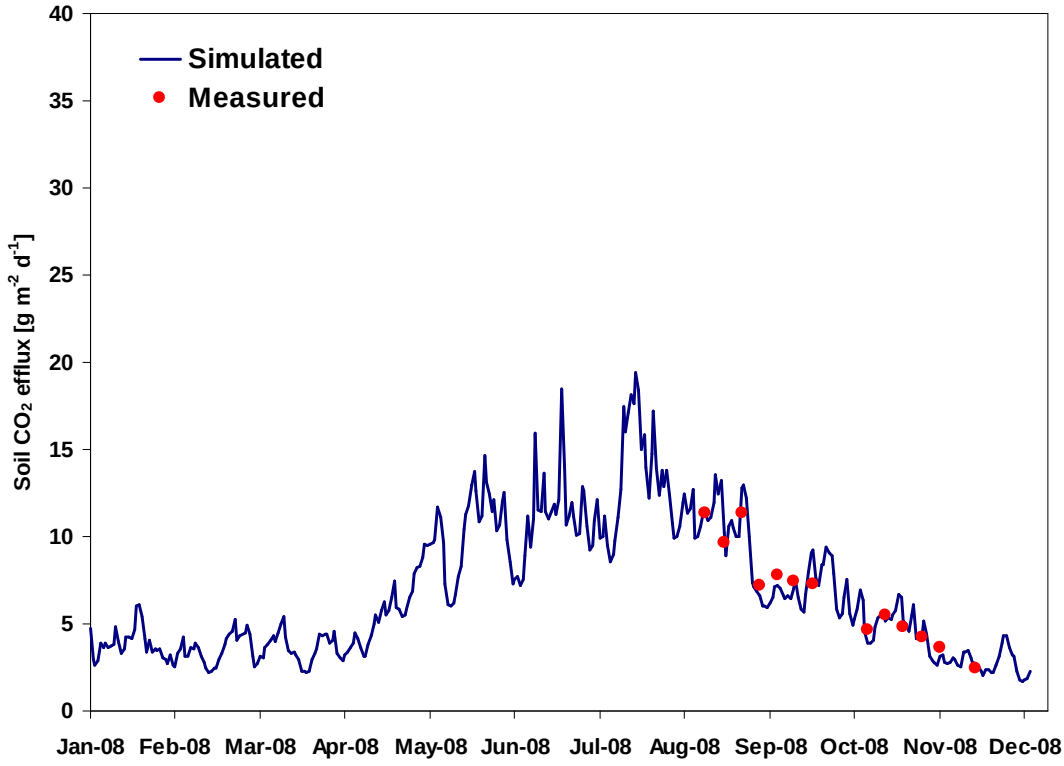

Figure 80: Mean simulated and mean measured values of soil CO_2 efflux for the year 2008 for grid M (calibration, R^2 = 94%)

A new calibration (parameterization) of 2008 for transects WA and WB resulted in a good fit of mean measured and mean simulated values for soil CO_2 efflux, while the validation of the 2007 parameterization for 2008 showed good R^2 values but generally overestimated the efflux (figures 78 & 79).

A good fit of soil CO_2 efflux with measured values could mostly be found during winter months. Therefore the fit of mean measured soil CO_2 efflux for grid M with mean simulated values for 2008 (figure 80), which included mainly values of the non-growing period, was good.

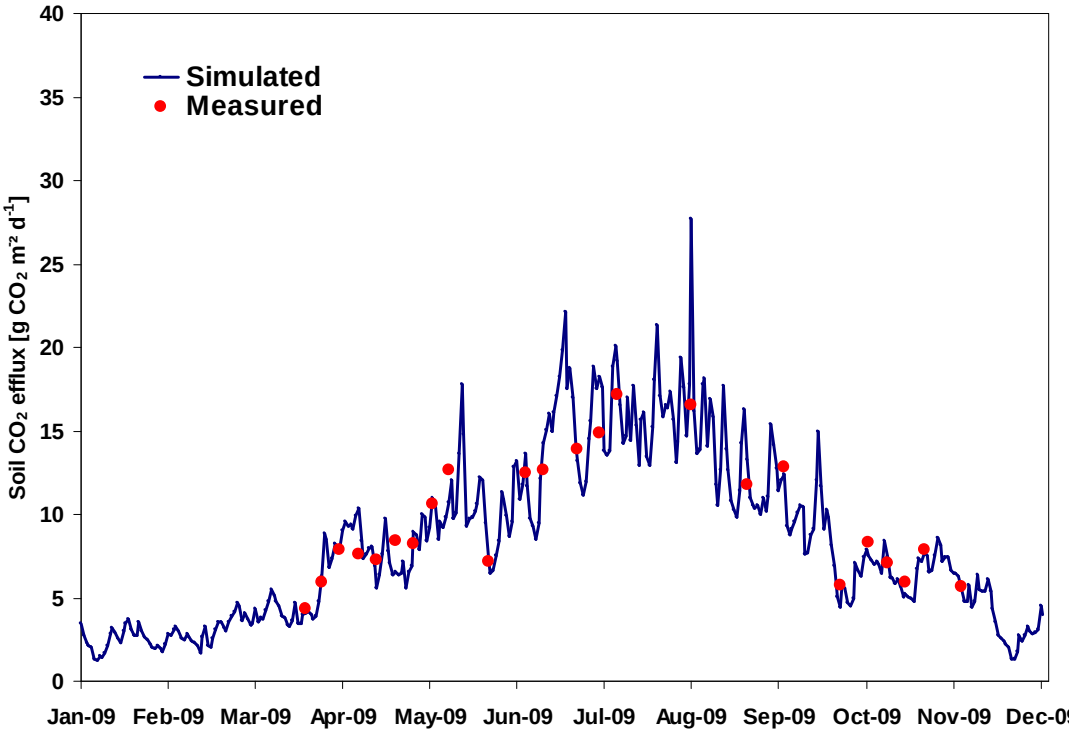

Figure 81: Mean simulated and mean measured values of soil CO_2 efflux for the year 2009 for transects WA and WB (new calibration, R^2 = 84%)

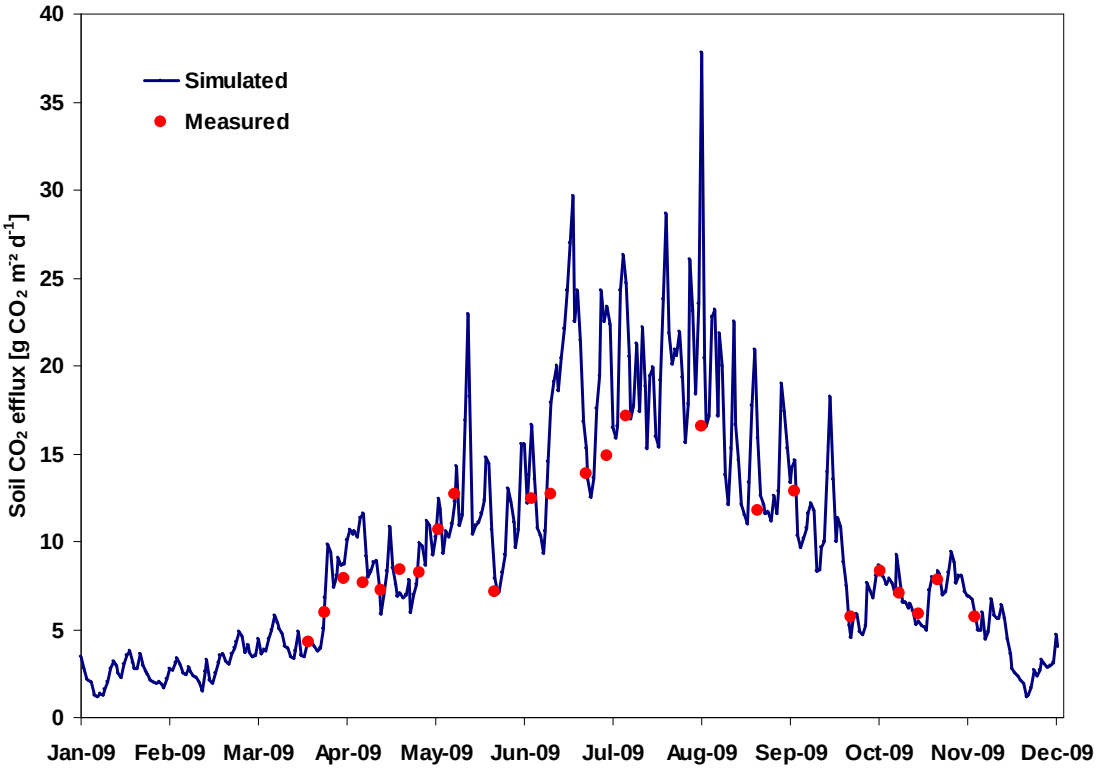

Figure 82: Mean simulated and mean measured values of soil CO_2 efflux for the year 2009 for transects WA and WB (validation of 2007 parameter combinations, R^2 = 81%)

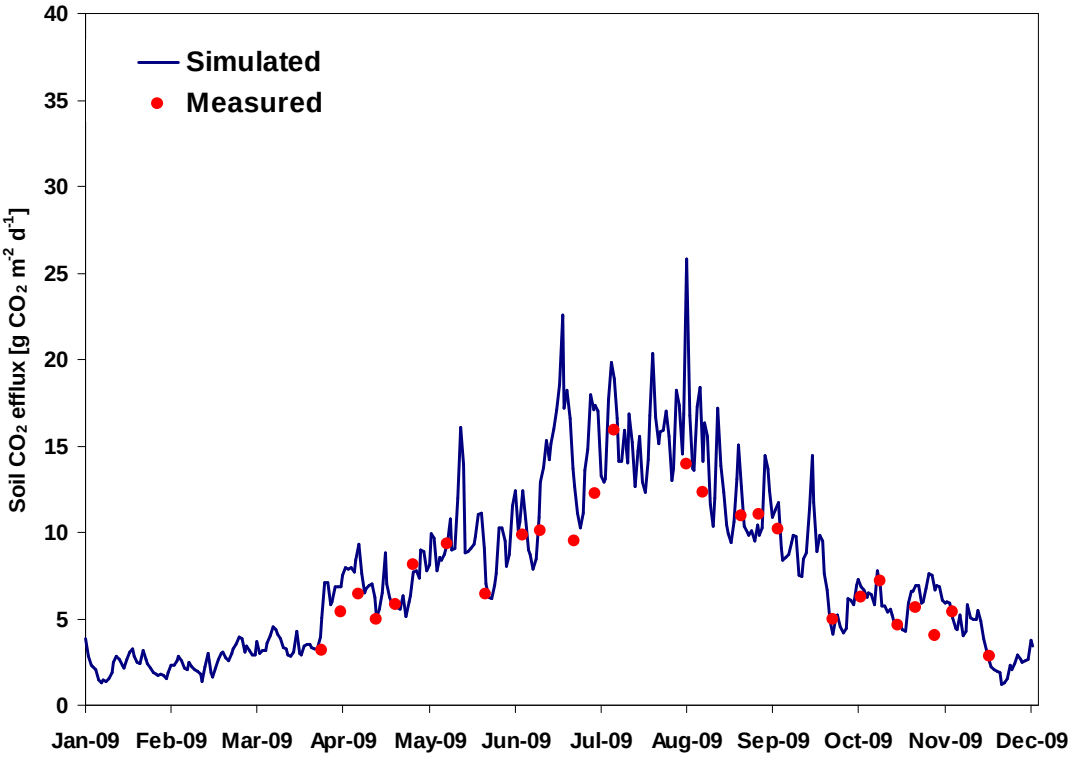

Figure 83: Mean simulated and mean measured values of soil CO_2 efflux for the year 2009 for grid M (new calibration, R^2 = 83%)

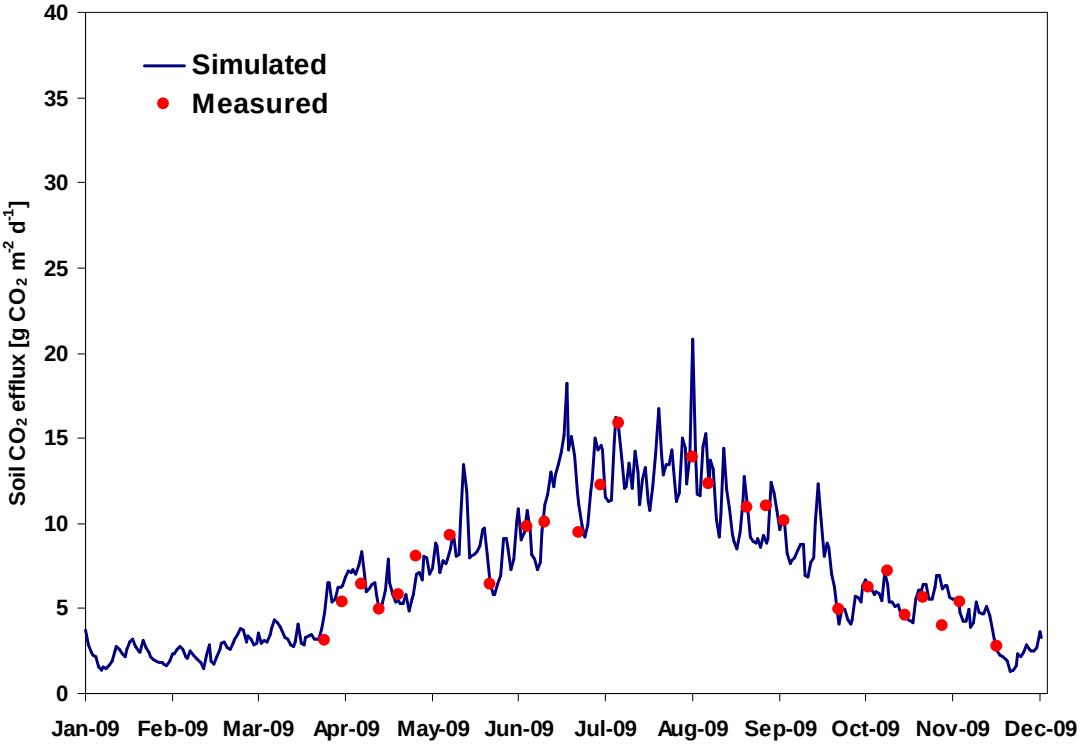

Figure 84: Mean simulated and mean measured values of soil CO_2 efflux for the year 2009 for grid M (validation of parameter combinations from 2008, R^2 = 84%)

The simulation of mean soil CO_2 efflux for 2009 resulted in high coefficients of determination (figures 81-84), but values were generally overestimated, especially during summer months. The validation of the parameter combinations from 2008 for grid M resulted in a better fit than the new parameterization of 2009. Coefficients of determination for individual measurement points can be found in table A5 (appendix).

Although mean simulated soil CO_2 efflux was in accordance with measured soil CO_2 efflux, spatial variability among the individual points was high, as shown in figure 85 for WA and WB for the year 2007. Spatial variability expressed in the spatial coefficient of variation for individual dates was higher for measured values compared to simulated values. The coefficient of variation for measured soil CO_2 efflux was on average 11% higher than simulated soil CO_2 efflux for transects WA/WB and grid M for the year 2008. This could be referred to the insufficient characterization of individual points with regard to organic matter content or root biomass. Samples were only taken for few points and transferred to all points.

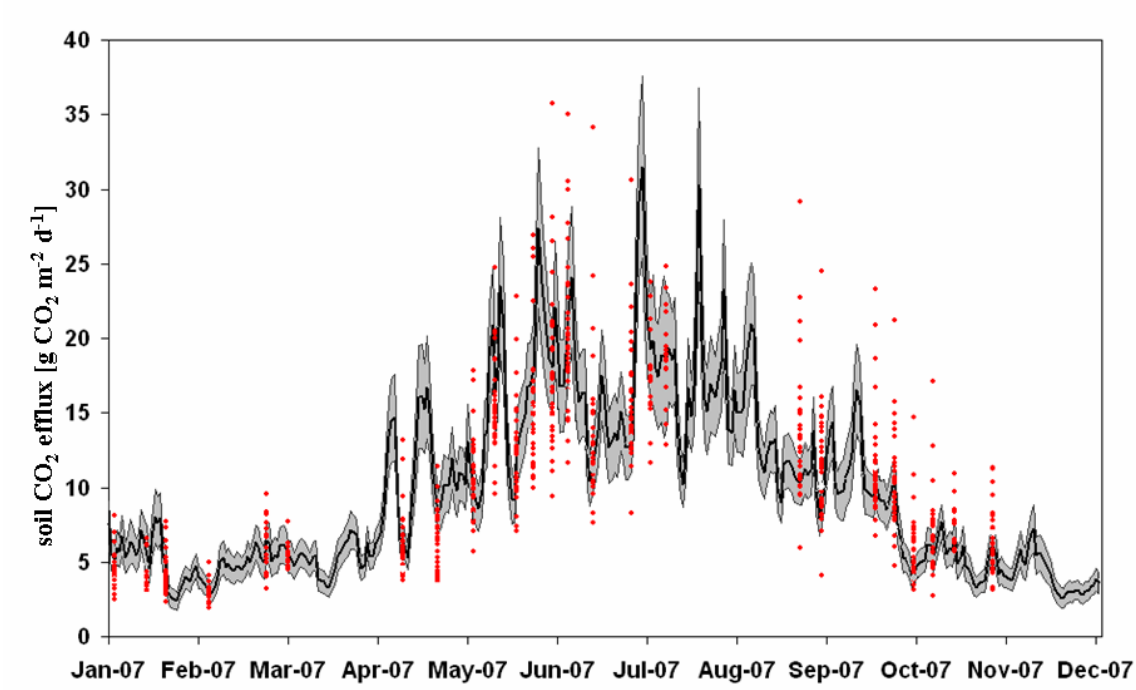

Figure 85: Mean simulated (thick black line) and measured (red dots) soil CO_2 efflux of transects WA and WB for 2007. The simulated confidence interval is displayed in grey (mean soil CO_2 efflux ± standard deviation)

Standard deviation and therefore spatial variability was higher during the growing period, compared to standard deviation of the non-growing period (figures 86 and 87).

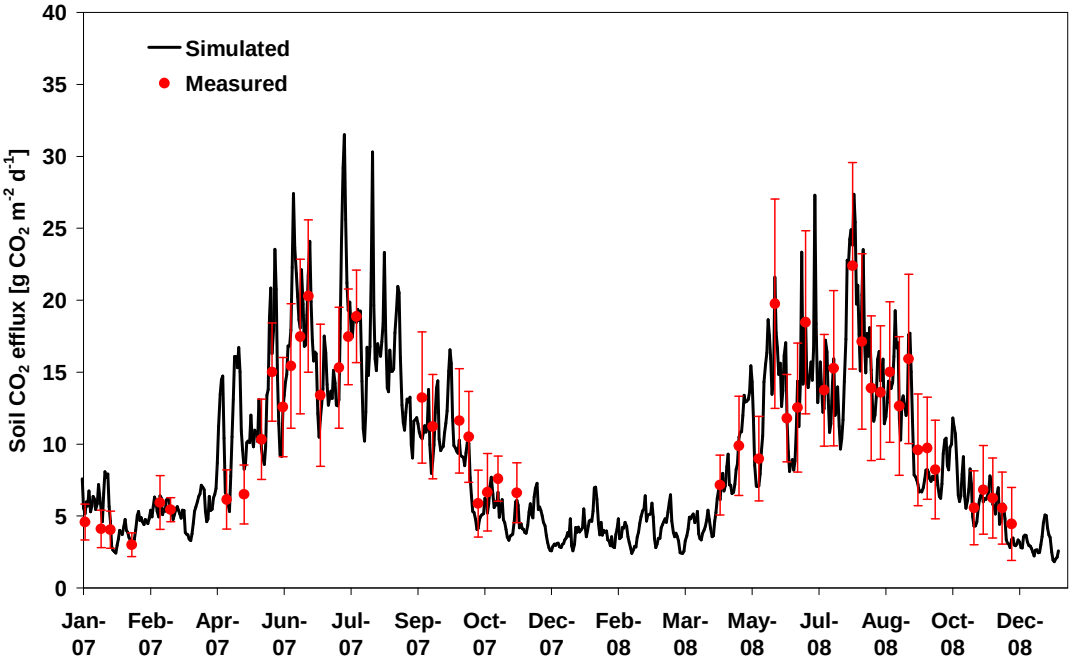

Figure 86: Mean measured and mean simulated soil CO_2 efflux for transects WA and WB with standard deviation of measurements for the years 2007-2008

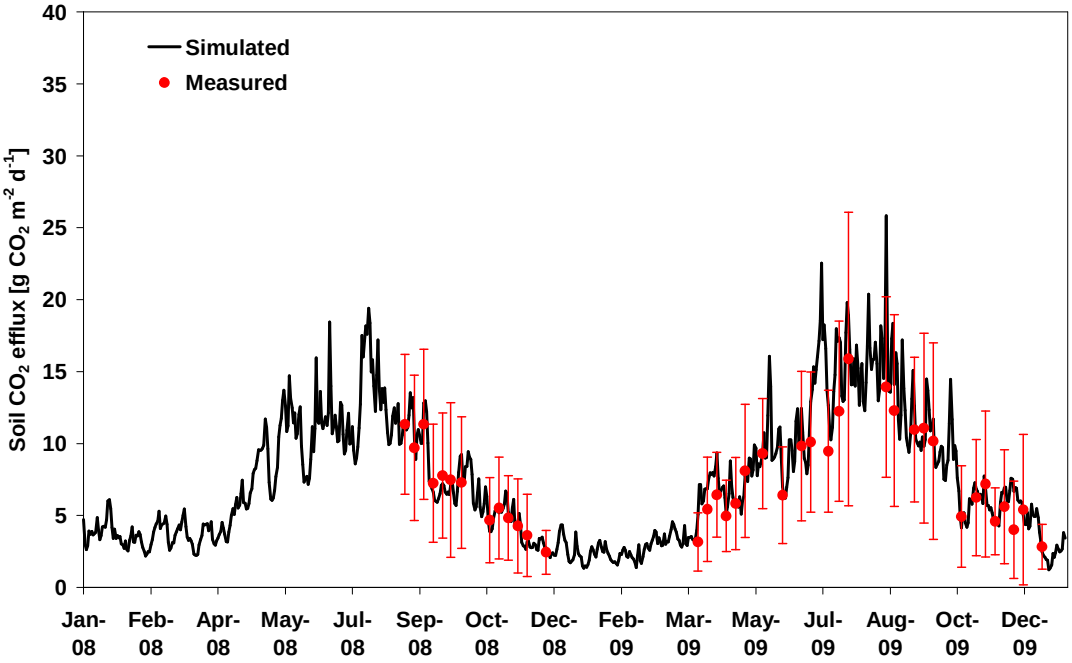

Figure 87: Mean measured and mean simulated soil CO_2 efflux for grid M with standard deviation of measurements for the years 2008-2009

5.2.4 Heterotrophic vs. autotrophic respiration

The simulated results of heterotrophic and autotrophic respiration identified heterotrophic respiration as the dominant type of respiration in the Wüstebach catchment, which resembles the findings of the measurements (Chapter 4.1.3).

In contrast to measurement results the percentage of heterotrophic respiration was higher for the simulation, between 88-97% (Figure 88, table 22). According to Hanson et al. (2000) the contribution of autotrophic respiration to total respiration can be anything from 10…95%. Buchmann (2000) discovered a percentage of less than 30% of autotrophic respiration to total soil respiration in her study on a *Picea abies* forest stand in Northeast Germany using root exclusion methods. Saiz et al. (2007) identified autotrophic respiration as the dominant soil respiration component with 54.7% for their Sitka spruce stand using PATCIS.

Table 22: Comparison of measured and simulated percentage of heterotrophic and autotrophic respiration to total soil respiration from 2008 to 2010

measurement point	heterotrophic respiration [%]		autotrophic respiration [%]	
	measured	simulated	measured	simulated
M1 / M1a	48	97	52	3
M7 / M7a and M7b	65	97	35	3
M16 / M16_metal	64	97	36	3
M18 / M18a	72	97	28	3
M23 / M23a	71	97	29	3
M24 / M24a and M24b	43	98	57	2
M29 / M29a	79	97	21	3
M32 / M32 metal	74	94	26	6
M33 / M33 metal	74	95	26	5

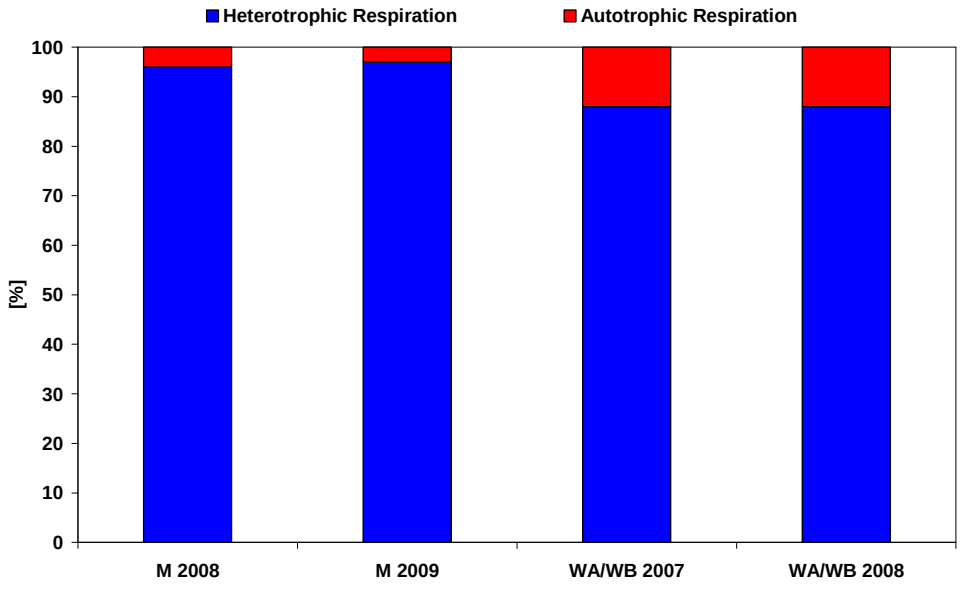

Figure 88: Percentage of heterotrophic and autotrophic respiration for grid M and transects WA/WB for individual years

Individual points did not show a great variability in the proportion of heterotrophic respiration and autotrophic respiration. Simulation of measurement points displayed in chapter 4.1.3 in the context of root exclusion did not resemble the measured values of heterotrophic respiration (figure 89). This large difference could partly be referred to a high uncertainty in root biomass analysis (difficulties in finding a representative spot, difficult separation of roots and soil, which results in loss, especially of fine roots) or as discussed in chapter 4.1.3 to uncertainty in root exclusion methods.

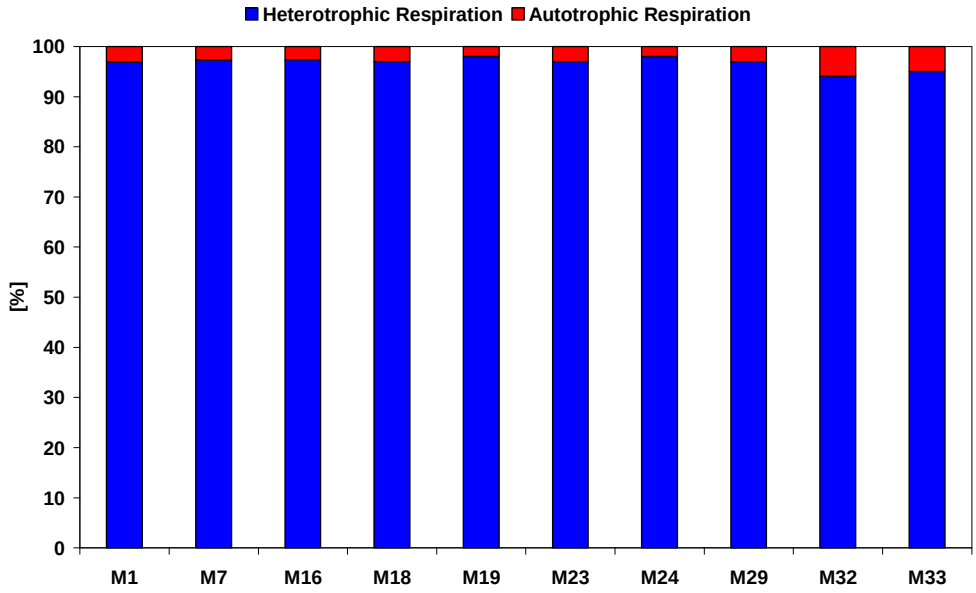

Figure 89: Simulated percentage of heterotrophic and autotrophic respiration for rootless points of grid M

Figure 90 shows the simulated seasonal variation for WA and WB 2007 (further years and measurement plots were similar) in both heterotrophic and autotrophic soil respiration. The contribution of both components to total soil respiration did not vary considerably over the year. The detected seasonal variability in the proportion of heterotrophic and autotrophic respiration in chapter 4.1.3 could not be confirmed by the simulation. A significant contribution of autotrophic respiration to total soil respiration during the growing season, as found by Saiz et al. (2007), could not be detected for the simulation. One reason for this is the lack of seasonal variability in input parameters such as root biomass. Due to the large physical effort involved in the analysis of root distribution, a possible seasonal variability in root biomass was excluded from observation. Based on the existence of mature full-grown trees, a high seasonality of root growth was not expected.

The seasonal variability visible in the measurements (chapter 4.1.3) on the other hand could not be related to growing period and non-growing period. Differences in the

proportion of heterotrophic and autotrophic respiration were not dependent of seasonal cycles, as they were existent during winter months and summer months. An incorrect measurement, possible root ingrowth or degradation of roots by microorganisms could be more appropriate explanations.

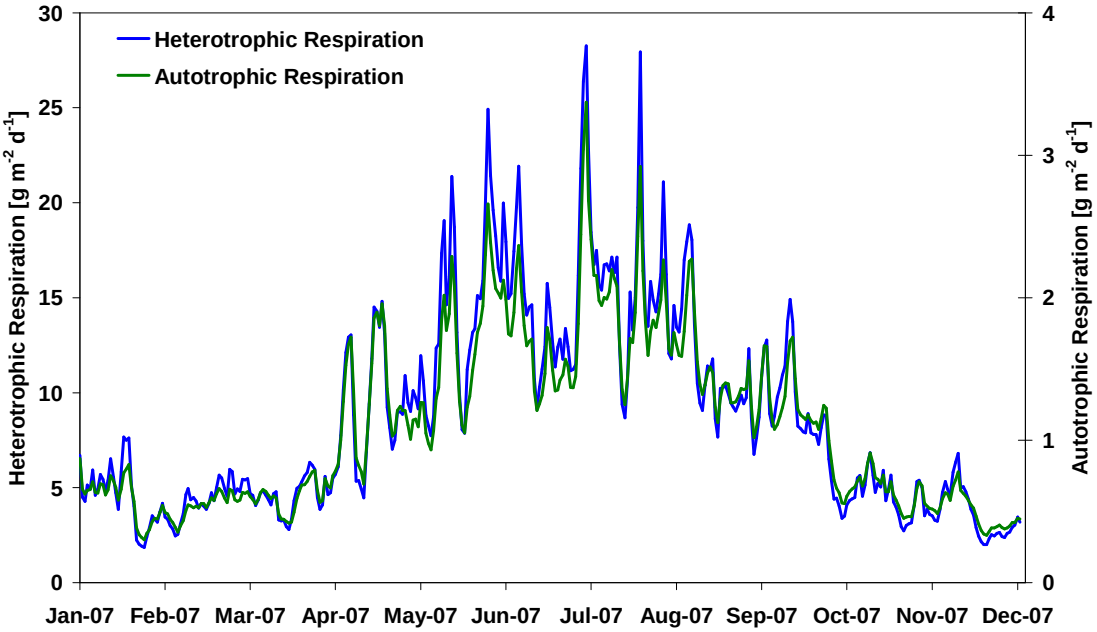

Figure 90: Simulated seasonal variation in autotrophic and heterotrophic respiration of transects WA/WB for 2007

5.2.5 Modifications of environmental conditions and their effect on soil CO_2 efflux

Some measurement points were modified by layer removal, which was used to test model output. The removal of layers as described in chapter 4.1.4 was simulated for the four affected measurement points.

Layer Removal

The measurement points M8 and M14 were simulated without the litter layer, measurement points M9 and M13 were simulated without litter layer and organic layers.

Table 23: Sum of measured and simulated soil CO_2 efflux (g m^{-2} d^{-1}) for measurement points affected by layer removal (M8, M9, M13, and M14) and their corresponding control points (M8a, M9a, M13a, M14) for the year 2009

∑ 2009	M8a	M8	M9a	M9	M13a	M13	M14a	M14
measured	193	140	120	53	194	58	207	140
simulated	225	187	163	94	259	76	160	157

Compared to measured values for most points simulated values overestimated the soil CO_2 efflux (table 23). Simulated soil CO_2 efflux for M8 in 2008 otherwise showed a good fit with measured values with a tendency to underestimation rather than overestimation

(figure 91 a/b). The simulation of 2009 for M8 resulted in an overestimation of the measurement values (figure 92).

a)

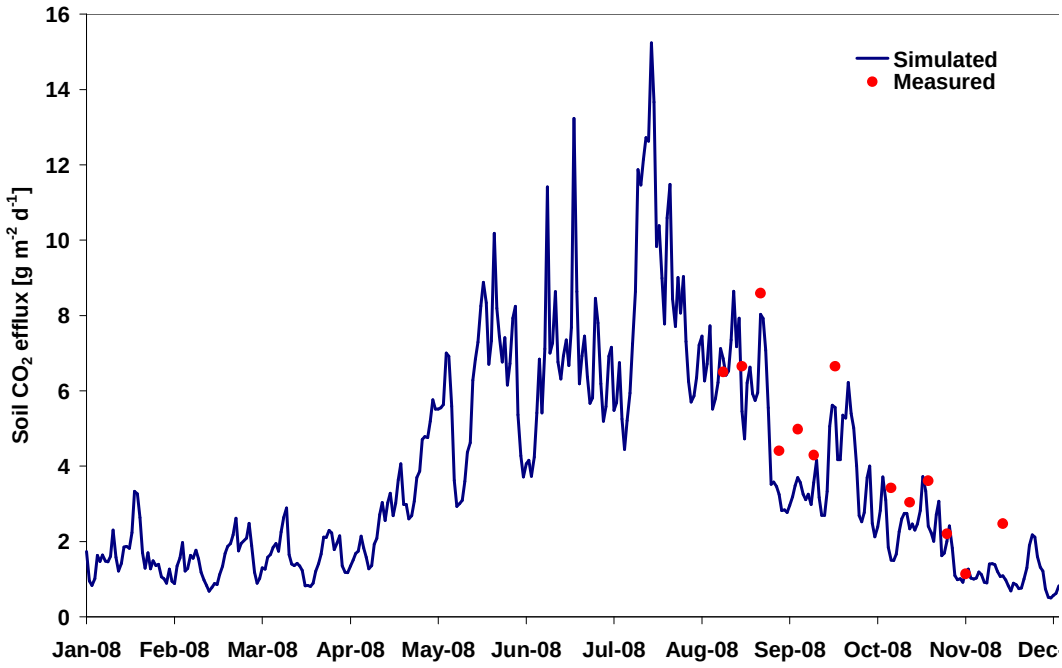

b)

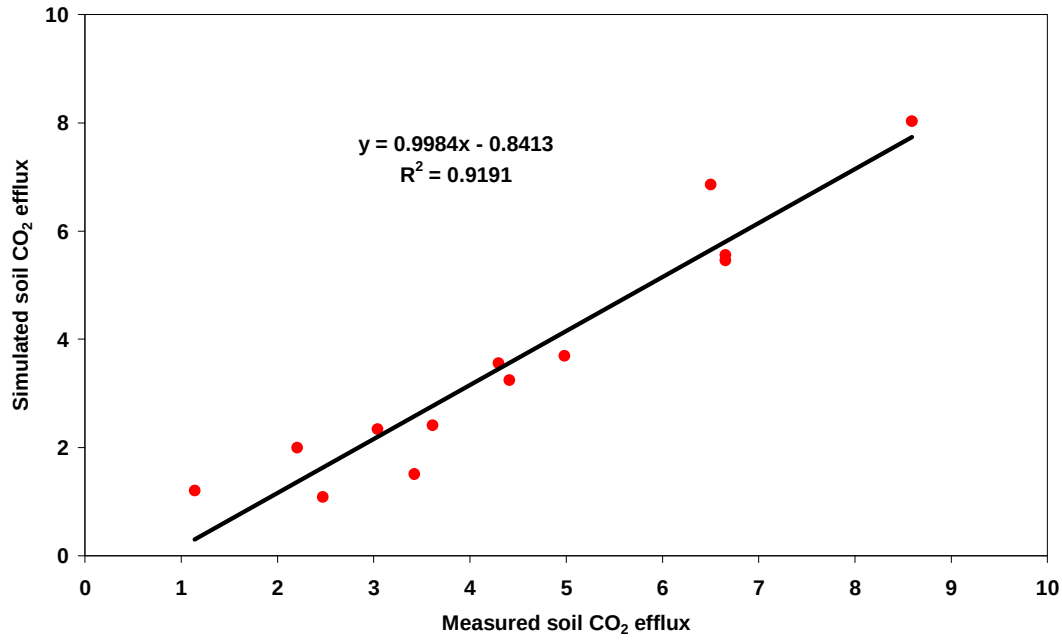

Figure 91: Simulated and measured soil CO_2 efflux of M8 affected by litter layer removal for 2008 (a) and linear regression of measured soil CO_2 efflux vs. simulated soil CO_2 efflux (b)

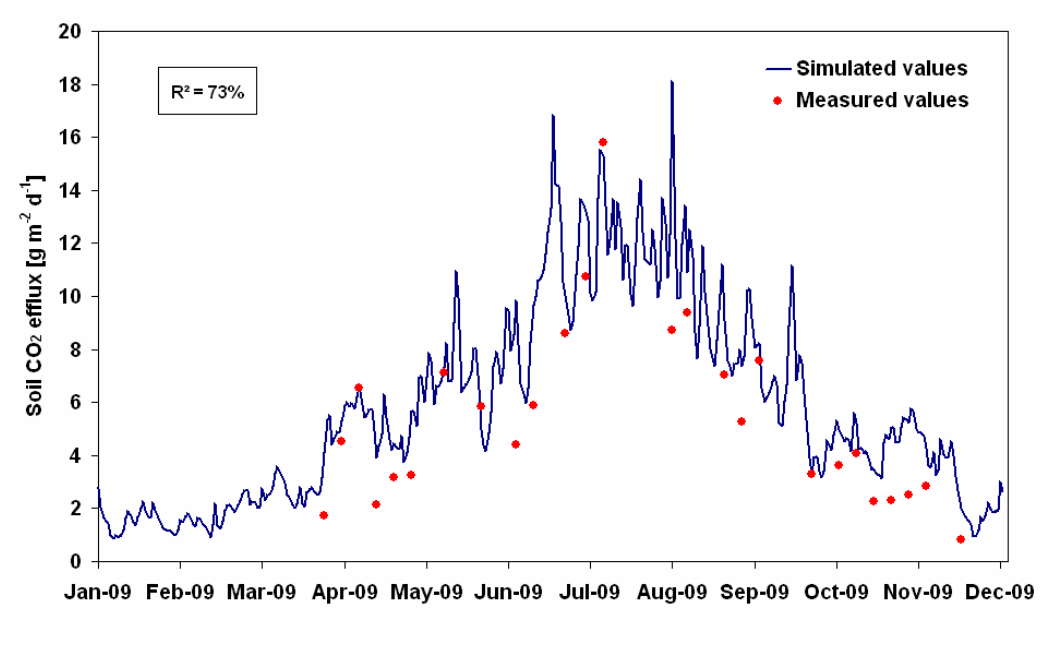

Figure 92: Simulated and measured soil CO_2 efflux of M8 affected by litter layer removal for 2009

Measurement points M9 and M13 without litter and organic layers showed good simulation results for 2008, while in 2009 fluxes were largely overestimated for both points (figure 93).

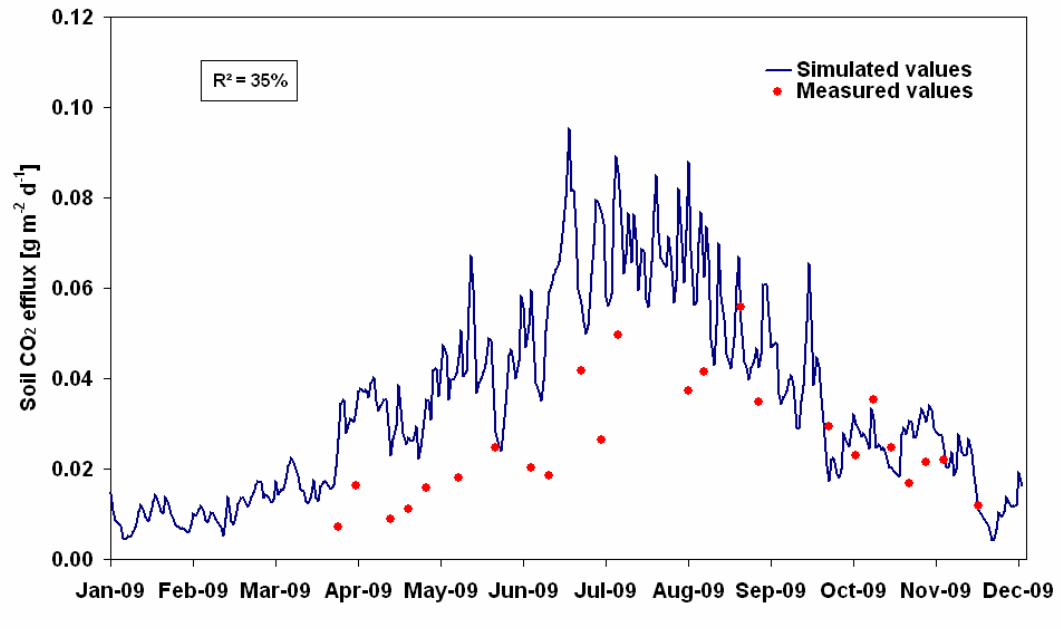

Figure 93: Simulated and measured soil CO_2 efflux of M9 affected by litter layer and organic layer removal for 2009

In general the simulation of layer removal displayed the actual measured layer removal in a sufficient way for measurement point M8 and M14, which showed significant

correlations ($p < 0.05$).A significant relationship for measurement points M9 and M13 was not detectable ($p > 0.05$).

6 Discussions

6.1 Concept of analysis

Several methods to analyse the spatial and temporal patterns of soil CO_2 efflux on a field scale have been applied. The observed temporal patterns included hourly, weekly and seasonal structures, while observed spatial patterns ranged from a cm- to m-scale. The main conclusion from the analyzing concept is that soil temperature plays a major role in the explanation of patterns of CO_2 efflux

6.1.1 Factors controlling temporal patterns

The analysis of measured soil CO_2 efflux and soil temperature data showed that the daily and the seasonal course of soil CO_2 efflux follows that of soil temperature. The high impact of soil temperature on soil CO_2 efflux is resembled in the results of exponential regression analysis with high values for coefficients of determination. Measured soil moisture showed a contrary course to measured soil CO_2 efflux throughout the year. In comparison to soil temperature, soil moisture plays only a minor role in temporal patterns, depending on characteristics of individual measurement points. Measurement points with comparably low or high soil moisture showed a larger impact of soil moisture on soil CO_2 efflux than points with medium soil moisture conditions.

6.1.2 Factors controlling spatial patterns

The analysis of measured soil CO_2 efflux, soil temperature and soil moisture showed that spatial patterns are time-persistent. Within-site variation was very high for soil CO_2 efflux as shown by high coefficients of variation. Soil temperature otherwise resembled a very low within-site variation which excludes soil temperature as important factor controlling spatial patterns. Using median values of soil CO_2 efflux over the whole measurement period drastically decreases spatial pattern. Thickness of litter layer and distance from the next tree partly explained spatial patterns for some of the measurement points. The variogram analysis did not reveal spatial correlation of soil CO_2 efflux on the considered scale. The analysis of mean relative differences (MRD) helped to characterize outliers and to calculate field averages. For individual points extreme values of soil temperature and soil moisture helped to explain patterns.

6.2 The modelling concept

The second goal of this study was to analyse if a process-based model system is able to reproduce measured data and to simulate temporal patterns.

6.2.1 Reproducing temporal patterns

The results of the simulations of individual measurement points indicated that it is possible to reproduce the courses of soil CO_2 efflux with the soil respiration model PATCIS. It was shown that soil temperature and soil organic matter displayed the most important factors controlling soil CO_2 efflux. Similar to analysis of measurements soil

CO_2 efflux and soil temperature showed a comparable seasonal course while the course of soil moisture was contrary. The parameterization of the model using a Latin Hypercube analysis remains questionable due to the wide variety of equally suitable parameters (equifinality) detected through this method.

Model input was of moderate quality due to the high effort involved in obtaining representative soil organic matter and root biomass values for 89 measurement points. The transfer of analysed root biomass and soil organic matter for few points to the complete measurement grid probably resulted in a large error. This error is of high importance for the simulation due to the high influence of soil organic matter on model output.

7 Conclusions

In this chapter the results of this study are evaluated in respect to their usefulness for analysis of spatio-temporal patterns. Returning to the posed research question in chapter,

- Is temperature the main factor controlling soil CO_2 efflux?
- Does temperature play a major role in the spatial patterns of soil CO_2 efflux?
- Which other factors determine spatial and temporal patterns?
- Is it possible to upscale from monitoring network scale to catchment scale?
- Is the model PATCIS feasible and does it help to answer the stated research questions?

The following concluding remarks can be made. As shown by measurement analysis as well as by simulation analysis, temperature plays the most important role in controlling temporal patterns of soil CO_2 efflux in the observed catchment area. With regard to spatial patterns temperature could not be identified as a main driver, as shown by analysis of MRD and variogram analysis.

Other factors responsible for spatial patterns could be identified qualitatively, including thickness of litter layer, and distance from the next tree. A general outstanding parameter relevant for all measurement points was not detectable. Measurements and simulations hint at a low importance of autotrophic respiration in comparison with heterotrophic respiration, which would assign the distribution of roots only a minor role in spatial patterns of soil CO_2 efflux. Soil organic matter otherwise was identified as a major parameter controlling soil CO_2 efflux in the simulation. A more precise and comprehensive sampling of soil organic matter might have led to the detection of potential spatial patterns of soil organic matter, which then might have been of help explaining spatial patterns in soil CO_2 efflux.

Analysis of measurements showed that, when looking at median values over a longer period of time, spatial variability of soil CO_2 efflux was low, apart from single measurement points, which showed a constantly higher or lower soil CO_2 efflux during the whole measurement period. Those outlier points were linked with extreme values of soil temperature, soil moisture or thickness of litter layer.

This ties in with the next question, whether upscaling from measurement plot to catchment scale is feasible or not. Keeping in mind that over a longer period of time soil CO_2 efflux for most points of the measurement network was similar, except from individual outliers, upscaling of values to catchment scale does seem feasible. Small-scale structures, e.g. extreme values, would get lost, but the general overall mean soil CO_2

efflux would remain. As shown by this study the method of mean relative differences is a useful tool to identify points characterizing field averages for upscaling.

With regard to the application of a soil respiration model the simulation results are encouraging. It could be shown that the process-based model PATCIS can be applied for the considered catchment area in order to calculate soil CO_2 efflux and to illustrate temporal patterns. With regard to further application of this model in the catchment area, an improvement of input parameter quality should be considered, especially concerning soil organic matter content and root biomass. More elaborate methods to separate heterotrophic and autotrophic respiration, such as isotope labelling, would be appropriate to provide a solid basis of comparison of measured versus simulated soil CO_2 efflux. Further research should also be concentrated on linking analysis of micro-scale patterns (e.g. laboratory scale, few cm) to analysis of field scale patterns in order to achieve a more profound understanding of spatial and temporal patterns of soil CO_2 efflux and detect underlying relationships of soil CO_2 efflux and environmental parameters. The restructuring of forest, as planned short-term, can be a unique opportunity to capture patterns of soil CO_2 efflux in a rapidly changing environment and therefore deliver valuable information in view of an upcoming global climate change.

8 Summary

The objective of this study was the analysis of temporal and spatial patterns of soil respiration on a catchment scale. This study is part of the DFG-financed project Transregio 32, which deals with the analysis of spatial and temporal patterns of matter fluxes on different scales. For investigation of local CO_2-fluxes from soil a catchment area of 27 ha in a spruce stand of the Eifel National Park was chosen and 89 measurement points, placed along two transects and one measurement grid, were installed. Soil respiration was measured weekly using a closed-dynamic chamber system, along with soil temperature (in 5 and 11 cm depth) and soil moisture (integral of 15 cm) for each measurement point. Additionally soil samples for the characterization of soil structure, including texture, density, root distribution and organic matter content, were taken.

In a first step the measured values were evaluated with regard to temporal and spatial patterns. These values were reproduced through a 1-dimensional simulation using a soil respiration model in a second step.

The results of the measurements show that temperature plays an important role in the explanation of existing temporal patterns of soil respiration. Soil moisture exerts an influence on the temporal development of soil-CO_2-fluxes, when extremely high or extremely low values of soil moisture are present. Spatial patterns are partly explained through the thickness of litter layer and through the distance from the next tree. The analysis of mean relative differences (MRD) proves satisfactory with regard to the identification of outliers and representative field averages.

The application of the soil respiration model PATCIS (Fang & Moncrieff 1999) was helpful, as it resulted in a good accordance of simulated and measured values of soil CO_2 efflux. The assumption, that temperature plays a major role in the variability of soil respiration, was verified by the model. Additionally the amount of organic matter in soil was identified as a second important factor explaining patterns in soil respiration. Since the measurement of soil organic matter involves a high effort and was therefore reduced to a minimum, the characterization of unsampled measurement points may be affected by large extrapolation errors, which in turn can be responsible for a high modelling error.

Future investigations in the observed catchment area should involve a detailed spatial examination of different soil parameters, especially of soil organic matter, to further reduce possible errors in simulation.

8 Zusammenfassung

In der vorliegenden Arbeit werden die zeitlichen und räumlichen Muster der Bodenrespiration auf Einzugsgebietsgröße untersucht. Diese Arbeit steht im Kontext des DFG-finanzierten Projektes Transregio 32, welches sich mit der Untersuchung räumlicher und zeitlicher Muster von Stoffflüssen auf unterschiedlichen Skalen beschäftigt. Zur Untersuchung der lokalen CO_2-Flüsse aus dem Boden wurde ein Einzugsgebiet von 27 ha in einem Fichtenwaldgebiet des Nationalparks Eifel ausgewählt und insgesamt 89 Messpunkte entlang zweier Transekte und eines Messnetzes errichtet. Die Messungen der Bodenrespiration wurden wöchentlich mittels eines geschlossenen dynamischen Kammersystems durchgeführt. Parallel wurden sowohl Bodentemperatur (in 5 und 11 cm Tiefe) als auch Bodenfeuchte (über ein Integral von 15 cm Tiefe) pro Messpunkt erfasst. Zusätzlich wurden Bodenproben zur Charakterisierung der Bodenbeschaffenheit bezüglich Körnung, Dichte, Durchwurzelung und Kohlenstoffgehalt entnommen und analysiert.

In einem ersten Schritt werden die gemessenen Werte in Hinsicht auf zeitliche und räumliche Muster ausgewertet. Diese Werte werden in einem zweiten Schritt durch eine 1-dimensionale Modellierung mit einem Bodenrespirationsmodell nachgebildet.

Die Ergebnisse der Messungen zeigen, dass der Temperatur die bedeutendste Rolle in der Erklärung der vorhandenen zeitlichen Muster der Bodenrespiration zukommt. Die Bodenfeuchte hat vor allem dann einen Einfluss auf die zeitliche Entwicklung der Boden-CO_2-Flüsse, wenn sie extrem hohe oder extrem niedrige Werte aufweist. Räumliche Muster der Bodenrespiration sind teilweise durch die Mächtigkeit der Streuschicht / organischen Auflage und durch den Abstand zum nächsten Baum zu erklären. Die Analyse der Mittleren Relativen Differenzen (MRD) erweist sich als hilfreich im Hinblick auf die Identifikation von Ausreißern und repräsentativen Feldmittelwerten.

Die Anwendung des Bodenrespirationsmodells PATCIS (Fang & Moncrieff 1999) war erfolgreich, da sie in einer guten Übereinstimmung von gemessenen und simulierten Werten resultierte. Die Annahme, dass Temperatur eine sehr große Rolle in der zeitlichen Variabilität der Bodenrespiration spielt, wurde durch das Modell verifiziert. Zusätzlich wurde der Anteil organischen Materials im Boden als bedeutender Faktor identifiziert. Da aufgrund des hohen Aufwands nur an einzelnen Messpunkten alle Bodeneigenschaften erhoben wurden, kann es bei der Charakterisierung der weiteren Messpunkte zu Fehlern bei den Extrapolationen kommen, die wiederum zu nicht unerheblichen Modellfehlern führen können.

Um mögliche Fehler in der Simulation weiter zu reduzieren wäre eine hoch aufgelöste räumliche Betrachtung unterschiedlicher Bodenparameter, insbesondere des organischen Materials, angebracht.

9 References

AG Bodenkunde (2005) Bodenkundliche Kartieranleitung. - BGR u. Geologische Landesämter der Bundesrepublik Deutschland 5th edition.: 438 p, Hannover

Ammer Ch (2000) Untersuchungen zum Einfluss von Fichtenaltbeständen auf die Entwicklung junger Buchen. Shaker, Aachen

Ammer Ch, Wagner S, (2005) An approach for modelling the mean fine-root biomass of Norway spruce stands. Trees 19: 145-153

Armstrong M (1998) Basic Linear Geostatistics. Springer, Berlin, New York: 139 p

Beven K (2006) A manifesto for the equifinality thesis. Journal of Hydrology 320: 18-36

Billings SA, Richter DD, Yarie J (1998) Soil carbon dioxide fluxes and profile concentrations in two boreal forests. Canadian Journal of Forest Research 28: 1773-1783

Boone RD, Nadelhoffer KJ, Canary JD, Kaye JP (1998) Roots exert a strong influence on the temperature sensitivity of soil respiration. Nature 396: 570-572

Borken W, Savage K, Davidson EA et al (2005) Effects of experimental drought on soil respiration and radiocarbon efflux from a temperate forest soil. Global Change Biology, doi: 10.1111/j.1365-2486.2005.01058.x

Bowden RD, Nadelhoffer KJ, Boone RD, Melillo JM, Garrison JB (1993) Contributions of above-ground litter, below-ground litter, and root respiration to total soil respiration in a temperate mixed hardwood forest. Canadian Journal of Forest Research 23: 1402-1407

Brooks RH, Corey AT (1964) Hydraulic properties of porous media: Hydrology Papers, Colorado State University: 24 p

Brumme R (1995) Mechanisms of carbon and nutrient release and retention in beech forest gaps. Plant Soil 168/169: 593–600

Buchmann N (2000) Biotic and abiotic factors controlling soil respiration rates in Picea abies stands. Soil Biology and Biochemistry 32: 1625-1635

Bunnell FL, Tait DEN, Flanagan PW, Van Cleve K (1977) Microbial respiration and substrate weight loss. Soil Biology and Biochemistry 9: 33–40

Certini G, Corti G, Agnelli A, Sanesi G (2003) Carbon dioxide efflux and concentrations in two soils under temperate forests. Biol Fertil Soils 37: 39-46

Cook FJ, Thomas SM, Kelliher FM, Whitehead D (1998) A model of one-dimensional steady-state carbon dioxide diffusion from soil. Ecol. Model. 109:155–164

Crill PM (1991) Seasonal patterns of methane uptake and carbon dioxide release by a temperate woodland soil. Global Biogeochemistry Cycles 5: 319-334

Davidson EA, Belk E, Boone RD (1998) Soil water content and temperature as independent or confounded factors controlling soil respiration in a temperate mixed hardwood forest. Global Change Biology 4: 217–227

Davidson EA, Richardson AD, Savage KE et al. (2005) A distinct seasonal pattern of the ratio of soil respiration to total ecosystem respiration in a spruce-dominated forest. Global Change Biology, doi: 10.1111/j.1365-2486.2005.01062.x

Davidson EA, Janssens IA, Luo Y (2006) On the variability of respiration in terrestrial ecosystems: moving beyond Q10. Global Change Biology, 154-164

Díaz-Pinés E, Schindlbacher A, Pfeffer M, Jandl R, Zechmeister-Boltenstern S, Rubio A (2010) Root trenching: a useful tool to estimate autotrophic soil respiration? A case study in an Austrian mountain forest. European Journal of Forest Research 129(1): 101-109

Diekkrüger B (1996) SIMULAT - ein Modellsystem zur Berechnung der Wasser- und Stoffdynamik landwirtschaftlich genutzter Standorte. *In:* O Richter, D Söndgerath and B Diekkrüger (Editors), Sonderforschungsbereich 179 "Wasser- und Stoffdynamik in Agrarökosystemen". Landschaftsökologie und Umweltforschung: 30-47

Drexhage M (1994) Die Wurzelentwicklung 40-jähriger Fichten (*Picea abies* [L.] Karst.) in der Langen Bramke. Ber. ForschungszentrumWaldökosysteme. Göttingen Reihe A: Bd. 111

Epron D, Farque L, Lucot E et al (1999) Soil CO_2 efflux in a beech forest: the contribution of root respiration. Annals of Forest Science 56: 289–295

Fang C, Moncrieff J (1999) A model for soil CO_2 production and transport 1: model development. Agric. For. Meteor. 95: 236–255

Fang C, Moncrieff JB (2001) The dependence of soil CO_2 efflux on temperature. Soil Biol. Biochem. 33: 155–165

Feddes RA, Kowalik PJ, Zaradny H (1978) Simulation of field water use and crop yield PUDOC, Wageningen, Netherlands. ISBN 90-220-0676-X

Forward DF (1965) The respiration of bulky organs. *In*: Steward FC (ed.), Plant Physiology. IVA. Metabolism: Organic Nutrition and Nitrogen Metabolism. Academic Press, New York: 311-376

Freijer JI, Leffelaar PA (1996) Adapted Fick's law applied to soil respiration. Water Resour. Res. 32: 791-800

Friedrich J (1992) Räumliche Variation bodenchemischer und -physikalischer Merkmalsgrößen sowie der Wurzelverteilung in Buchen- und Fichtenwaldökosystemen. Berichte des Forschungszentrums Waldökosysteme, Reihe A: Bd. 83

Giertz S, Hiepe C, Steup G, Sintondji L, Diekkrüger B (2010) Hydrological processes and soil degradation in Benin. *In*: Speth P, Christoph M, Diekkrüger B (Eds.): Impacts of Global Change on the Hydrological Cycle in West and Northwest Africa. Springer, Heidelberg, Germany: 168-197

Glinski J, Stepniewski W (1985) Soil Aeration and Its Role for Plant. CRC press: 176-178

Graf A, Weihermüller L, Huisman J A, Herbst M, Bauer J, Vereecken H (2008) Measurement depth effects on the apparent temperature sensitivity of soil respiration in field studies. Biogeosciences Discuss 5: 1867-1898

Gruber F (1994.) Morphology of coniferous trees: possible effects of soil acidification on the morphology of norway spruce and silver fir. *In:*D Godbold, A Hüttermann (editors) Effects of acid rain on forest processes. John Wiley & Sons, Inc., New York: 265-324.

Hanson PJ, Wullschleger SD, Bohlman SA, Todd DE (1993) Seasonal and topographic patterns of forest floor CO_2 efflux from an upland oak forest. Tree Physiology 13:1–15

Hanson PJ, Edwards NT, Garten CT, Andrews JA (2000) Separating root and microbial contributions to soil respiration: A review of methods and observations. Biogeochemistry 48: 115-146

Hanson PJ, O'Neill EG, Chambers MLS (2003) Soil respiration and litter decomposition. In Hanson PJ, Wullschleger SD (ed) North American Temperate Deciduous Forest Responses to Changing Precipitation Regimes. Ecological Studies 166, Springer, New York, p. 472

Herbst M, Prolingheuer N, Graf A, Huisman JA, Weihermüller L, Vanderborght J (2009) Characterization and understanding of bare soil respiration spatial variability at plot scale. Vadose Zone Journal 8: 762-771

Hilf HH (1927) Wurzelstudien an Waldbäumen. Die Wurzelausbreitung und ihre waldbauliche Bedeutung. Schaper, Hannover

Hornung U, Messing W (1984) Poröse Medien Methoden und Simulation. Verlag Beiträge zur Hydrologie I. Nippes, Kirchzarten, Germany

Horwath WR, Pregitzer KS, Paul EA (1994) ^{14}C allocation in tree-soil systems. Tree Physiol. 14: 1163–1176

Hui D, Luo Y (2004) Evaluation of soil CO_2 production and transport in Duke Forest using a process based modelling approach. Global Biogeochemical Cycles 18: GB4029

IPCC (2007) Climate Change 2007. The Scientific Basis. Cambridge University Press, p. 996

Janssens IA, Lankreijer H et al (2001) Productivity overshadows temperature in determining soil and ecosystem respiration across European forests. Global Change Biology 7: 269–278

Janssens IA, Dore S, Epron D et al. (2003) Climatic influences on seasonal and spatial differences in soil CO_2 efflux. *In:* Valentini R (editor) Fluxes of Carbon, Water and Energy of European Forests. Springer, Berlin: 233–253

Janssens IA, Pilegaard K (2003) Large seasonal changes in Q_{10} of soil respiration in a beech forest. Global Change Biol. 9: 911–918

Jarvis P, Linder S (2000) Constraints to growth of boreal forests. Nature 405: 904–905

Kirschbaum MUF (1995) The temperature dependence of soil organic matter decomposition, and the effect on global warming on soil organic C storage. Soil Biol. Biochem. 27: 753–760

Lavigne MB, Boutin R, Foster RJ, Goodine G, Bernier PY, Robitaille G (2003) Soil respiration responses to temperature are controlled more by roots than by decomposition in balsam fir ecosystems. Can. J. For. Res. 33: 1744–1753

Lee M-S, Nakane K, Nakatsubo T, Koizumi H (2003) Seasonal changes in the contribution of root respiration to total soil respiration in a cool-temperate deciduous forest. Plant Soil 255: 311–318

Leiros MC, Trasar-Cepeda C, Seoane S, Gil-Sotres F (1999) Dependence of mineralization of soil organic matter on temperature and moisture. Soil Biol. Biochem. 31(3): 327-335

Lenhart T, Eckhardt K, Fohrer N, Frede H-G (2002) Comparison of two different approaches of sensitivity analysis. Physics and Chemistry of the Earth 27: 645-654

Linn DM, Doran JW (1984) Effect of water-filled pore space on carbon dioxide and nitrous oxide production in tilled and nontilled soils. Soil Science Society of America Journal 48: 1267–1272

Lloyd J, Taylor JA (1994) On the temperature dependence of soil respiration. *Functional Ecology* 8: 315-323

Longdoz B, Yernaux M, Aubinet M (2000) Soil CO_2 efflux measurements in a mixed forest:: impact of chamber disturbances, spatial variability and seasonal evolution. Global Change Biology 6: 907-917

Lundegard H (1927) Carbon dioxide evolution of soil and crop growth. Soil Sci. 23: 417–454

Luo Y, Wan S, Hui D, Wallace L (2001) Acclimatization of soil respiration to warming in a tall grass prairie. Nature 413: 622– 625

McDowell NG, Marshall JD, Hooker TD, Musselman R (2000) Estimating CO_2 flux from snowpacks at three sites in the Rocky Mountains. Tree Physiology 20: 745-753

Meharg AA (1994) A critical review of labelling techniques used to quantify rhizosphere carbon-flow. Plant and Soil 166: 55-62

Meyer W (1994) Geologie der Eifel. Stuttgart. 618 p. ISBN 978-3-510-65161-0

Mitchell S, Beven K, Freer J (2009) Multiple sources of predictive uncertainty in modelled estimates of net ecosystem CO_2 exchange. Ecol. Model. 220: 3259–3270

Moncrieff J, Fang C (1999) A model for soil CO_2 production and transport 2: Application to a Florida Pinus elliotte plantation. Agric. For. Meteor. 95 (4): 237-256

Monteith JL (1976) Vegetation and atmosphere II. Academic Press: 343 p

Müller K, Wagner S (2003) Fine-root dynamics in gaps of Norway spruce stands in the Germany Ore mountains. Forestry 76:149–158

Nadelhoffer KJ, Raich JW (1992) Fine Root Production Estimates and Belowground Carbon Allocation in Forest Ecosystems. Ecology 73 (4): 1139-1147

Nakane K, Yamamoto M, Tsubota H (1983) Estimation of root respiration rate in a mature forest ecosystem. Jpn. J. Ecol. 33: 397–408

Oberbauer SF, Gillespie CT, Cheng W, Gebauer R, Sala Serra A., Tenhunen JD (1992) Environmental effects on CO_2 efflux from riparian tundra in the northern foothills of the Brooks Range, Alaska, USA. Oecologia 92: 568-577

Orchard VA, Cook FJ (1983) Relationship between soil respiration and soil moisture. Soil Biol. Biochem. 15: 447-453

Parsons WFJ, Miller SL, Knight DH (1994) Root gaps dynamics in a lodgepole pine forest: ectomycorrhizal and nonmycorrhizal fine root activity after experimental gap formation. Can J For Res 24: 1531–1538

Parton WJ, Ojima DS, Cole C, Schimel DS (1993) A general model for soil organic matter dynamic: sensitivity to litter chemistry, texture and management. in Quantitative Modelling of Soil Forming Processes. Soil Science Society of America, Madison: 147–167 p

Potter CS, Randerson J, Field CB, Matson PA, Vitousek PM, Mooney HA, Klooster SA (1993) Terrestrial ecosystem production: a process model based on global satellite and surface data. Global Biogeochem. Cycle 7: 811–841

Puhe J (1994) Die Wurzelentwicklung der Fichte (*Picea abies* [L.] Karst.) bei unterschiedlichen chemischen Bodenbedingungen. Berichte des Forschungszentrums Waldökosysteme Göttingen, Reihe A, Volume 108

Pumpanen J, Ilvesniemi H, Hari P (2003) A process-based model for predicting soil carbon dioxide efflux and concentration. Soil Science Society of America Journal 67: 402–413

Qi Y, Xu M (2001) Separating the effects of moisture and temperature on soil CO_2 efflux in a coniferous forest in the Sierra Nevada Mountains. Plant and Soil 237: 15-23

Raich JW, Rastetter EB, Melillo JM, Kicklighter DW, Steudler PA, Peterson BJ, Grace AL, Moore B, Vorosmarty CJ (1991) Potential net primary productivity in South America: application of a global model. Ecological Appl. 1: 399–429

Raich JW, Schlesinger WH (1992) The global carbon dioxide flux in soil respiration and its relationship to vegetation and climate. Tellus 44B: 81-99

Raich JW, Tufekcioglu A (2000) Vegetation and soil respiration: Corrleation and controls. Biogeochemistry 48: 71-90

Randerson JT, Thompson MV, Malmstrom CM, Field CB, Fung IY (1996) Substrate limitations for heterotrophs: implications for models that estimate the seasonal cycle of atmospheric CO_2. Global Biogeochemical Cycles 10: 585-602

Rayment MB, Jarvis PG (2000) Temporal and spatial variation of soil CO_2 efflux in a Canadian boreal forest. Soil Biol Biochem 32: 35–45

Reichstein M, Rey A, Freibauer A et al (2003) Modelling temporal and large-scale spatial variability of soil respiration from soil water availability, temperature and vegetation productivity indices. Global Biogeochemical Cycles 17: 1104

Richter D (1995) Ergebnisse methodischer Untersuchungen zur Korrektur des systematischen Messfehlers des Hellmann-Niederschlagsmessers. Berichte des Deutschen Wetterdienstes 194, Offenbach am Main

Ritchie JT (1972) A model for predicting evaporation from a row crop with incomplete cover. Water Resources Research 8: 182-190

Rockel B, Will A, Hense A (2008) The Regional Climate Model COSMO-CLM (CCLM). Meteorologische Zeitschrift 17(4): 347-348

Romell LG (1932) Mull and duff as biotic equilibria. Soil Sci. 34 (3): 161-188

Rout SK, Gupta SR (1989) Soil respiration in relation to abiotic factors, forest floor litter, root biomass and litter quality in forest ecosystems of Siwaliks in north India. Acta Oecologica/ Oecologica Plantarum 10: 229-244

Rustad LE, Campbell JL, Marion GM, Norby RJ, Mitchell MJ, Hartley AE, Cornelissen JHC, Gurevitch J (2001) Ameta-analysis of the response of soil respiration, net nitrogen mineralization, and aboveground plant growth to experimental ecosystem warming. Oecologia 126: 543-562

Saiz G, Black K, Reidy B, Lopez S, Farrell EP (2007) Assessment of soil CO_2 efflux and its components using a process-based model in a young temperate forest site. Geoderma 139: 79–89

Scheffer F, Schachtschabel P (2002) Lehrbuch der Bodenkunde. Heidelberg, Berlin, p. 593

Schlesinger WH (1977) Carbon balance in terrestrial detritus. Annual Review of Ecology and Systematics 8: 51-81

Schlesinger WH, Andrews JA (2000) Soil respiration and the global carbon cycle. Biogeochemistry 48: 7–20

Sciuto G, Diekkrüger B (2010) Influence of soil heterogeneity and spatial discretization on water balance modelling in a headwater forest catchment. Vadose Zone Journal 9: 955:969

Schöller W (2002): Waldgeschichte, Waldzustand und Waldbehandlung im geplanten Nationalpark Eifel. *In:* NATUR- UND UMWELTSCHUTZAKADEMIE NRW (ed.): Nationalpark Eifel. Eine Idee nimmt Gestalt an. NUA Seminarbericht 8. Recklinghausen: 39-45

Schwind W (1984): Der Eifelwald im Wandel der Jahrhunderte ausgehend von Untersuchungen in der Vulkaneifel. Düren, Eifelverein: 240 p

Shi PL, Zhang XZ, Zhong ZM, Ouyang H (2006) Diurnal and seasonal variability of soil CO_2 efflux in a cropland ecosystem on the Tibetan Plateau. Agr. Forest Meteorol. 137: 220–233

Simlab (2011) Software package for uncertainty and sensitivity analysis. Joint Research Centre of the European Commission. Downloadable for free at: http://simlab.jrc.ec.europa.eu

Skopp J, Jawson MD, Doran JW (1990) Steady-state aerobic microbial activity as a function of soil water content. Soil Sci. Soc. Am. J. 54: 1619–1625

Smith RE (1992) Opus: An integrated simulation model for transport of nonpoint-source pollutants at the field scale: Volume I, Documentation, 1. USDA, Agricultural Research Service, Springfield: 120 p

Smith RE, Parlange J-Y (1978) A parameter-efficient hydrologic infiltration model. Water Resources Research 14: 533-538

Søe ARB, Buchmann N (2005) Spatial and temporal variations in soil respiration in relation to stand structure and soil parameters in an unmanaged beech forest. Tree Physiology 25: 1427-1436

Sowell JB, Spomer GG (1986) Ecotypic variation in root respiration rate among elevational populations of Abies lasiocarpa and Picea engelmannii. Oecologia 68: 375–379

Stöcker H (1995) Taschenbuch mathematischer Formeln und moderner Verfahren. 3rd edition, Harri Verlag

Stone EL, Kalisz PJ (1991) On the maximum extent of tree roots. For Ecol Manage 46: 59–102

Suarez DL, Šimunek J (1993) Modelling of carbon dioxide transport and production in soil 2. Parameter selection, sensitivity analysis, and comparison of model predictions to field data. Water Resources 29: 499-513

Subke J-A, Inglima I, Cotrufo MS (2006) Trends and methodological impacts in soil CO_2 efflux partitioning: a metaanalytical review. Global Change Biology: 921-943

Tang JW, Baldocchi DD, Qi Y, Xu LK (2003) Assessing soil CO_2 efflux using continuous measurements of CO_2 profiles in soils with small solid-state sensors. Agr. Forest Meteorol. 118: 207–220

Taskinen O, Ilvesniemi H, Kuuluvainen T, Leinonen K (2003) Response of fine roots to an experimental gap in a boreal *Picea abies* forest. Plant Soil 255:503–512

Vachaud G, Passerat De Silans A, Balabanis P, Vauclin M (1985) Temporal stability of spatially measured soil water probability density function. Soil Sci. Soc. Am. J. 49: 822–828

Van Cleve K, Oliver L, Schlentner R, Viereck LA, Dymess CT (1983) Productivity and nutrient cycling in taiga forest ecosystems. Canadian Journal of Forest Research 13: 747-766

Van Cleve K, Sprague D (1971) Respiration rates in the forest floor of birch and aspen stands in interior Alaska. Arctic and Alpine Research 3: 17-26

Van Genuchten MT (1980) A closed-form equation for predicting the hydraulic conductivity of unsaturated soils. Soil Sci. Soc. Am. J. 44: 892-898

Whelan BM, McBratney AB, Minasny B (2002) Vesper 1.5 – Spatial prediction software for precision agriculture. In Robert PC, Rust RH, Larson WE (eds) Precision Agriculture, Proceedings of the 6th International Conference on Precision Agriculture, ASA/CSSA/SSSA, Madison, Wisconsin, 14p. Retrieved from http://www.usyd.edu.au/agriculture/acpa/software/vesper.shtml (April 2010)

Wiedemann E (1927) Der Wurzelbau älterer Waldbäume. Forstarchiv 3: 229–233

Wood BD, Keller CK, Johnstone DL (1993) In situ measurement of microbial activity and controls on microbial CO_2 production in the untreated zone. Water Resour. Res. 29: 647-659

Xu M, Qi Y (2001) Soil-surface CO_2 efflux and its spatial and temporal variations in a young ponderosa pine plantation in northern California. Global Change Biol. 7: 667–677

Yuste JC, Baldocchi DD et al (2007) Microbial soil respiration and its dependency on carbon inputs, soil temperature and moisture. Global Change Biology 13: 2018-2035

10 Appendix

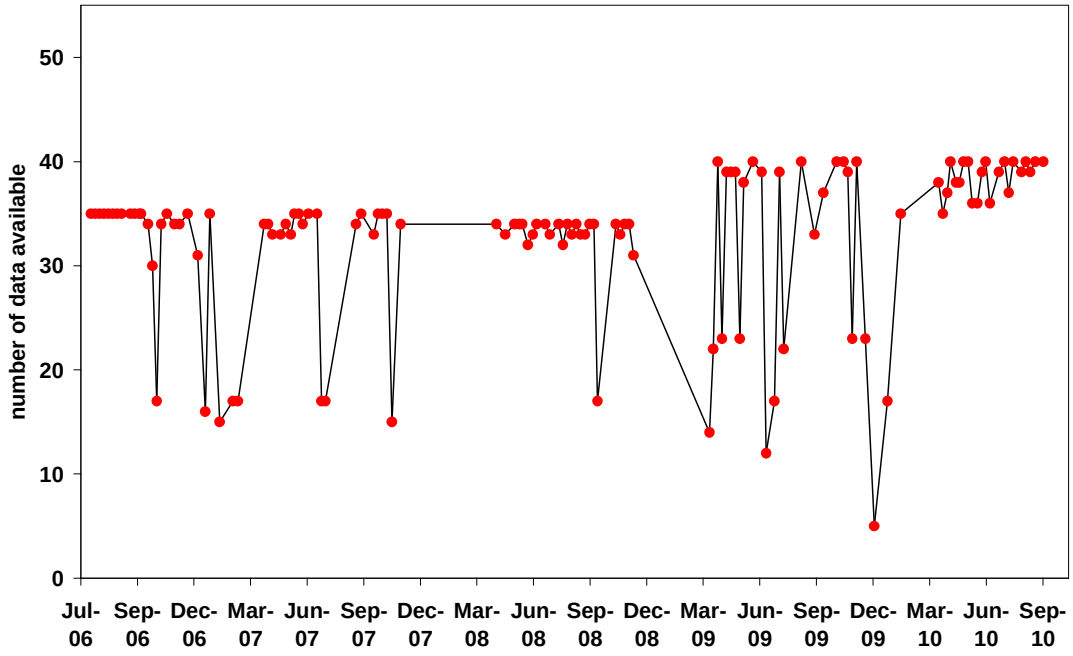

Figure A1: Overview of available data of soil CO_2 efflux for transects WA and WB from 2006 to 2010 (source: illustration of own data)

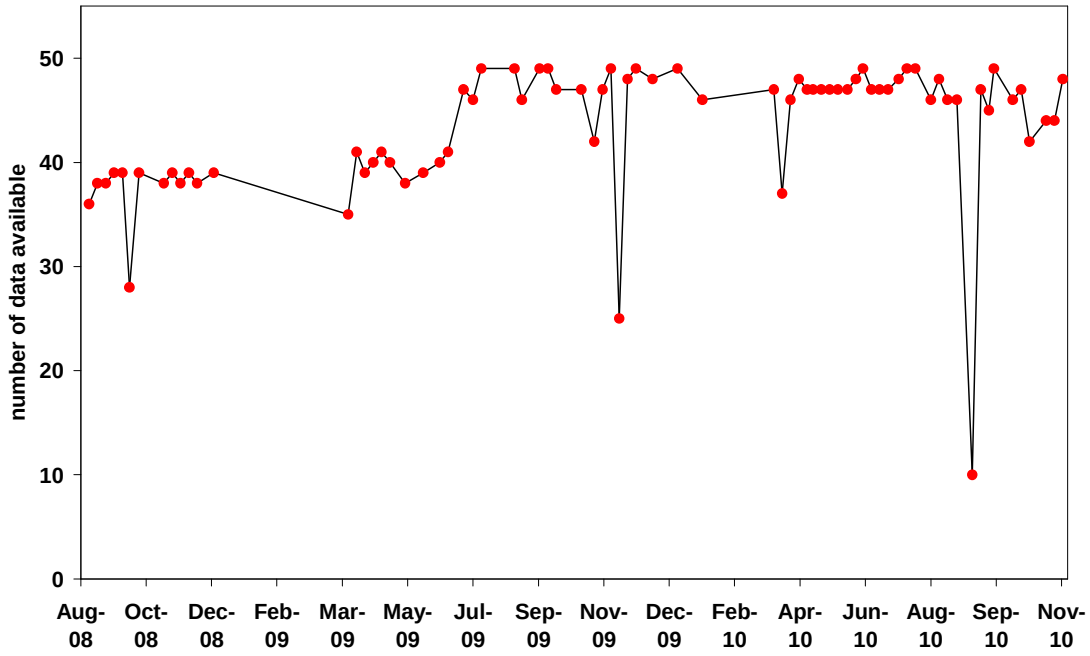

Figure A2: Overview of available data of soil CO_2 efflux for grid M from 2008-2010 (source: illustration of own data)

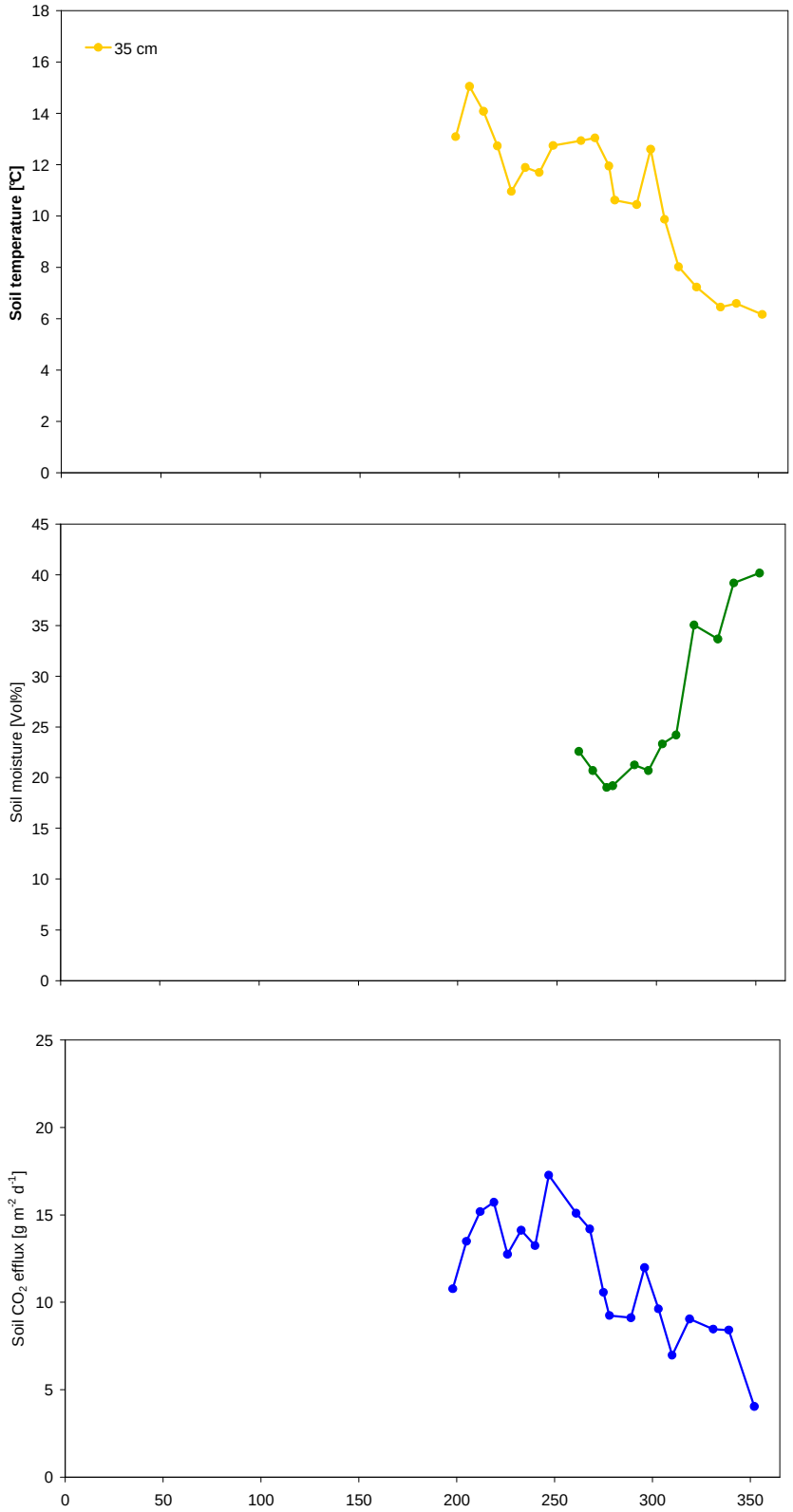

Figure A3: Seasonal course of soil temperature, soil moisture (over an integral of 15 cm) and soil CO_2 efflux for transects WA and WB for the measurement year 2006 (source: illustration of own data)

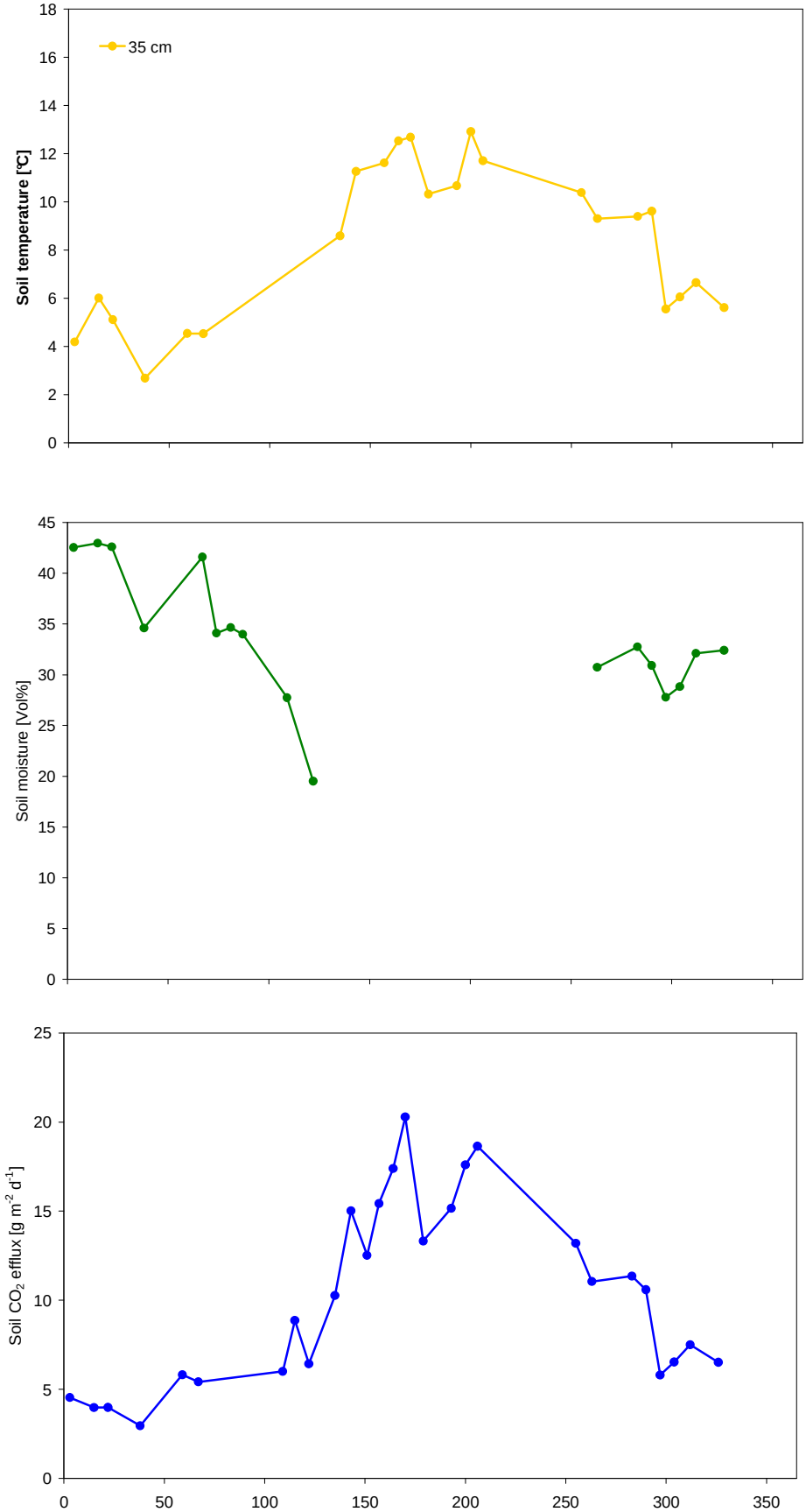

Figure A4: Seasonal course of soil temperature, soil moisture (over an integral of 15 cm) and soil CO_2 efflux for transects WA and WB for the measurement year 2007 (source: illustration of own data)

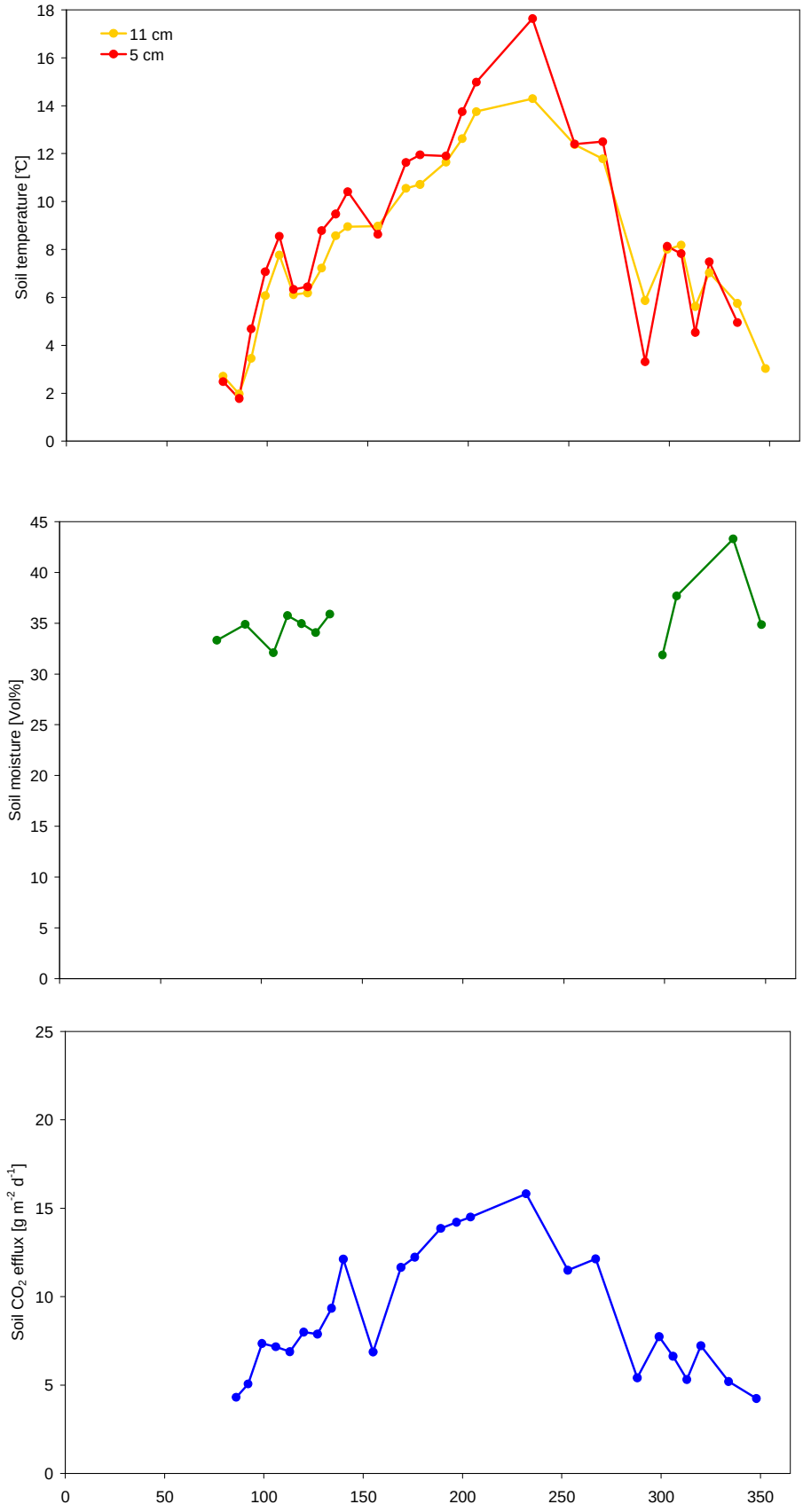

Figure A5: Seasonal course of soil temperature, soil moisture (over an integral of 15 cm) and soil CO_2 efflux for transects WA and WB for the measurement year 2009 (source: illustration of own data)

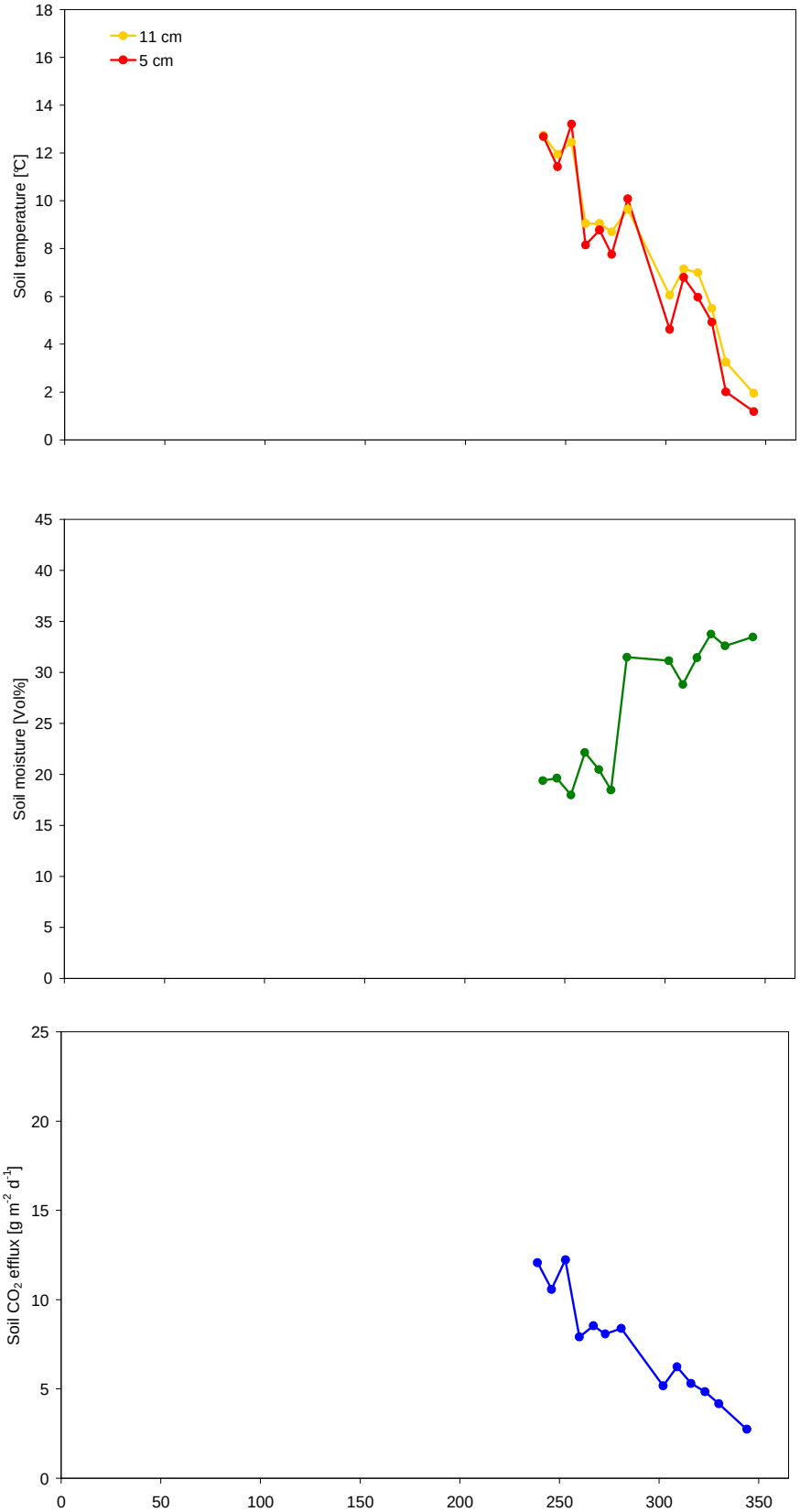

Figure A6: Seasonal course of soil temperature, soil moisture (over an integral of 15 cm) and soil CO_2 efflux for grid M for the measurement year 2008 (source: illustration of own data)

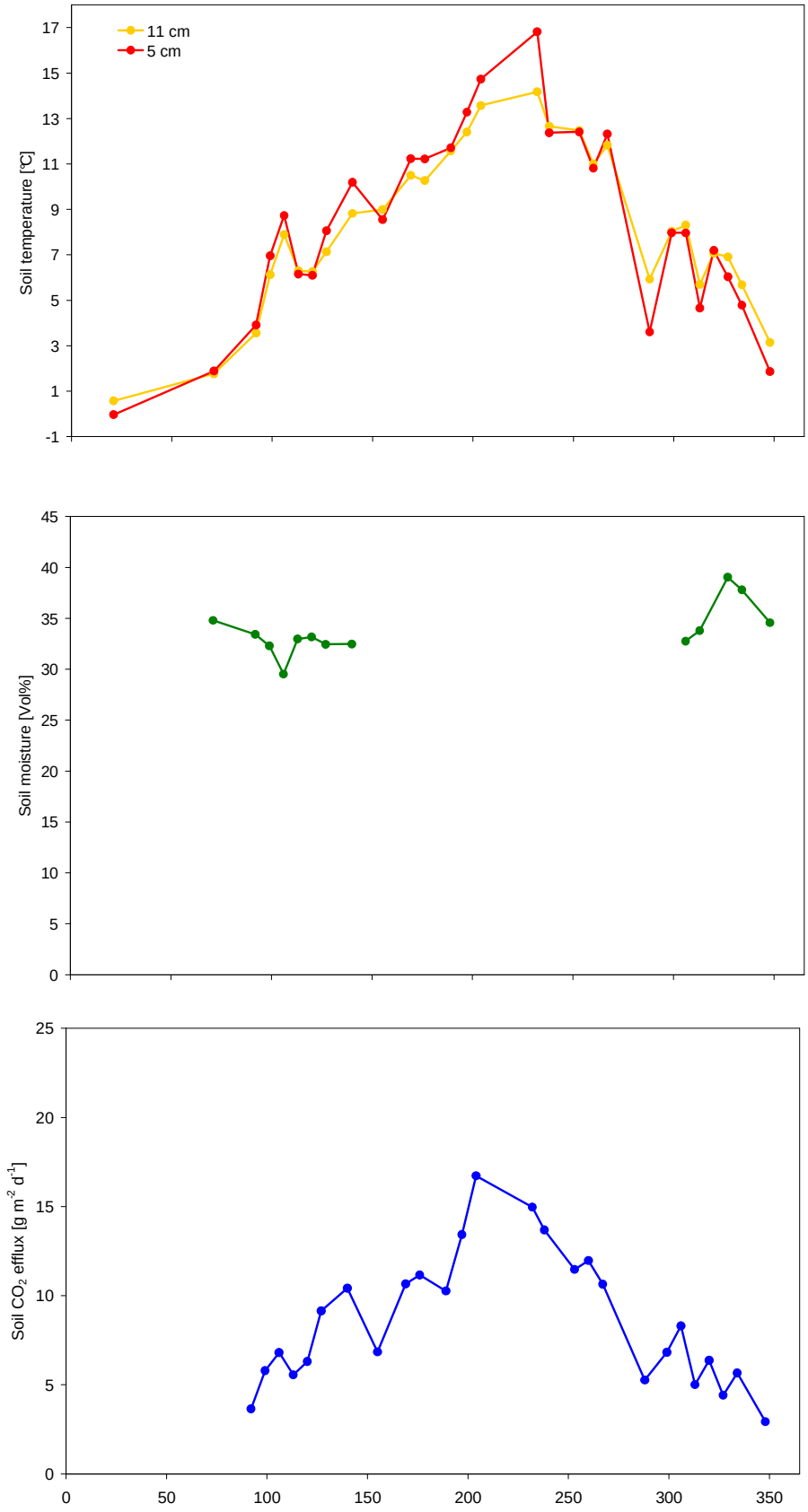

Figure A7: Seasonal course of soil temperature, soil moisture (over an integral of 15 cm) and soil CO_2 efflux for grid M for the measurement year 2009 (source: illustration of own data)

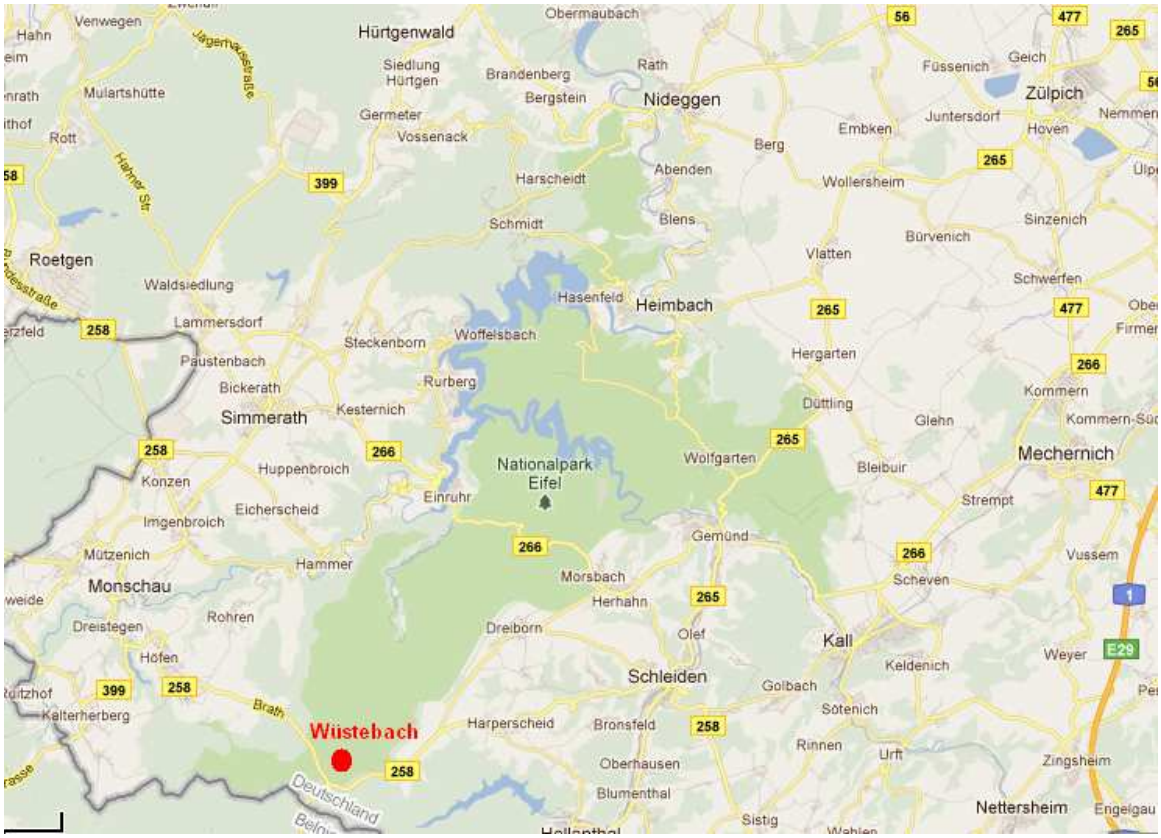

Figure A8: Map of the Rureifel region (source: own illustration with data from Google maps)

Table A1: Soil moisture [Vol%] over an interval of 15 cm measured inside and outside collars (own data)

	03/09/2008	24/09/2008	30/09/2008	08/10/2008
M16	23	33	24	
M16 in collar	26	28	26	
M19	59	56	46	
M19 in collar	54	50	57	water column
M32	24	26	30	36
M32 in collar	28	31	33	31
M33	30	27	35	
M33 in collar	37	34	35	

Table A2 Soil temperature [°C] at a depth of 5 cm measured inside and outside collars (own data)

	03/09/2008 *5 cm*	10/09/2008 *5 cm*	17/09/2008 *5 cm*	24/09/2008 *5 cm*	30/09/2008 *5 cm*
M16	11.4	13	8.2	8.8	7.8
M16 in collar	11.2	13.2	8.7	8.8	7.8
M19	11.9	12.6	8.4	8.8	7.5
M19 in collar	11.6	12.9	8.7	9	7.9
M32	12.1	13.2	9.8	9.4	8.1
M32 in collar	12.1	13.7	9.7	9.4	8
M33	12.2	13.3	9.5	9.2	8.5
M33 in collar	12.2	13.5	9.5	9.5	7.9

Table A3 Soil temperature [°C] at a depth of 11 cm measured inside and outside collars (own data)

	03/09/2008 *11 cm*	10/09/2008 *11 cm*	17/09/2008 *11 cm*	24/09/2008 *11 cm*	30/09/2008 *11 cm*
M16	11.9	12.1	8.9	8.8	8.3
M16 in collar	11.4	12.4	8.9	8.8	8.1
M19	12.2	11.9	9.3	9	8.4
M19 in collar	12.3	11.8	9.1	9	8.3
M32	12.4	12.5	9.7	9.3	8.8
M32 in collar	12.4	12.7	9.7	9.3	8.4
M33	12.7	12.5	9.3	9.3	8.8
M33 in collar	12.7	12.7	9.3	9.2	8.4

Table A4 Pearson Correlation Coefficients for soil CO_2 efflux (CO_2), soil temperature in 11 cm depth (T_{11}; 11 cm was chosen because the temperature data for 5 cm was not available over such a long period of time) and soil water content over an interval of 15 cm (θ_{15}) for transects WA and WB. The Pearson Correlation Coefficients were highly significant for coefficients > 0.7 ($p < 0.01$). (own data)

Year	Date	Interval	Pearson Correlation Coefficient		
		d	CO_2	T_{11}	θ_{15}
	03.01.				
	15.01.	12	0.78	0.73	0.62
	22.01.	7	0.84	0.83	0.50
	07.02.	16	0.77	0.81	0.71
	08.03.	29	0.36	0.75	0.73
2007	**20.09.**	196	0.45	-0.20	0.82
	10.10.	20	0.71	0.84	0.83
	17.10.	7	0.72	0.82	0.87
	24.10.	7	0.81	0.61	0.82
	08.11.	15	0.86	0.92	0.87
	22.11.	14	0.49	0.46	0.83
	02.04.				
	16.04.	14	0.42	0.31	0.85
	23.04.	7	0.84	0.52	0.82
	30.04.	7	0.30	0.81	0.88
	07.05.	7	0.33	0.73	0.80
2009	**14.05.**	7	0.84	0.45	0.81
	26.10.	165	0.65	0.20	0.21
	02.11.	7	0.62	0.81	0.82
	30.11.	28	0.85	0.43	0.76
	26.03.		0.81	0.39	0.89
	02.04.	7	0.53	0.21	0.85
	09.04.	7	0.52	0.79	0.73
	14.04.	5	0.67	0.92	0.58
	28.04.	14	0.53	0.30	0.56
2010	**05.05.**	7	0.61	0.30	0.95
	12.05.	7	0.72	0.75	0.92
	19.05.	7	0.62	0.74	0.91
	27.05.	8	0.44	0.65	0.94
	03.06.	7	0.41	0.85	0.92
	16.06.	15	0.52	0.78	0.90
	30.06.	14	0.50	0.21	0.91

Table A5 Coefficients of determination of individual measurement points for simulated vs. measured soil CO_2 efflux (param. = parameterization; own data)

	2007	2008	2008 param. of 2007	2009	2009 param. of 2007		2008	2009 param. of 2009	2009 param. of 2008
WA1	81	88	88	61	57	**M1**	85	51	58
WA2	93	83	77	63	60	**M2**	92	50	45
WA3	85	88	88	69	68	**M3**	79	50	49
WA4	93	87	81	65	57	**M6**	84	69	65
WA5	83	83	84	76	76	**M7**	91	70	70
WA6	90	56	56	45	45	**M8**	92	73	67
WA7	82	76	74	30	44	**M9**	60	35	35
WA8	80	81	81	88	88	**M10**	97	74	73
WA9	92	74	75	79	78	**M11**	86	80	78
WA10	79	83	82	58	55	**M12**	85	53	59
WA11	79	66	64	84	76	**M13**	51	19	19
WA12	88	73	73	68	68	**M14**	84	83	86
WA13	83	75	76	57	51	**M15**	79	49	46
WA14	81	77	77	57	55	**M16**	99	69	68
WA15	82	69	69	24	24	**M16metal**	81	65	65
WA16	90	96	96	67	55	**M18**	86	26	*27*
WA17	87	94	94	55	57	**M19**	92	47	30
WB1	81	72	76	60	47	**M19metal**	74	4	2
WB2	82	72	82	49	53	**M20**	64	0	0
WB3	68	85	84	56	59	**M21**	73	68	66
WB4	84	85	85	55	57	**M22**	92	47	47
WB5	89	77	78	46	47	**M23**	85	59	57
WB6	74	92	90	75	73	**M24**	65	33	34
WB7	87	83	85	60	57	**M25**	97	74	75
WB8	95	75	75	46	46	**M26**	78	63	63
WB10	88	53	54	29	25	**M27**	64	42	54
WB11	75	72	72	37	38	**M28**	92	74	75
WB12	93	73	73	37	37	**M29**	85	35	40
WB13	82	70	69	29	26	**M30**	91	85	83
WB14	91	77	77	56	48	**M31**	80	71	70
WB15	68	86	87	64	57	**M32**	84	67	66
WB16	86	92	92	65	57	**M32metal**	88	74	72
WB17	86	95	95	43	43	**M33**	86	70	60
WB18	77	92	92	43	46	**M33metal**	71	66	65
						M34	72	57	54